UNIVERSIDADE DE LISBOA
FACULDADE DE CIÊNCIAS
DEPARTAMENTO DE BIOLOGIA VEGETAL

Variability of physicochemical and biological parameters in the Sado Estuary: integration of *in situ* observations and satellite data

Beatriz Isabel Estrada Biguino

Mestrado em Ciências do Mar

Dissertação orientada por:
Doutora Maria Fátima Sousa (FCUL) e Doutora Ana Cristina Brito (FCUL)

2020

Acknowledgments

I would like to properly acknowledge the persons and institutions that allowed the development of this dissertation.

First of all, I want to thank my advisors, Dr. Fátima Sousa and Dr. Ana Brito, who without hesitation accepted to be my guides. Thank you for your dedication, support and investment in my work and in me.

A special acknowledgment to Dr. Carolina Sá. From the beginning, you were a third advisor, always available for me and my difficulties. Thank you for your kindness and support.

I would like to thank the Marine and Environmental Sciences Centre (MARE, ULisboa), where I developed most of this dissertation. To the AQUASADO project, in particular to Dr. Ana Brito, I express my gratitude for having allowed the development of my dissertation within the scope of the project and for having integrated me as a member of the team since the first day. I would like to thank the AQUASADO team for all the help in the field campaigns and in the analysis of the samples, especially to Joana Cruz, Joshua Heumüller and Rui Cereja, to whom my project was demanding.

An acknowledgment to the *Instituto Hidrográfico*, specially to Dr. Carlos Borges and Dra. Carla Palma, for ensuring all the sampling campaigns in the estuary within the AQUASADO project. A note of thanks also to the maritime police and the Captaincy of the Port of Setúbal for the support provided during the project.

A word of gratitude to Dr. Dmitri Boutov, for teaching me how to work with the CTD and the current meter sensor. For coming to meet me whenever I needed help if something unexpected was happening with the instruments, even if it was just a problem with batteries.

Giulia Sent and Mara Gomes, I thank you for being my companions in this challenge that was the dissertation and for your help in the sampling campaigns and with the data processing. Thank you for the words of motivation and for the shared moments of despairs.

My MOGloides friends Rita Cunha and Nuno Luís, distance master's colleagues. Thank you for your help, friendship and care during all this process.

To Vertigem Azul, Maria João Fonseca and Pedro Narra, for the interest shown in my dissertation and for making your boats available so that I could do a more complete study on the estuary dynamics.

João Casal, a sincere thank you for not hesitating in lending me your boat when I suddenly needed it to be able to continue my dissertation. Thank you for your help and friendship.

Artur, my private sailor that, for 26 hours, helped me collect current data when I was too tired to do it by myself. You turned out to be the best scientist in the world. Despite the long and difficult hours and the scares caught during those nights of sampling, it was a spectacular adventure. You were my companion and safe haven, but the truth is that you are it every day. Thank you for your motivation, for assuming my problems as yours, for all your love.

Finally, to my parents and siblings, I thank you for this opportunity, for your constant support and concern, for my life. You are my definition of a perfect family.

This dissertation was developed within the framework of AQUASADO Project (MAR – 02.01.01-FEAMP-0051) – Promoting sustainable aquaculture in the Sado estuary. Website: www.aquasado.pt

Funded by:

Resumo

Os sistemas estuarinos desde sempre captaram a atenção do ser humano. Os estuários estão entre os ecossistemas mais produtivos do mundo, têm uma elevada biodiversidade, que é característica destes sistemas, e oferecem zonas mais protegidas, com enorme importância para funções de proteção, alimentação e berçário para várias espécies. São, portanto, áreas influenciadas pela atividade do Homem, que se habituou a explorar estes sistemas nas vertentes económicas e sociais, por exemplo, através da construção de portos, da atividade piscatória ou do turismo marítimo. Como consequência desta exploração, existe impacto da atividade antropogénica na dinâmica dos estuários, que deve ser devidamente avaliada. No entanto, a análise deste tipo de ambientes apresenta inúmeros desafios. Além do forçamento antropogénico, os estuários têm fortes interações com a atmosfera, condição que confere uma variação sazonal aos parâmetros físico-químicos da água. Adicionalmente, a mistura diária de água doce, vinda do rio, com água salgada, que entra pela foz, promove uma variação constante desses parâmetros e influencia a componente biológica da região. Estes fatores, bem como a recorrente interação com a costa, conferem uma condição natural complexa aos estuários.

O presente estudo aborda este dinamismo e a variabilidade dos parâmetros físico-químicos no estuário do Sado, o segundo maior estuário de Portugal e um dos maiores da Europa. Devido à sua rica biodiversidade, produtividade e valor estético, o estuário do Sado foi definido como reserva natural em 1980, a fim de promover a sua preservação, evitando possíveis impactos antropogénicos nos seus processos e características naturais.

Os primeiros estudos oceanográficos realizados no estuário do Sado decorreram nos anos 70. No entanto, após 40 anos, ainda é um desafio conseguir compreender na íntegra a dinâmica deste estuário e é crucial estudá-lo utilizando uma abordagem que integre observações *in situ* (com um regime de amostragem frequente, feito em profundidade e que acompanhe o ciclo de maré) com dados de satélite, para permitir uma análise temporal e espacial mais completa.

Seguindo esse objetivo, foram realizadas campanhas *in situ* entre setembro de 2018 e setembro de 2019 no estuário do Sado, para recolher dados físico-químicos (temperatura, salinidade, fluorescência, turbidez, intensidade e direção das correntes) e biológicos (concentração de clorofila *a*). Essas campanhas foram realizadas com uma periodicidade mensal utilizando um CTD (Condutividade, Temperatura, Profundidade), um correntómetro e uma sonda multiparamétrica, e recolheram-se amostras de água para posterior quantificação de concentrações de clorofila *a* e matéria em suspensão (SPM). Adicionalmente, em novembro de 2018 e junho de 2019, a recolha de dados foi feita ao longo do ciclo de maré, em condições de marés vivas e de marés mortas. Os resultados indicaram que a região da embocadura do estuário é espacialmente homogénea, verificando-se, ocasionalmente, uma ligeira estratificação da coluna de água. A variabilidade dos parâmetros físico-químicos observada aparentou ser consequência de forçamentos antropogénicos e da variabilidade sazonal ou pontual das condições meteorológicas. Na região do estuário analisada, foi possível observar valores de salinidade tipicamente oceânicos, podendo concluir-se que o rio teve pouca influência na região mais exterior do estuário. Após comparados os resultados obtidos com os de estudos anteriores, pareceu ter existido uma diminuição da influência do rio na embocadura do estuário nos últimos anos, uma vez que se obtiveram valores de salinidade mais elevados ao longo do ano em análise, e uma maior amplitude térmica da água. A circulação no estuário aparentou ser feita através dos dois canais de navegação, sendo o canal sul, a via mais relevante de entrada e saída de água. Observou-se que a maré teve um papel determinante na direção da circulação no estuário. Ademais, a direção da corrente foi uniforme ao longo da coluna de água, contrariando estudos anteriores.

Com vista a melhorar o conhecimento sobre a dinâmica deste sistema estuarino, avaliou-se também a variabilidade intra-anual e interanual da temperatura da superfície do mar (TSM) e da concentração de clorofila *a* através de deteção remota por satélite. O primeiro desafio, foi o de perceber quais os sensores mais apropriados para um estudo em sistema estuarino, que apresentassem dados fiáveis e com elevada qualidade espacial e temporal. Estudou-se a viabilidade em utilizar a base de dados de TSM do *Group for High Resolution Sea Surface Temperature* (GHRSST) através da versão 4.1 da análise *Multiscale Ultrahigh Resolution* (MUR) disponibilizada pelo grupo. Estes dados foram validados com sucesso, por terem apresentado uma boa concordância com os valores de temperatura recolhidos *in situ*, principalmente na região do estuário mais próxima do oceano. No entanto, revelaram ter uma baixa resolução espacial. Ainda assim, foi percetível a sensibilidade deste produto em detetar variações sazonais ao longo do estuário. Foi feita uma análise deste parâmetro de junho de 2002 a setembro de 2019 e viu-se que anos de TSM mais baixas, parecem estar associados a anos de índice NAO positivo.

Para analisar a concentração de clorofila *a* no estuário, utilizaram-se os produtos do Sentinel-3 OLCI (*Ocean and Land Colour Instrument*) para serem validados com os dados *in situ*, e os produtos MERIS, para se alcançar uma maior cobertura temporal e fazer-se uma análise histórica da variação de clorofila *a* no estuário de 2002 a 2012. A análise da clorofila estimada a partir do Sentinel-3 deu uma indicação de que esses dados eram mais apropriados para a área de estudo, devido à resolução espacial do sensor e à boa aplicação a águas costeiras. Foi possível observar concentrações mais elevadas de clorofila *a* nos canais mais interiores do estuário. Adicionalmente, as concentrações máximas de clorofila *a* foram encontradas durante a primavera em todo o estuário. No entanto, a correlação entre os valores de satélite e os obtidos *in situ* não foi a ideal ($R^2 = 0,33$). Uma das fontes de erro associada aos dados do Sentinel-3 poderá ser a presença de matéria em suspensão que parece ter interferido na quantificação de clorofila *a*, principalmente durante a campanha de 8 de novembro de 2018. Dos resultados obtidos no presente estudo, foi também detetada uma tendência para um decréscimo da concentração de clorofila *a* na região, de 2002 a 2012. De 2002 a 2019, também a TSM tendeu a diminuir no estuário. No entanto, seria importante complementar o presente estudo com uma análise estatística que detetasse a significância das tendências observadas.

Dada a complexidade dos ambientes costeiros, os algoritmos disponíveis (quer de correção atmosférica, quer de determinação de variáveis biogeoquímicas) ainda não são totalmente eficientes e outros componentes oticamente ativos (*e.g.*, partículas em suspensão ou matéria orgânica dissolvida) podem interferir nas estimativas da concentração de clorofila *a*. No entanto, quando foram analisadas as bases de dados MERIS e Sentinel-3, utilizaram-se os algoritmos desenvolvidos para águas costeiras e foi possível observar que, com o tempo, houve um aumento da qualidade dos produtos de satélite disponíveis. Como tal, é importante que se continuem a desenvolver novos algoritmos direcionados para ambientes costeiros, utilizando como base os resultados obtidos pelos exercícios de validação de produtos de satélite já realizados por vários autores em diferentes áreas do planeta. O presente estudo permitiu uma caracterização da dinâmica do estuário do Sado na atualidade a partir das campanhas *in situ* e pareceu indicar que poderão ter existido algumas alterações na sua natural dinâmica nos últimos anos. No entanto, seria importante prolongar a análise *in situ* seguindo uma abordagem frequente acompanhando ciclos de maré completos. Posteriormente, mantendo-se a tendência dos resultados obtidos, seria importante perceber o que esteve na origem destas alterações e quais as consequências que estas poderão ter no futuro do ecossistema.

Palavras-chave: Estuários, Circulação de Água, Deteção Remota, TSM, Clorofila *a*

Abstract

Estuarine systems have always captured the attention of Man. Estuaries are among the most productive ecosystems in the world. They have a high biodiversity, that is characteristic of these systems, and offer sheltered areas, with enormous importance for protection, feeding and nursery functions for several species. Therefore, they are areas influenced by the activity of Man, that explores these systems economically and socially, through, for example, the construction of ports, fishing or maritime tourism. As a result of this exploration, an impact of the anthropogenic activity on the dynamics of the estuaries is verified, which must be properly assessed. However, the analysis of these types of environments presents numerous challenges. In addition to anthropogenic forcing, estuaries have strong interactions with the atmosphere, a condition that gives a seasonal variation to the physicochemical parameters of the water. Additionally, the daily mixture of fresh water, coming from the river, with salt-water, which enters through the estuary, promotes a constant variation of these parameters and influences the biological component of the region. These factors, as well as the continuous interaction with the coast, give estuaries a complex natural condition.

The present study addresses this dynamism and the variability of the physicochemical parameters of the water in the Sado estuary, the second largest estuary in Portugal and one of the largest in Europe. Due to its rich biodiversity, productivity and aesthetic value, Sado estuary was defined as a natural reserve in 1980, in order to promote its preservation, avoiding possible anthropogenic impacts in its natural processes and characteristics.

The first oceanographic studies carried out in the Sado estuary took place in the 70s. After 40 years, it is still challenging to understand the dynamics of this estuary and is crucial to integrate *in situ* observations (with frequent sampling, in depth and throughout the tidal cycle) with satellite data, to enable an extended temporal and spatial analysis.

Following that objective, *in situ* campaigns were conducted between May 2018 and September 2019 in Sado estuary, to collect physicochemical (temperature, salinity, fluorescence, turbidity, intensity and direction of the currents) and biological (chlorophyll *a* concentration) data. These campaigns were conducted on a monthly basis using a CTD (Conductivity, Temperature, Depth), a current meter sensor and a multiparameter sonde, and water samples were collected for laboratory quantification of chlorophyll *a* concentrations and suspended particulate matter (SPM). Additionally, in November 2018 and June 2019, the data collection was made along the tidal cycle, in both spring and neap tide conditions. The results indicated that the outermost area of the estuary is spatially homogeneous, with occasional stratification of the water column. The observed variability of the physicochemical parameters appeared to be a consequence of anthropogenic forcing and of seasonal or occasional variations of the weather conditions. In the analyzed region of the estuary, it was possible to observe salinity values typically oceanic, so it is assumed that the river had a low influence in the outermost region of the estuary. When compared with the results of previous studies, it was possible to infer that there was a decrease in the influence of the river in the outermost region of the estuary in the past years, since higher salinity values were obtained throughout the year under analysis, and that is currently observed a greater thermal amplitude of the water. The circulation in the estuary appeared to be made in the two navigation channels, being the South channel the most relevant route for water exchange. It was observed that the tide played a determining role in the direction of the circulation in the estuary. In addition, and contrary to the results of previous studies, the direction of the current was uniform along the water column.

In order to improve knowledge about the dynamics of this estuarine system, the intra-annual and interannual variability of the sea surface temperature (SST) and the chlorophyll *a* concentration through satellite remote sensing was studied.

The feasibility of using the SST database of the Group for High Resolution Sea Surface Temperature (GHRSST) was studied through version 4.1 of the Multiscale Ultrahigh Resolution (MUR) analysis made available by the group. These data were successfully validated, as they showed a good agreement with the temperature values collected *in situ*, mainly in the region of the estuary closest to the ocean. However, they appeared to show a low spatial resolution. Even so, the sensitivity of the product in detecting seasonal variations along the estuary was noticeable. An analysis of this parameter was carried out from June 2002 to September 2019 and it was observed that years of lower SST values seemed to be associated with years of positive NAO index.

To analyze the chlorophyll *a* concentration in the estuary, the products of the Sentinel-3 OLCI (Ocean and Land Color Instrument) were used for validation with the *in situ* data. MERIS products were also used to achieve a greater temporal coverage and to present a historical analysis of the variation of chlorophyll *a* in the estuary. The analysis of chlorophyll estimated from Sentinel-3 gave the indication that these data were more appropriate for the study area, due to the spatial resolution of the sensor and its better application to coastal waters. It was possible to observe higher concentrations of chlorophyll *a* in the innermost channels of the estuary. Additionally, the maximum concentrations of chlorophyll *a* were observed during spring throughout the estuary. However, the correlation between the satellite values and those obtained *in situ* was not ideal ($R^2 = 0.33$). One of the sources of error associated with the Sentinel-3 data may be the presence of suspended matter that appears to have interfered with the quantification of chlorophyll *a*, especially during the campaign of 8 November 2018. From the results obtained in the present study, it was also observed a trend towards a decrease in the concentration of chlorophyll *a* in the region, from 2002 to 2012 (MERIS data). From 2002 to 2019, the SST also tended to decrease in the estuary. However, it would be important to complement the present study with a statistical analysis that would detect the significance of the observed trends.

Due to the complexity of coastal environments, the algorithms available (whether for atmospheric correction or for determining biogeochemical variables) are not yet fully efficient because other optically active components (*e.g.* Suspended Particulate Matter or Colored Dissolved Organic Matter) can interfere with the estimations of chlorophyll *a* concentrations. However, in the present work, when MERIS and Sentinel-3 databases were analyzed, algorithms developed for coastal waters were used and it was possible to observe that, over time, there was an increase in the quality of the available satellite products. It is important to continue to develop new algorithms for coastal environments, using as a basis the results obtained by the validation exercises of satellite products already carried out by various authors in different areas of the planet. The present study allowed to describe the dynamic of the Sado estuary, based on *in situ* campaigns and it was concluded that some changes in the natural behavior of the estuary may have occurred in the past years. However, it would be important to prolong the *in situ* analysis following a frequent sampling approach along full tidal cycles. Subsequently, if the trend of the results obtained is maintained, it would be important to understand the origin of these changes and what consequences could they have on the future of the ecosystem.

Keywords: Estuaries, Water Circulation, Remote Sensing, SST, Chlorophyll *a*

Table of Contents

Figure Captions

Tables Index

List of Acronyms

ADEC	Alaska Department of Environmental Conservation
AMSRE	Advanced Microwave Scanning Radiometer-EOS
AUV	Autonomous Underwater Vehicle
AVHRR	Advanced Very High Resolution Radiometer
CCI	Climate Change Initiative
CDOM	Colored Dissolved Organic Matter
CZCS	Coastal Zone Color Scanner
DCM	Deep Chlorophyll Maximum
EC	European Commission
EES	Environmental, Energy and Science Group (New South Wales Government)
ESA	European Space Agency
FSI	Falmouth Scientific Inc
NOAA	National Oceanic and Atmospheric Administration
ICNF	*Instituto de Conservação da Natureza e das Florestas*
GHRSST	Group for High Resolution Sea Surface Temperature
HPLC	High Performance Liquid Chromatography
IPMA	*Instituto Português do Mar e da Atmosfera*
IST	*Instituto Superior Técnico*
JPL	Jet Propulsion Laboratory
MERIS	Medium Resolution Imaging Spectrometer
MODIS	Moderate Resolution Imaging Spectroradiometer
MUR	Multiscale Ultrahigh Resolution
NAO	North Atlantic Oscillation
NASA	National Aeronautics and Space Administration
NEODAAS	NERC Earth Observation Data Acquisition and Analysis Service
NXIC	Non-eXternal Inductive Conductivity
OLCI	Ocean and Land Colour Instrument
PO.DAAC	Physical Oceanography Distributed Active Archive Center
SeaWiFS	Sea-viewing Wide Field-of-view Sensor
SNAP	Sentinel Application Platform
SNIRH	*Sistema Nacional de Informação de Recursos Hídricos*
TEOS-10	Thermodynamic Equation of Sea Water 2020
USA	United States of America
VIIRS	Visible Infrared Imaging Radiometer Suite
WWTP	Wastewater Treatment Plant

Chapter 1

Introduction

Estuaries are very dynamic transitional environments (Day *et al.*, 2012). They are influenced by discharges from rivers, which transport large amounts of nutrients and organic matter, and simultaneously by oceanic waters, that allow the renewal of water and cause a great variation in salinity which determines the existing biodiversity. The high concentrations of nutrients, that comes also from the continuous interaction of the water with the coast, implicit in the morphology of an estuary, leads to high primary production (Mateus *et al.*, 2008). For these reasons, estuaries are especially important areas of habitat and nutrition with very characteristic food chains, that contribute to its relevance as a nursery area (NOAA, 2020a). Therefore, estuaries are recognized as ecologically important and efforts should be made to preserve them (Day *et al.*, 2012). However, these environments tend to be difficult to analyze, due to all the external forcing to which they are subjected. The daily mixture of fresh water, that comes from the river, and salt-water, that enters into the estuary through its mouth, promotes a constant variation of the physical and chemical parameters of the estuary, that influences the biological component of the region. Additionally, these variables are sensitive to atmospheric conditions and, therefore, show seasonal variations (Mateus *et al.*, 2008).

A large fraction of the population lives in the adjacent area of estuaries due to the increased social and commercial potential of these environments. The appropriate management of the estuaries is necessary for their preservation. Thus, its scientific understanding is of great practical importance (Wolanski *et al*., 2013) and integrating knowledge of geology, hydrology, chemistry, physics and biology is essential (Day *et al.*, 2012). The Sado estuary in particular, is one of the biggest estuaries in Portugal, has a unique morphology and biodiversity and has an enlarged commercial interest, as there is a great dependence of the population of the region on the estuary and its resources (Caeiro, 2004).

The Sado estuary was previously characterized considering its circulation regime and the variability of its physical, chemical and biological parameters, with *in situ* observations and numerical models (*e.g.*: Ambar *et al.*, 1982; Maretec, 2002a). However, it has been weakly analyzed by satellite, probably due to the complex dynamics of these areas that increases the difficulty in deriving accurate products. Satellite remote sensing is of great importance as it allows a high temporal and spatial coverage, at virtually no cost. For example, it is possible to retrieve Sea Surface Temperature data from all around the world, simply by accessing to the Group for High Resolution Sea Surface Temperature (GHRSST) database. Also, the use of satellite remote sensing allows performing a historical analysis of the region, through the study of the intra and

interannual variability of the parameters of the estuary. The integration of *in situ* observations with satellite data is, therefore, essential to fully understand the estuarine dynamics, as this is a key tool to evaluate how the estuary has been changing through time and if it has been responding to the global climatic variation.

1.1 The Sado Estuary

Sado River begins in Serra da Vigia (southwest of Ourique) at 232 m high, and flows northwards until it reaches the Atlantic Ocean, through an estuarine environment, in Setúbal (Portugal). It travels a course of ≈ 175 km in a Southeast-Northwest orientation (ICNF, 2020).

The Sado estuary is the second largest national estuary and one of the largest in Europe. Due to its rich biodiversity, productivity and aesthetic value, it was defined as natural reserve in 1980, in order to promote its preservation, avoiding possible interferences in the natural processes and characteristics that distinguish it from other estuaries. The reserve has a navigable area of about 23,160 ha and includes about 28 km of the river (ICNF, 2020).

Using the morphologic classification of Pritchard (1952), Sado estuary can be considered as a coastal plain type estuary, since it is long, shallow, with shoals, that resulted from the subsidence of the Sado basin (Sousa and Lourenço, 1980).

In the protected area, there is a high number of bird species that find the perfect place to nest or hibernate, of mammals, reptiles and amphibians that in the vast areas of marsh obtain perfect nursery areas (ICNF, 2020). Also, it is possible to find seagrass meadows in Sado estuary. They are important in maintaining healthy estuarine environments and play a critical role in primary production (Cunha, 2009). This estuary is also the habitat of the only community of dolphins, *Tursiops truncatus*, resident in an estuarine environment in Portugal (Costa, 2015). Currently the community is composed of 27 individuals and this, like many other species in the estuary, is threatened by the human activity, that in the peninsula of Setúbal and Troia, has a great incidence in the estuary.

For all its characteristics, the estuary is also a privileged place for the practice of aquaculture, and the Sado's oyster (*Crassostrea (Magallana) angulata*) is the main example of this activity in Setúbal. During the 60s and 70s, there was an important production of oyster in the estuary that got strongly weakened, possibly due to the high levels of pollution of the water (Coutinho, 2003). Nowadays, it is recovering its statute of one of the most iconic symbols of the region.

Coutinho (2003) divided the Sado estuary into three sections, according to the topography and morphology of the region. The first section (S1, represented in orange in Figure 1.1), the Setúbal Bay, with an average depth of 10 m, is the region where the contact between the ocean and the estuary mouth occurs, through an embouchure of approximately 1.5 km and maximum depth of 40 m (Brito *et al*., 2003). This communication channel is divided in two different courses separated by intertidal shoals, the North channel, that allows access to the Port of Setúbal, and the South channel, which runs to the city of Alcácer do Sal.

The second section (S2), in blue in Figure 1.1, is the one that includes a vast intertidal zone, where the Marateca and Comporta channels are located. In this region, the influence of the tides is very evident and is the factor that allows the water circulation. That leads to great variations in the volume and depth of the channels, naturally with a very reduced depth (Coutinho, 2003).

The third section (S3), in green in Figure 1.1, corresponds to the main channel of the Sado river, evident in the area of Alcácer do Sal, denominated as the channel of Alcácer. This channel

has an average of 5 m depth and a very irregular and seasonal flow that varies, on average, from 0.7 m^3/s in the summer to 60.0 m^3/s in the winter (Coutinho, 2003; Brito *et al.*, 2003).

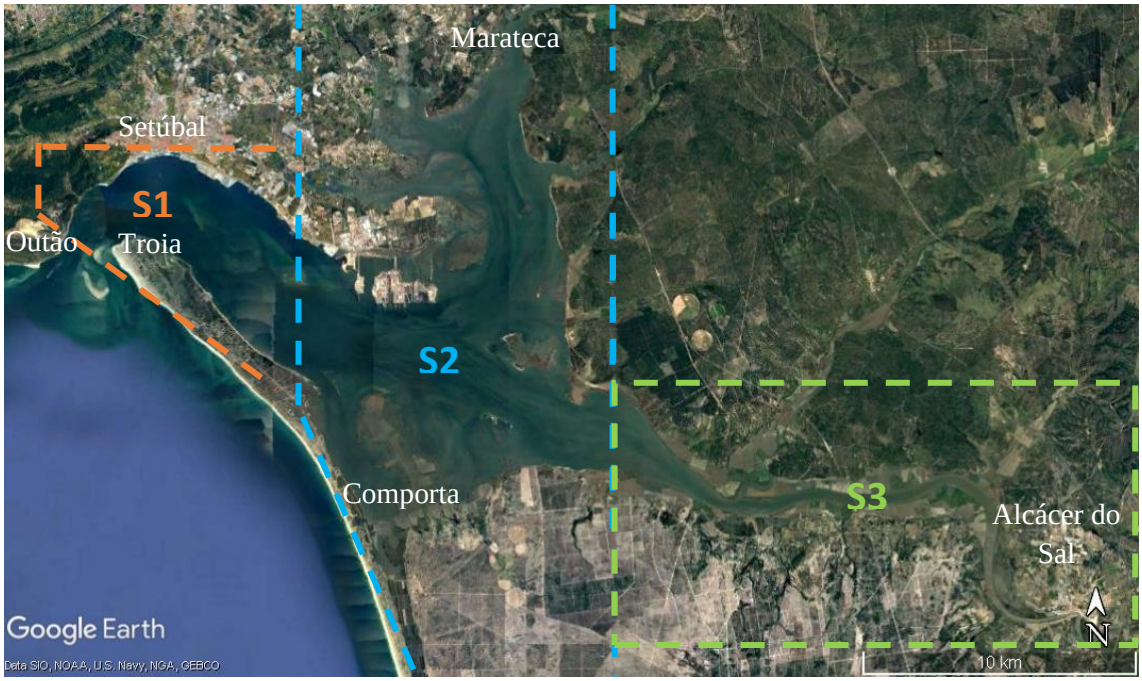

Figure 1.1. Configuration of the Sado estuary with the division into 3 sections. Adapted from Coutinho (2003).

The Sado river is characterized by having a low flow rate and for a reduced displacement of water, as it is under the influence of the arid climate of Alentejo, where the river spring is located. Also, the river does not suffer great differences of altitude during its course to the mouth, has 2% of inclination in the initial section and practically zero in the final one (Sousa and Lourenço, 1980). Lastly, is fed by several streams that do not have a substantial flow.

In general terms, there is a strong influence of the effect of the tide on the circulation in the estuary (Sousa and Lourenço, 1980). Previous studies showed that during high water, water tends to enter the bay predominantly through the North channel and exit through the South channel at low water and there is a trend towards a strong asymmetry between tidal regimes in the two channels with stronger streams in the southern channel of the estuary (Ambar *et al.*, 1982).

In order to have a better understanding of the dynamic of the estuary, Sado river flow was analyzed. Data of the daily average flow from *Sistema Nacional de Informação de Recursos Hídricos* (SNIRH) were used to complement this analysis. The data used were collected in *Moinho da Gamitinha*, the sampling station suggested by SNIRH's team as being the most suitable for this study (see location in Figure 1.2). In the database, daily average values were available from October 1940 to December 2019, there being missing values in some periods of the series. Figure 1.3 shows the temporal variation of the daily average outflow of the Sado river in the station aforementioned.

Figure 1.2. Location of Moinho da Gamitinha station.

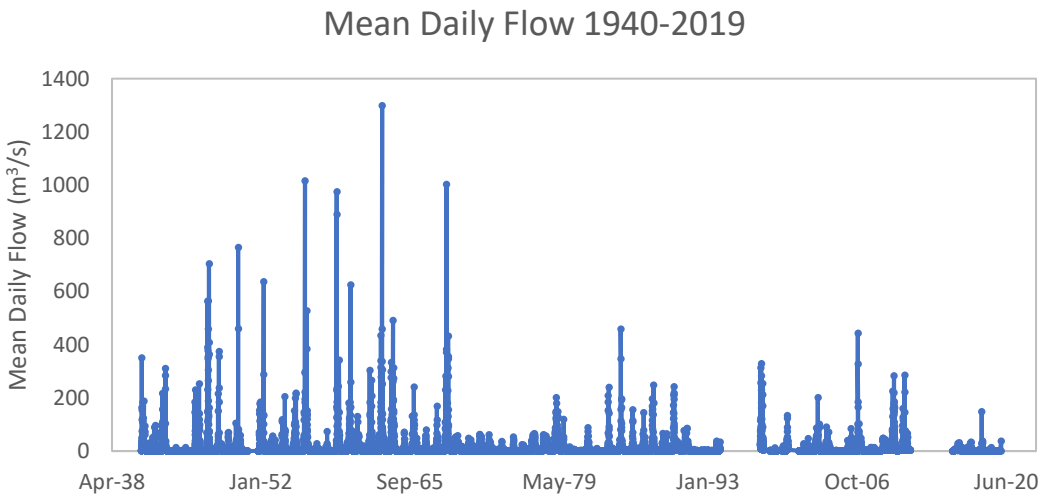

Figure 1.3. Daily average outflow of the Sado river, in the period between 16 OCT 1940 and 31 DEC 2019, measured at Moinho da Gamitinha. Data provided by SNIRH.

These data (Figure 1.3) highlights two distinct periods. The first, from the beginning of the series until 1969, shows peaks with high daily outflows, frequently with values exceeding 500 m^3/s. The second period, from 1969 onwards, presents much lower outflows. Particularly between 1969 and 1978, there were no values higher than 100 m^3/s. This change in the flow regime could be related with the construction of dams along the course of the river (1967 – *Roxo dam*; 1972 – *Monte da Rocha dam;* Sales, 2015). Table 1.1 shows the average and maximum daily flow of the two mentioned periods.

Table 1.1. Mean and maximum values of the average daily flow measured at Moinho da Gamitinha, before and after 1969.

	Average Daily Flow (m^3/s) - *Moinho da Gamitinha*	
	Mean	Maximum
16 OCT 1940 to 31 DEC 1969	9.7	1298.5
01 JAN 1970 to 31 DEC 2019	5.6	458.8

Figure 1.4 shows the Sado river flow anomalies between 1941 and 2019, using the data of Figure 1.3 and considering the average of the values measured between this period as the reference. Only the data of the years that did not presented gaps of one or more months were considered. It is clear that 1963 was characterized by having a big positive anomaly, as opposed to 2019, one of the years with the lowest flow rates of the analyzed period. Also, it is plausible to deduce that there was a decrease of the river flow since 1941, given the trend towards negative anomalies represented by the dashed line (fitting the anomalies) in Figure 1.4. Of relevance is also the lack of positive anomalies in the last decade (although the absence of data in some years).

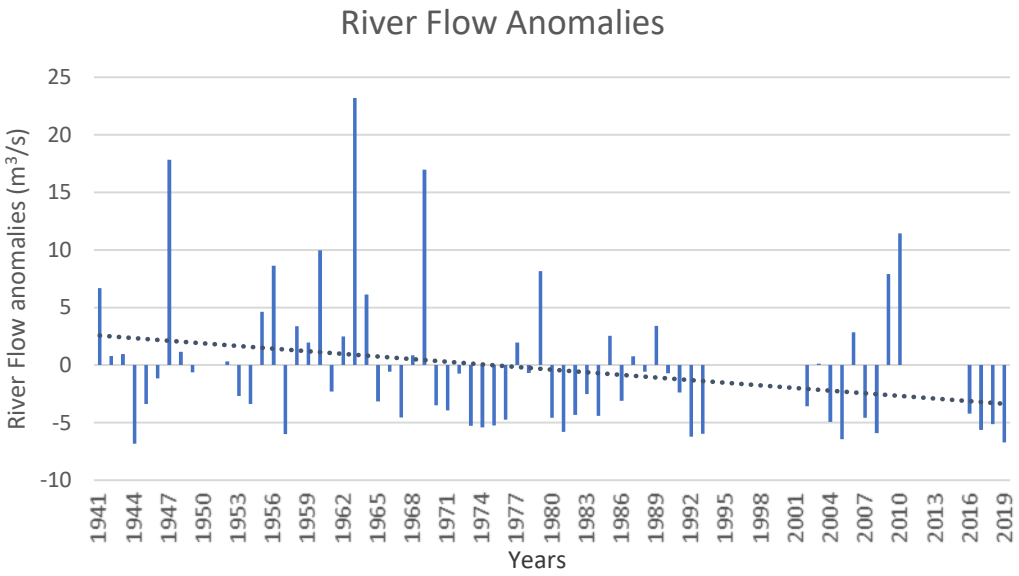

Figure 1.4. Sado river flow anomalies between 1941 and 2019, being the reference, the average of the values measured between this period. Only the data of the years that did not presented gaps of one or more months were considered. The dashed line represents the trend of the river flow anomalies in the period referred. Data provided by SNIRH (Moinho da Gamitinha).

Figure 1.5 presents the monthly values of Sado's flow at *Moinho da Gamitinha* between 2002 and 2011. This period was chosen to allow the analysis made in Chapter 3 with MERIS satellite products, that provided data between 2002 to 2012 (flow data regarding 2012 were not available in SNIRH's database). As it would be expected, the river presented a higher mean flow during the winter months and minimum values during summer.

.

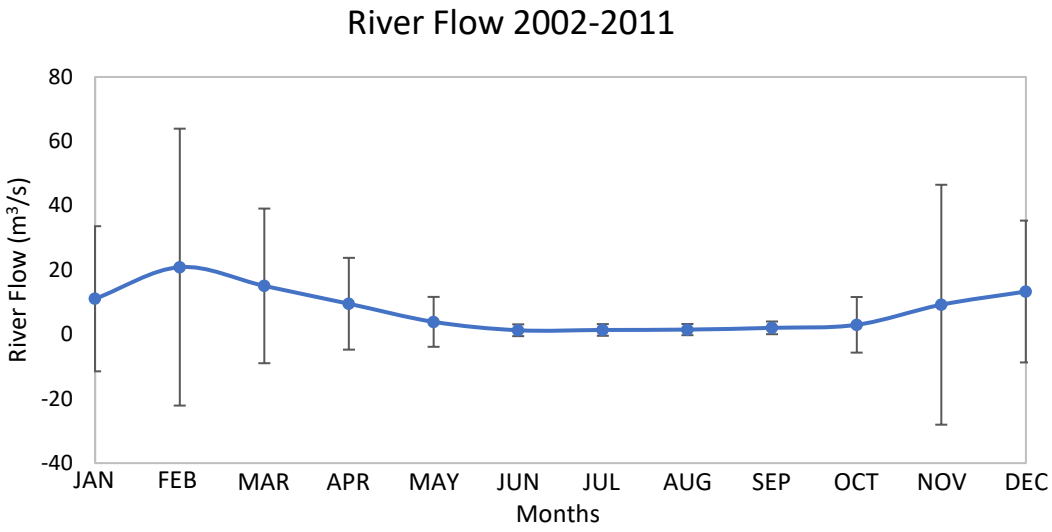

Figure 1.5. Mean monthly river flow measured at Moinho da Gamitinha between 2002 and 2011, with the respective standard deviation. Data provided by SNIRH.

1.2 Aims of this study

The main objective of this study was to analyze the temporal variability of physicochemical and biological parameters of the Sado estuary integrating two types of data: i) *in situ* observations and ii) satellite data. This temporal analysis was carried out at different time scales: tidal and seasonal, using *in situ* data, and interannual, after the integration of the satellite products. Consequently, this dissertation is divided into two main chapters, as described below.

Chapter 2 is focused on the variability of temperature, salinity, turbidity, fluorescence and direction and intensity of currents (physicochemical parameters) at the outermost area of the Sado estuary, observed during *in situ* campaigns, at two different time scales: tidal and seasonal. In this chapter it is essentially intended to describe the circulation in the estuary, mainly the regime of water exchange at the mouth of the estuary, and to understand how the behavior of the remaining parameters can be defined throughout time. The first studies taken as a reference go back to the 1970s. Given the dynamic regime of this ecosystem, the climatic forcing and the anthropogenic pressure that is currently verified in the area, it is aimed to analyze if the estuary changed in the past years. If so, there is the purpose to try to clarify the reason for the observed changes and study possible trends and consequences derived from the new conditions.

Chapter 3 intends to extend the temporal and spatial coverage of the previous analysis with the use of satellite data. The first step is to understand which are the satellite products more appropriate for this study area, in order to analyze the variability of the Sea Surface Temperature (SST) and the chlorophyll *a* in the Sado estuary. After validating those products with the *in situ* observations, an evaluation of the general temporal and spatial pattern of those parameters was performed. The use of satellite data allows to investigate the temporal variation of these parameters using a more robust database and of greater spatial coverage. Likewise, it allows to discuss future scenarios for this estuary.

Chapter 2

Tidal and seasonal variability of physicochemical parameters using *in situ* observations

2.1 Introduction

Estuaries have been described very broadly as the portion of the earth's coastal zone where there is interaction of ocean water, fresh water, land and atmosphere. Although the dynamics of an estuary can be described in a very generalized way, estuaries are characterized as much by similarities as by differences (Day *et al.*, 2012). The Sado estuary is an example of that, having distinctive properties. The first oceanographic studies carried out in the Sado estuary occurred throughout the 1970s with the work of Wollast (1978, 1979). Wollast (1978, 1979) studied the variation of the temperature and salinity in the estuary and recorded hydrologic and current data without analyzing the direction of the currents. However, these results were too preliminary to allow any solid conclusion about the physical oceanography of the estuary (Sousa and Lourenço, 1980). Later, several studies that focused on the physical characterization of the estuary were conducted in the area (Sousa and Lourenço, 1980; Ambar *et al*., 1982; Ribeiro and Neves, 1982; Neves, 1985).

Sousa and Lourenço (1980) reported that the entrance of water in the Sado estuary was made mainly through the North channel, being the South channel the focal area of water outflux. The estuary was described by showing a pronounced asymmetry in both tidal regimes between the North and South channels, not only in current intensity (higher values were observed in the South channel), but also in the timing of the turn of the tide from ebb to flood (North channel with a faster reaction to the change of the tide). Also, the residual current was observed to be directioned from near Albarquel all the way up the northern channel while the southern channel showed a classical net estuarine circulation - the vertically integrated residual flow was seaward although the deep layers moved up-estuary and the surface layers moved towards the sea (Ambar *et al.*, 1982).

The oceanic water is believed to influence the entire estuary, as high salinity values were previously observed throughout the whole estuarine area (Sousa and Lourenço, 1980). Sousa and Lourenço (1980) observed that this parameter was vertically heterogeneous, so they referred that the Sado estuary was partially mixed. However, mean salinity values (tidal and vertical averages) were used together with current data, to calculate the stratification and circulation parameters

defined by Hansen and Rattray (1966) and, according to this criterion, the estuary was classified as having a low stratification (Ambar *et al*., 1982). Ribeiro and Neves (1982) suggested that the estuary behaved as a coastal lagoon, with salinity always above 28. The similarity with a coastal lagoon came mostly from the high salinity values that were measured throughout the whole estuarine region. This observation revealed a low mixture of fresh water with oceanic water, mixture that would have to be evident in a typical estuary (NOAA, 2020c). It was also observed that the water of the river tended to be colder than the ocean water (Ambar *et al*., 1982).

Considering the tidal cycle, the variation of the salinity and the temperature was observed to be low (Moreira, 1987). Nevertheless, the seasonal variation of these parameters was evident (Sousa and Lourenço, 1980). According to the study of Sousa and Lourenço (1980), in the first section of the estuary (S1 in Figure 1.1), during winter and summer, the surface temperature was ≈13 ºC and ≈17 ºC, respectively. As for the salinity, it reached values of 32 in winter and fitted between 35.0 and 35.7 during summer, for the same region of the estuary. Usually, during winter, the sea water was warmer than the water inside the estuary (or had almost the same temperature), occurring an inversion of that signal during summer (Ribeiro and Neves, 1982).

More recently, few oceanographic studies have been conducted in the estuary. Nevertheless, the application of the MOHID 2000 model in Sado estuary is worth to be mentioned. MOHID is a water modeling system initially developed to study the circulation in coastal and oceanic areas (Neves, 2000). Throughout its existence, the MOHID model has been successfully used in numerous case studies, among which are areas with very different characteristics, as the deep ocean (cases of the Northeast Atlantic, within the scope of the Omex project; Mediterranean Sea, under the EuroModel project), river and estuarine areas, coastal areas, lagoons and reservoirs (Maretec, 2000a). In Sado estuary, a hydrodynamic analysis and a simulation of the estuary was performed with MOHID, in order to evaluate its trophic level, as well as to identify the most important factors that influenced it (Maretec, 2002a). The circulation regime obtained using MOHID for the Sado estuary presented results in agreement with previous studies.

Since this region started to be occupied by humans, the estuary margins have slowly been modified. The salt pans, the landfills or the facilities of the port of Setúbal are undoubtedly some of the most visible structures resulting from the human settlement that led to the artificialization of the coast throughout time. Furthermore, they motivate frequent dredging works in the navigation channels, in order to maintain the navigability of the estuary. All these human influences lead to the destruction of intertidal zones, to the introduction of polluting sources within the estuary (from industrial units and ship movements) and influences the circulation in the estuary (Sousa, 2006). In addition to the changes resulting from human occupation, it is also possible to see modifications driven by environmental variations, such as climate change, specific atmospheric phenomena or changes in the river's flow, that vary the morphology of the estuary and the water physicochemical and biological conditions (EES Group, 2018). As about 40 years have passed since the first studies were carried out in the estuary, it is important to understand if the behavior of these water parameters changed through time, and if so, by what aspects were those changes driven. Moreover, a study based on *in situ* measurements made throughout the tidal cycle, with high frequency and in depth, in a monthly sampling regime, using a various set of instruments, was in need. This approach would allow a more accurate view of estuarine dynamics and, therefore, was used in the present study.

2.2 Sampling Strategy

The sampling strategy of this study consisted in monthly sampling collections and intense campaigns conducted along part of the tidal cycle and covering the entire tidal cycle (partial tidal cycle and full tidal cycle campaigns, respectively). Different parameters of water quality (*e.g.*: temperature, salinity, dissolved O_2, pH, nutrient and chlorophyll *a* concentrations) were measured. Monthly campaigns took place between September 2018 and September 2019, in stns. #6 and #7 (see Figure 2.1 and Table 2.1 for location). A total of 11 monthly campaigns were performed (Table 2.2).

The partial tidal cycles were covered during two periods: November 2018 and June 2019. For each period, two cycles were sampled to evaluate the differences between spring and neap tides. For this tidal study, an additional station, stn. #8 (Figure 2.1 and Table 2.1), was considered instead of stn. #6, that was not monitored given its proximity to the coast. In the end, a total of 4 partial tidal campaigns were performed. Stn. #8 is the station with the least information because was only monitored in those tidal campaigns.

Figure 2.1. Distribution of the sampling stations in Sado estuary.

Table 2.1. Sampling stations: designation and geographical coordinates.

Station (Stn.)	Designation	Coordinates	
		Latitude ˚ N	Longitude ˚ W
#6	Setúbal	38.51809	008.89838
#7	Outão	38.48667	008.93000
#8	Troia	38.49278	008.88167

All the monthly campaigns were planned to start the data collection at high water (HW). In the partial tidal cycle campaigns, sets of measurements were taken every two hours in each one of the stations, with more or less results depending on the available hours of day light. Due to the high variability of the data observable during these partial cycle campaigns, it was considered that, for better knowledge of the circulation in the estuary, it would be important to study complete tidal cycles. Therefore, one full tidal cycle campaign (13 h) was made in stns. #6 and #8, in June 2019, with measurements taken every 30 min. For these complete cycle campaigns, the collection of the data was not made exactly in stn. #6, but closer to the navigation channel, to avoid land interference (exact coordinates - 38˚ 31' 3.6" N 008˚ 53' 55.5" W). During these 2 campaigns, the boat was anchored during the entire period and the measurements were taken, every 3 m depth in stn. #6 and every 4 m in stn. #8. Stn. #7 was not considered for this study because, the results obtained up to then with the monthly campaigns, lead to the conclusion that this area is highly dynamic, with high instability, difficult to characterize with the monitorization of only one full tidal cycle. Additionally, stn. #7 is located in the middle of the main navigation channel so it would be difficult to stay there for 13 h.

2.3 Data and Methodologies

In situ observations were carried out using: i) a NXIC (Non-eXternal Inductive Conductivity) CTD for conductivity, temperature and depth, from the former Falmouth Scientific Inc. – FSI; ii) an EXO2 Multiparameter Sonde (from YSI) for water quality analysis; iii) a Doppler Current Sensor (4100, from Aanderaa, Norway) for current intensity and direction measurements. In order to make the reading easier, from now on, the multiparameter sonde is referred as MS and the current meter sensor as CS.

The CTD and the CS were used in all sampling campaigns, except in OCT 2018 (CS) and in DEC 2018 (CTD and CS) when unforeseen events prevented their use. Therefore, there is no data from these instruments during those months, as described in Table 2.2.

From the campaign of the 26th of June onwards, there is no record of CTD data because the instrument had an anomaly. Also, in August 2019, due to logistic constraints, the research boat needed to sample stn. #7 was not available, thus only stn. #6 was monitored (Table 2.2). For the full tidal cycle campaigns, it was only used the CS.

It should be mentioned that in stns. #7 and #8, the research boat never anchored and the profiles were always collected with the boat drifting whereas the collections in stn. #6 were made with the boat moored at a pontoon.

Table 2.2. Sampling dates and instruments used in each one of the stations (#6, #7 and #8). N represents the total number of profiles collected during the whole sampling period. LT – Local Time, CS – Current Meter Sensor, MS – Multiparameter Sonde, Sets - cycles of measurements made.

	Stations with data		
Sampling Dates	CTD	CS	MS
06 SEP 2018	#6, #7	#6, #7	#6, #7
03 OCT 2018	#6, #7	-	#6, #7
08 NOV 2018 Partial Tidal Cycle	#7 (4 sets), #8 (4 sets)	#7 (4 sets), #8 (4 sets)	#7, #8
16 NOV 2018 Partial Tidal Cycle	#7 (4 sets), #8 (4 sets)	#7 (4 sets), #8 (4 sets)	-
19 DEC 2018	-	-	#6, #7
16 JAN 2019	#6, #7	#6, #7	#6, #7
14 FEV 2019	#6, #7	#6, #7	#6, #7
28 MAR 2019	#6, #7	#6, #7	#6, #7
12 ABR 2019	#6, #7	#6, #7	#6, #7
24 MAY 2019	#6, #7	#6, #7	#6, #7
18 JUN 2019 Partial Tidal Cycle	#7 (5 sets), #8 (3 sets)	#7 (5 sets), #8 (3 sets)	#7, #8
[1] 19 JUN 2019 - 20 JUN 2019 Full Tidal Cycle		#8	
[2] 20 JUN 2019 - 21 JUN 2019 Full Tidal Cycle		#6	
26 JUN 2019 Partial Tidal Cycle	-	#7 (7 sets), #8 (7 sets)	#7, #8
10 JUL 2019	-	#6, #7	-
09 AUG 2019	-	#6	#6
23 SEP 2019	-	#6, #7	#6, #7
N	38	55	25

[1] 19 JUN 2019 15:30 LT – 20 JUN 2019 05:00 LT; [2] 20 JUN 2019 19:00 LT – 21 JUN 2019 08:30 LT.

2.3.1 CTD data

The CTD was kept at the surface of the water column for sensor stabilization during 2 min, before data for each profile were recorded. Only downcast data were used. Also, the data recorded in the first meter of the water column were discarded due to the dimensions of the CTD.

A relatively recent CTD calibration indicated that the following correction should be applied to the conductivity measurements:

$$y = 0.0699247975 + 0.997943785x \quad [2.1]$$

where x is the conductivity measured by the instrument and y the respective value after calibration. The difference between the uncalibrated conductivities and the respective calibrated values was of ≈ 0.02 mmho/cm for the profiles of every campaign (blue and orange profiles, respectively, in Figure 2.2). Equation 2.1 was applied to the whole set of conductivity measurements.

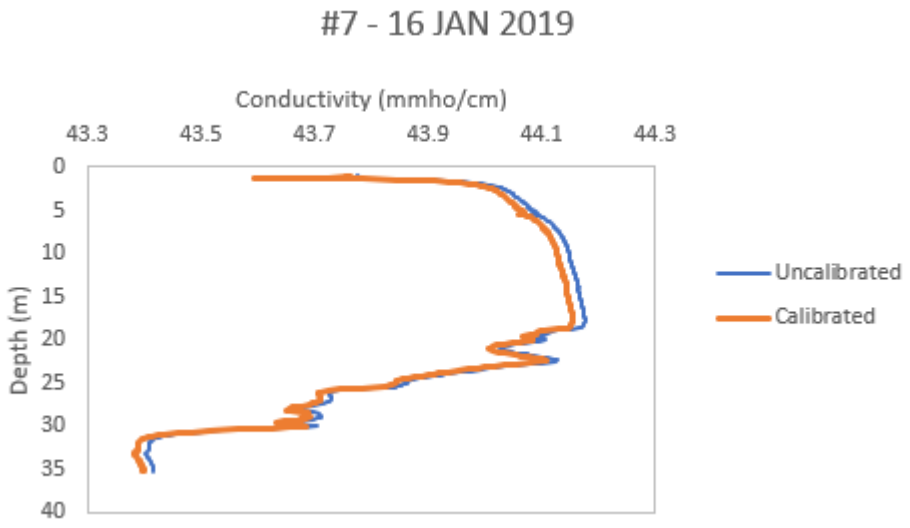

Figure 2.2. Conductivity values obtained with the CTD in JAN'19 campaign before (blue) and after the calibration (orange).

After correcting the conductivity, the practical salinity (PSS-78) was calculated using the Gibbs-SeaWater (GSW) Oceanographic Toolbox, software package of the Thermodynamic Equation of Sea-Water 2010 (TEOS-10), with the function gsw_SP_from_C (Practical Salinity from conductivity) using MATLAB software (McDougall and Barker, 2011).

Using the values of water temperature (T) and salinity (S), the density anomaly was also computed using the same toolbox, with the function gws_sigma0. This function calculates the density anomaly (σ_t, kg/m^3) with reference to the surface (0 dbar), according to equation 2.2:

$$\sigma_t = \rho_{S,T,0} - 1000 \qquad [2.2]$$

where ρ is the seawater density.

Additionally, the CTD allowed registering data of turbidity and of chlorophyll *a* concentrations, which, in this last case, were automatically derived from the CTD fluorescence readings (referred simply as fluorescence from this point forward).

After the data were treated, profiles of temperature, salinity, σ_t, turbidity, and fluorescence were plotted for the whole set of stations. Also, a T/S scatter diagram was plotted considering all data collected.

2.3.2 Current Meter Sensor data

The Current Sensor (CS) enables to gather several parameters at each measurement depth: i) intensity and direction of the current; ii) temperature; and iii) pressure. The depth of the water column at stns. #6, #7 and #8, was approximately 8, 38 and 20 m, respectively. In stns. #6, #7 and

#8, the measurements were made every 2, 5 and 4 m in the water column, respectively. At each station, the sensor was placed in the water and it was left stabilizing at every depth for about 2 min. The instrument measured the parameters cyclically and when the values appeared stabilized, a measurement cycle was chosen as the representative one.

Regarding the processing of the CS data, the first step was the computation of the pressure values (p in kPa) into depth values (D in m) using equation 2.3.

$$D = (p - 100)/10 \qquad [2.3]$$

Then, a correction to the current direction was applied. These data were collected in degrees relative to the magnetic north and needed to be transformed into degrees relative to the geographic north, by subtracting or adding the earth's magnetic declination to the first value. At the time of the measurements, the magnetic declination of the stations was the following (according to http://www.magnetic-declination.com):

- Stn. #6: 2˚ 5' W
- Stn. #7: 2˚ 6' W
- Stn. #8: 2˚ 5' W

Since these values were relative to West, they represented a negative declination and, therefore, once they have been transformed into degrees, they were subtracted to the ones collected with the current sensor, to obtain the geographic direction of the current.

The temperature values obtained by the CS, were not used in this chapter because they were much higher than the temperatures measured with the CTD and with the MS. The values obtained with these two instruments were close to each other and, as the instruments were calibrated in a recent past, it was assumed that they presented the most reliable values. Figure 2.3 presents an example of the data collected in stn. #6 and #7, during the 14 FEB 2019 campaign, to show the discrepancy of the temperature values obtained with the 3 instruments.

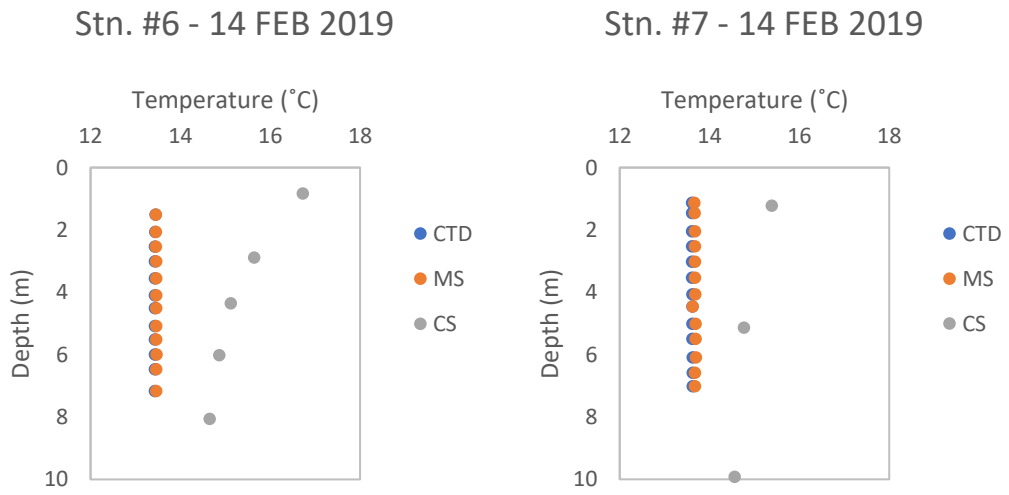

Figure 2.3. Temperature values obtained with the CTD, the MS and the CS in stns. #6 and #7, during the 14 FEB 2019 campaign.

The data were then arranged in polar vector graphics to characterize the currents according to its direction and intensity along the water column. The graphics were drawn with the software Grapher 14.

2.4 Results

2.4.1 Variability along the tidal cycle

2.4.1.1 Partial Cycle Campaigns

In this study, concerning the partial cycle campaigns, a total of 24 CTD profiles were acquired (Figure 2.5). For each profile, there is a time reference (Local Time, LT) relative to high water (HW). Every set of measurements is represented by "C" (partial **C**ycle measurement) followed by the number of the set.

It was possible to see that there were small variations of each parameter along the water column and throughout the tidal cycle (Figure 2.5). However, some profiles showed some unexpected values. As for temperature, most observations varied around 16 ºC, except in stn. #8, during the June campaign, when the temperature varied from 15 ºC to 19 ºC.

Regarding the salinity, almost all the profiles varied around 36.0. However, lower values, in about 3.5 units (*i.e.* 32.5) were observed at the surface in the 4th set (C4) of the campaign conducted in stn. #8 on the 16th November. Consequently, a similar pattern was observed in the σ_t profiles (Figure 2.5).

Most of the turbidity profiles showed values ranging between 0 and 10 FTU (Formazin Turbidity Units). Higher values, up to 25 FTU were observed during the 08 NOV 2018 and 18 JUN 2019 campaigns. Values of 13 and 24 FTU can be verified and they seem very high for the natural behavior of the estuary. The fluorescence profiles showed values mostly between 0 and 2 and with no relevant variations in depth and throughout the campaigns (Figure 2.5).

Although the general outlook of these profiles is of a regular behavior with small variations along the water column, in the campaign of June, a variation in the temperature, salinity and σ_t profiles (density anomaly) around 10 m depth was observed. This is shown in Figure 2.4, a partial zoom of Figure 2.5. This oscillation around 10 m was perceptible throughout that campaign in both stations but had a bigger pronunciation in the first and third set of measurements of stns. #7 and #8, respectively.

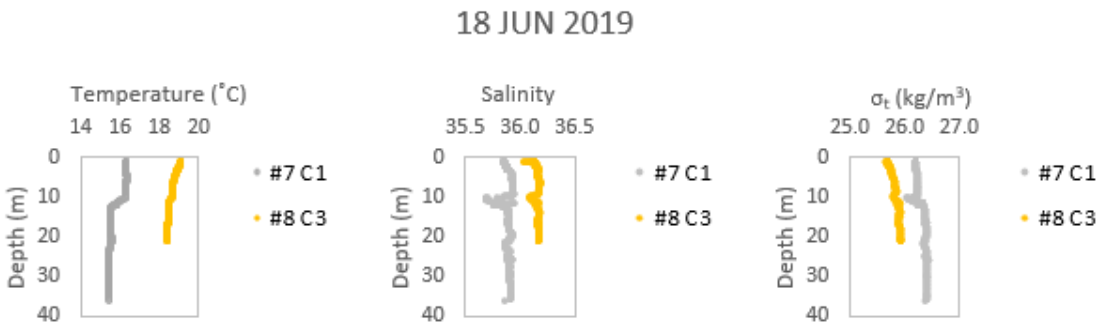

Figure 2.4. Temperature, salinity and σ_t profiles obtained in the first and third set of measurements at stn. #7 and #8, respectively, during the 18 June campaign.

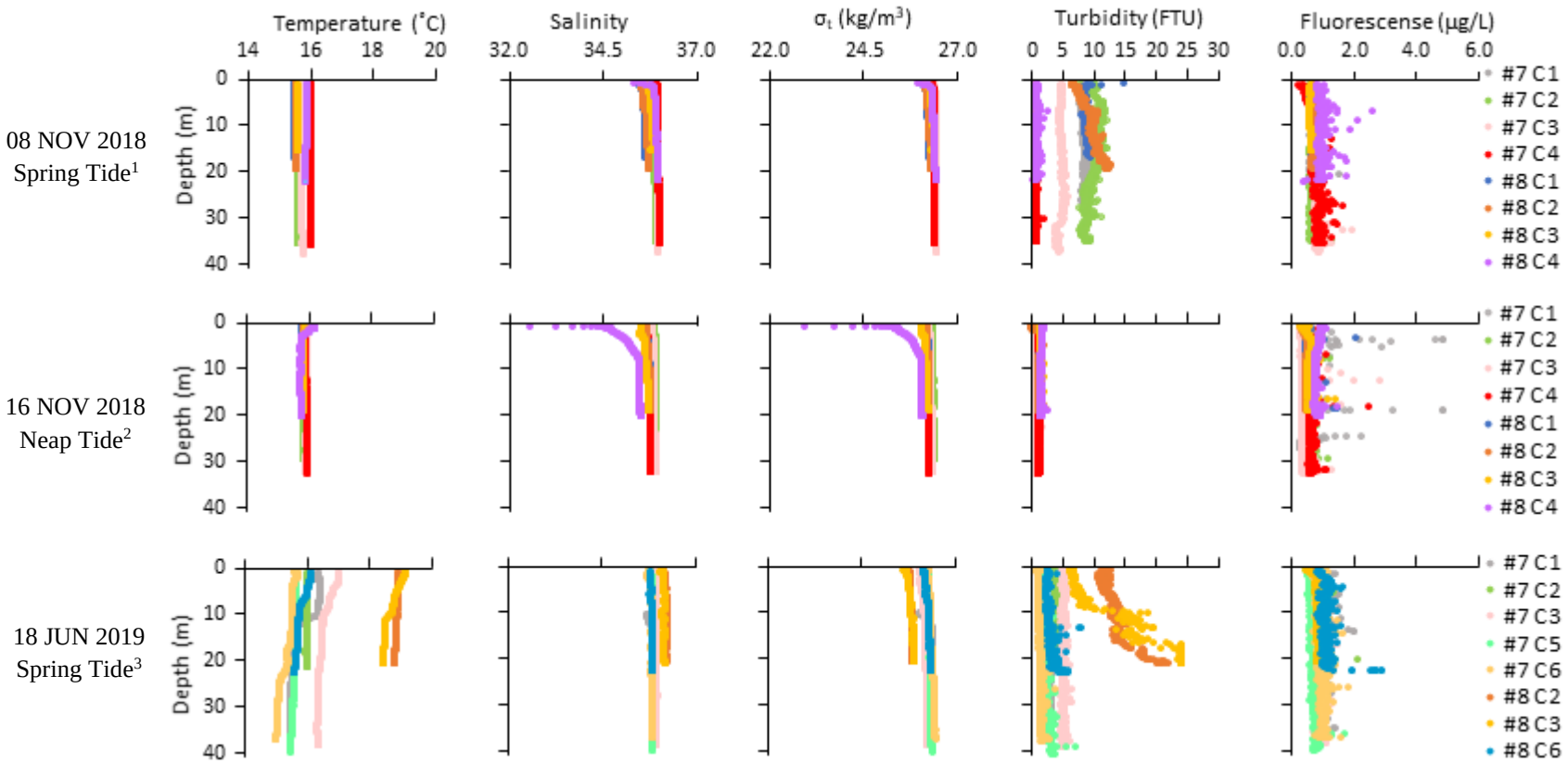

[1]Stn. #7: C1 – HW+5.0; C2 – HW+6.5; C3 – HW-3.3; C4 – HW+0.1. Stn. #8: C1 – HW+5.9; C2–HW-4.5; C3 – HW-2.5; C4 – HW+0.8.

[2]Stn. #7: C1 – HW+5.8; C2 – HW-6.3; C3 – HW-4.2; C4 – HW-0.3. Stn. #8: C1 – HW+6.1; C2–HW-5.4; C3 – HW-1.5; C4 – HW+0.2.

[3]Stn. #7: C1 – HW+4.0; C2 – HW+4.7; C3 – HW-4; C5 – HW-2.0; C6 – HW-0.1. Stn. #8: C2 – HW+5.7; C3–HW-4.9 h; C6 – HW+0.8.

Figure 2.5. Temperature (ºC), salinity, σ_t (kg/m³), turbidity (FTU) and fluorescence (µg/L) profiles obtained at stns. #7 and #8 during the different partial cycle campaigns using the CTD (C – partial cycle measurement, HW – high water).

The CS data obtained throughout the partial tidal cycle campaigns complemented the data obtained with the CTD. It is challenging to understand how the current intensity varies in depth, as there was no pattern in the variation of the current intensity along the water column throughout the tidal cycle (Figure 2.6 and Figure 2.7). Likewise, there was no constant agreement between the direction of the current at the surface and at the lowest level along the tidal cycle (showed in blue and green arrows, respectively, in Figure 2.6 and 2.7). This inconsistent behavior appeared to be similar in stn. # 7 and stn. #8, as a characteristic pattern was not observed at any of the stations. Between spring and neap tides, it was evident that higher current intensity values were observed in the campaigns conducted during spring tides, as would be expected. The June campaigns appeared to show a concordant behavior in terms of current intensity between some sampling points. However, these campaigns included more measurements throughout the tidal cycle than the campaigns conducted in November. It can also be seen that the direction of the current most often did not coincide with the tidal regime, contrary to the expectation.

This inconstant behavior of the current direction and intensity throughout time, could be justified by the small number of measurements that were done at each station throughout the tidal cycle. Also, a big amount of those measurements was made during slack water, which does not give much information about the circulation regime in the region.

.

2.4.1.2 Complete Cycle Campaigns

To achieve a more accurate characterization of the estuary circulation, an extra campaign was performed to fully cover the tidal cycle with measurements every 30 min, in stns. #6 and #8 (Figure 2.8).

For both stations, there was a general agreement between the direction at the surface current and the lowest level (blue and green arrows, respectively, in Figure 2.8), contrary to what was previously described in the analysis of the partial cycle campaigns. Additionally, the direction of the current coincided with the tide throughout the tidal cycle. There was a clear tendency for a current intensity decreasing with depth, as there were stronger currents at the surface. More intense currents were observed during the ebb than during the flood. As expected, during slack water, the currents reached minimum values in both stations (Figure 2.8).

It is also possible to see that the two stations responded in different timings to the changing of the tide (Figure 2.8). Also, in high water both stations seemed to show a direction of the current towards the center of the estuary. The opposite appeared to happen in low water, being the direction of the current towards land (except at the surface of stn. #8).

These data seem to indicate that the water flows in and out of the estuary through both channels, showing greater intensity in the South channel (the deepest one). Therefore, it is suggested that the southern channel is the most important in the exiting and at the entrance of water in the estuary (Figure 2.9). In Figure 2.9, the average current intensity obtained during flood is represented with a green arrow, and the obtained during ebb, is shown with a red arrow.

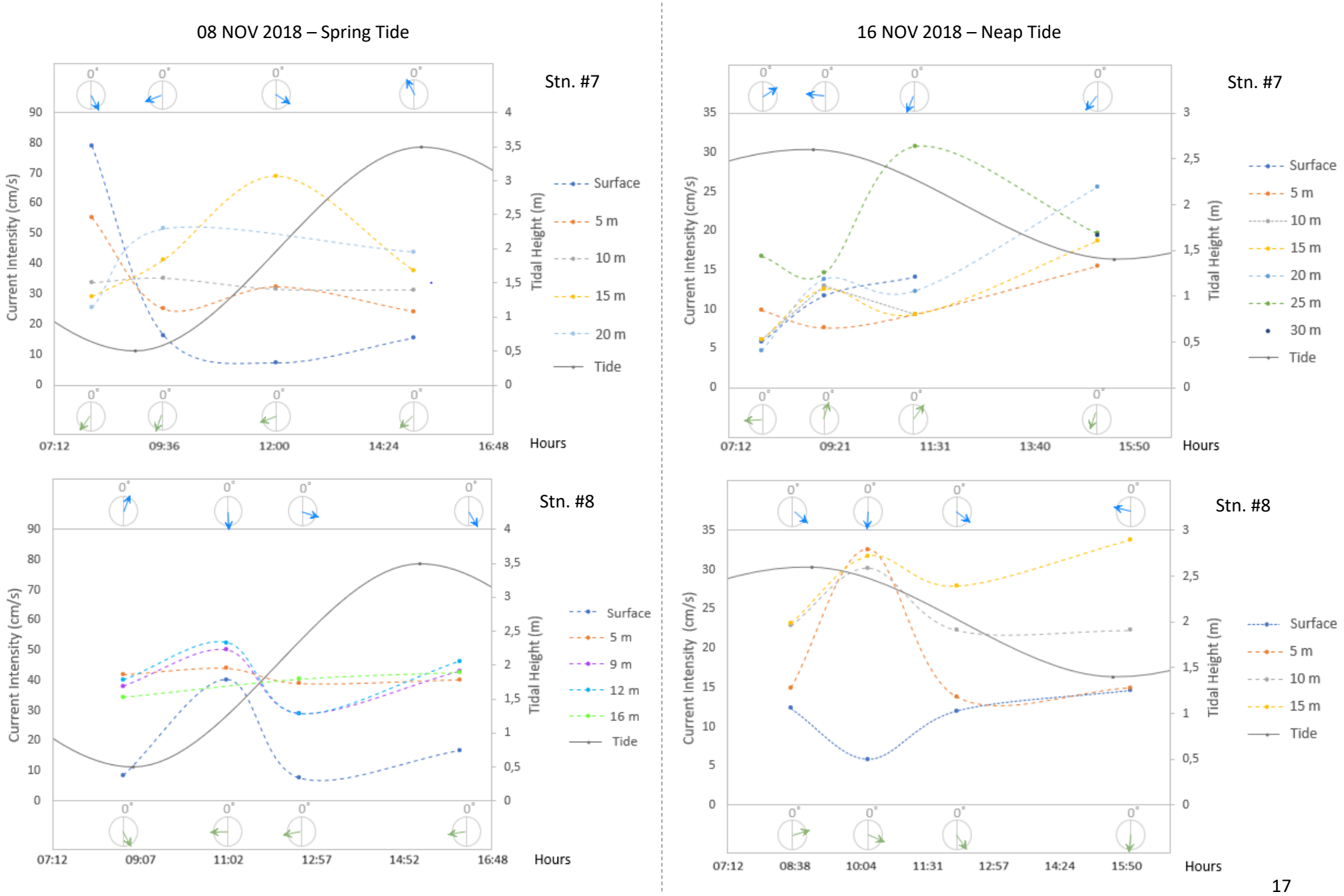

Figure 2.6. Intensity of the current at every depth level, in stns. #7 and #8, along the partial tidal cycle campaigns conducted in November 2018. Direction of the current at the surface and at the deepest level represented in blue and green arrows, respectively.

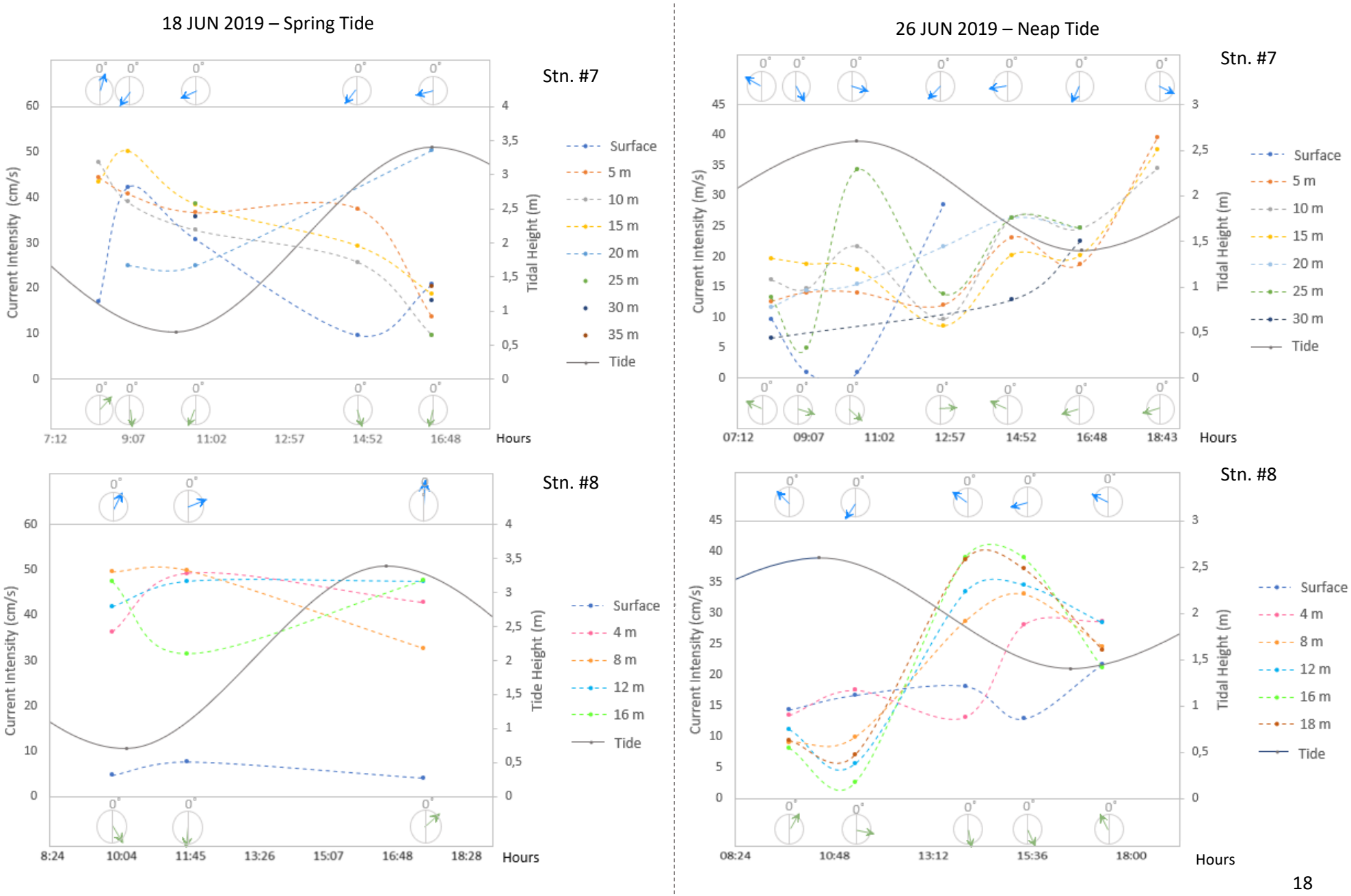

Figure 2.7. Intensity of the current at every depth level, in stns. #7 and #8, along the partial tidal cycle campaigns conducted in June 2019. Direction of the current at the surface and at the deepest level represented in blue and green arrows, respectively.

Stn. #8
19-20 JUN 2019

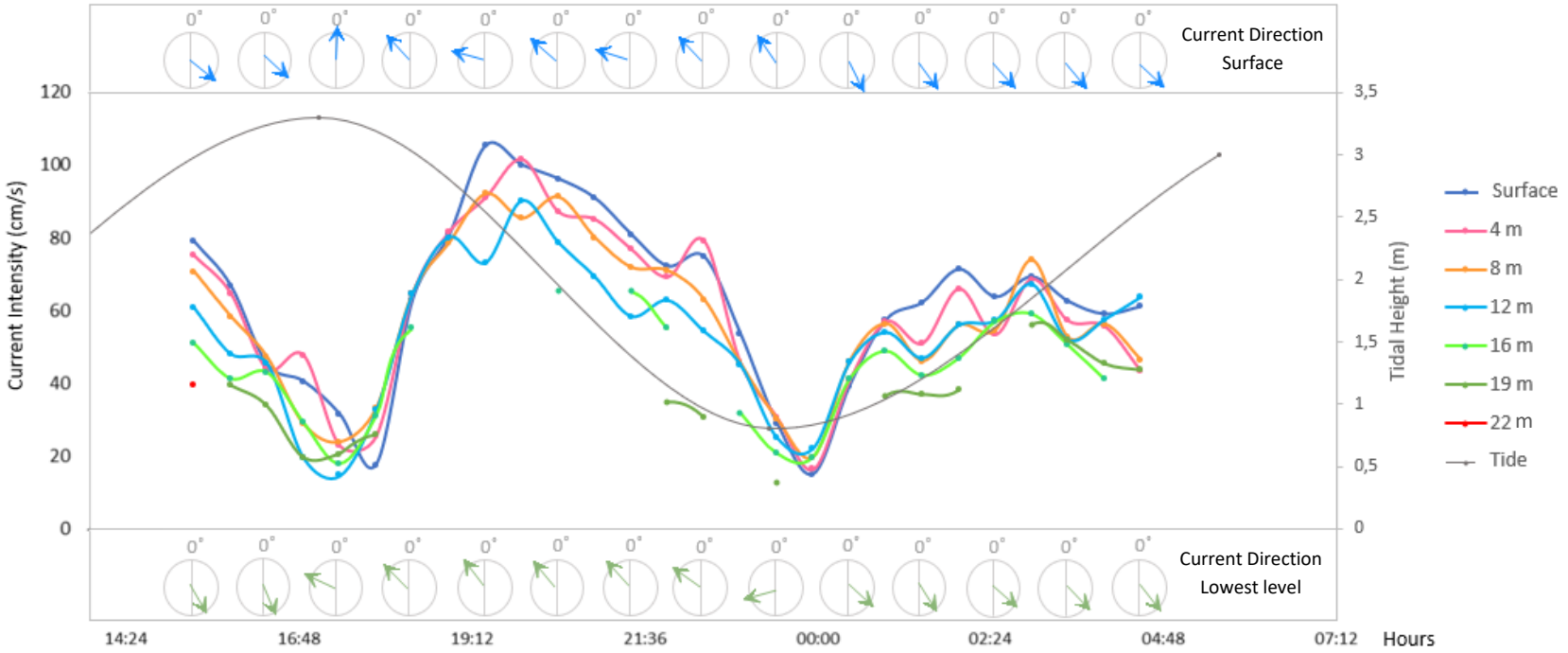

Stn. #6
20-21 JUN 2019

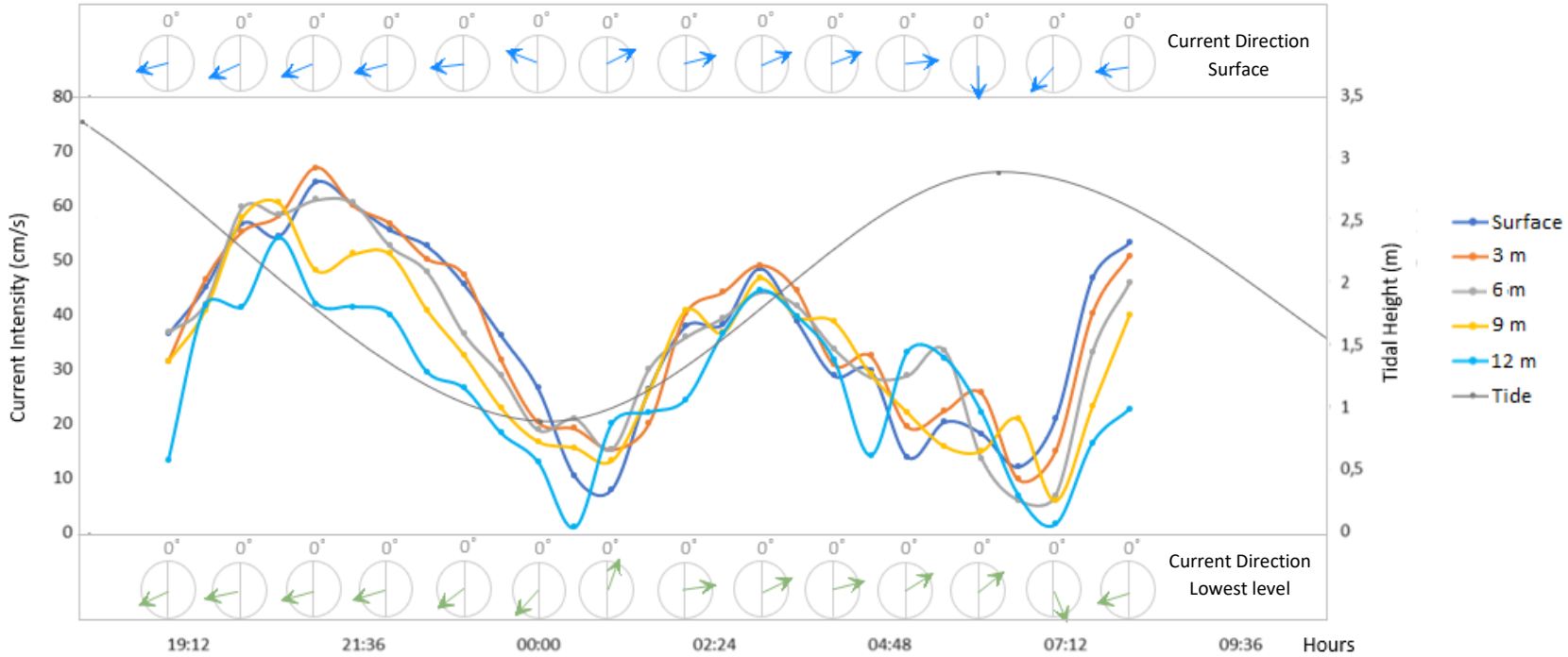

Figure 2.8. Intensity of the current at every depth level, in stns. #6 and #8, during the campaigns that completely covered the tidal cycle (June 2019). Direction of the current at the surface and at the deepest level represented in blue and green arrows, respectively.

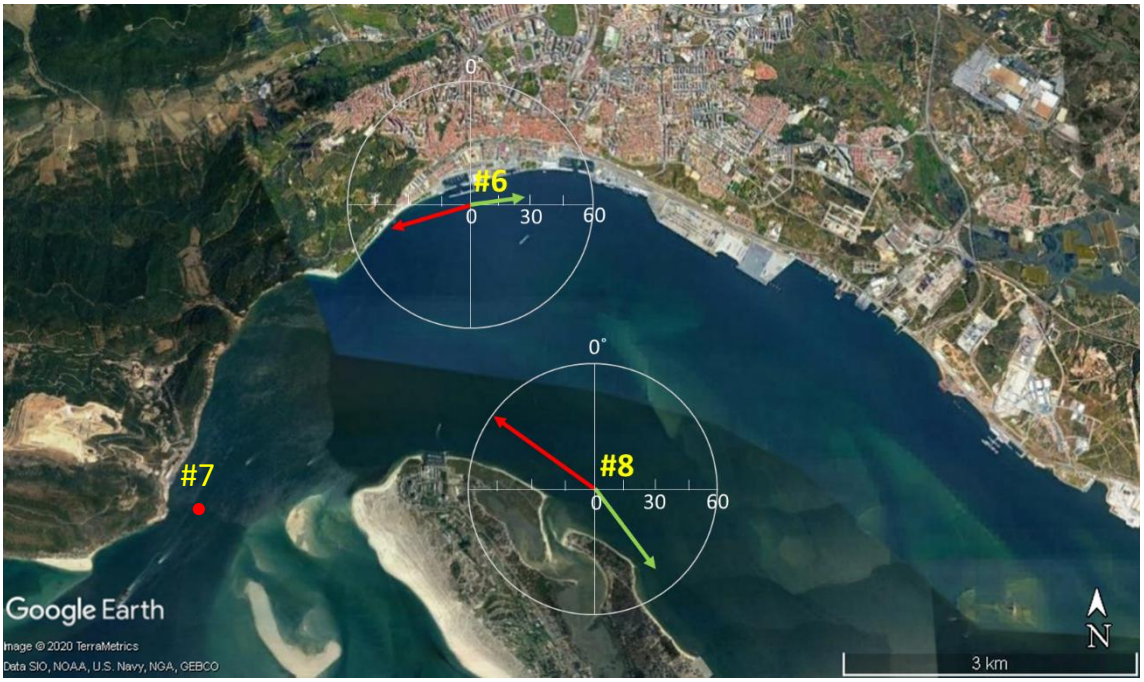

Figure 2.9. Average intensity and direction of the current obtained using all the data from the water column, at stns. #6 and #8 throughout the cycle campaign, during ebb (red arrow) and during flood (green arrow).

2.4.2 Seasonal Variability

At the end of the sampling period, it was possible to obtain the values of the analyzed parameters, averaged by season, considering the estuary as a whole, in depth and space (Table 2.3). Also, the mean values considering the entire estuary and the whole sampling period were calculated (entire period in Table 2.3). It is important to note that during autumn and spring there were more observations due to the partial cycle campaigns. It is possible to observe that the temperature presented the clearer seasonal behavior, showing a thermal amplitude of ≈ 5 ºC (Table 2.3). Sigma-t varied seasonally as expected (lower values during summer than in the winter months) and had an average of 26.2 kg/m^3 throughout the sampling period. As it would be predictable, salinity was higher in summer than in winter but, given the range of values observed throughout the year, this seasonal variability was low. Higher turbidity values were observed during the transition months, being the highest the ones from spring measurements. Similarly, spring presented the highest average values of fluorescence, being difficult to assume any seasonal behavior of this parameter along the rest the year (Table 2.3).

Table 2.3. Mean values obtained for each season and for the whole sampling period, considering the average of the 8 stations and of the water column for the analyzed parameters.

	Temperature (˚C)	**Salinity**	**σ_t (kg/m^3)**	**Turbidity (FTU)**	**Fluorescence (µg/L)**
Entire period	16.0	35.8	26.2	3.7	0.9
Summer	19.0	35.9	25.6	1.7	0.8
Autumn	17.3	35.8	25.9	3.3	0.7
Winter	13.8	35.7	26.7	1.0	0.8
Spring	16.2	35.9	26.2	5.1	1.4

To accomplish a detailed analysis of the seasonal variability of each parameter according to the sampling station, Figure 2.10 presents the whole set of temperature profiles, where in red are the profiles obtained during the summer, in orange the profiles obtained in autumn, in blue the profiles obtained during winter and in green the profiles collected during spring.

A clear thermal seasonal pattern is observable in all stations (Figure 2.10). The lowest temperature values were obtained in winter (blue profiles) and the highest values obtained in summer (red profiles), as expected. However, in stns. #6 and #7, the profiles with the highest temperatures were obtained in October 2018. October is frequently a very hot month and, when the campaign took place, this region was under the influence of summer.

After an analysis of each season in detail, it is interesting to describe some variations:

i) In stn. #7 during summer (red profile in Figure 2.10), it was possible to see a practically constant decrease of the temperature in depth. This profile was the only one that showed this behavior.

ii) The profiles obtained during fall (orange profiles in Figure 2.10), suggested that the water column was very well mixed during that time of the year, both in stn. #7 as in stn. #8.

iii) During winter, it was also possible to observe a homogeneous water column in stn. #6 and stn. #7. However, in stn. #7, the profile obtained in January, suggested that the water column was well-mixed only until 20 m depth, with a temperature decrease of almost 1 ºC until the bottom, at ≈ 30 m (Figure 2.10).

iv) In all the sampling stations, the profiles obtained during spring (green profiles in Figure 2.10) were the ones that showed the greatest range of values over the tidal cycle (comparing with the autumn profiles) and over time. In depth, some temperature variations in the first meters were noticeable.

v) Of the three stations, it was stn. #6 that tended to have the greatest mixture of the water column over time. However, is the station with the lowest water column.

Annex I shows in detail, the temperature profiles obtained in each campaign. It is interesting to note that stn. #6 had lower temperatures than stn. #7 in the winter months but higher values in summer and transition seasons.

The salinity profiles obtained with the CTD for the same 3 stations are shown in Figure 2.11. As in Figure 2.10, the color code was kept in order to facilitate the study of the seasonality of this parameter. Salinity data from stn. #6 seem to indicate the influence of seasonality but, as there is no consistency between stations, it is difficult to suggest any clear seasonal effect (Figure 2.11). From Table 2.3 it was possible to observe a slight seasonal behavior of this parameter when it was considered the average of the 3 stations, but, analyzing each station separately, it becomes more difficult to see that variability.

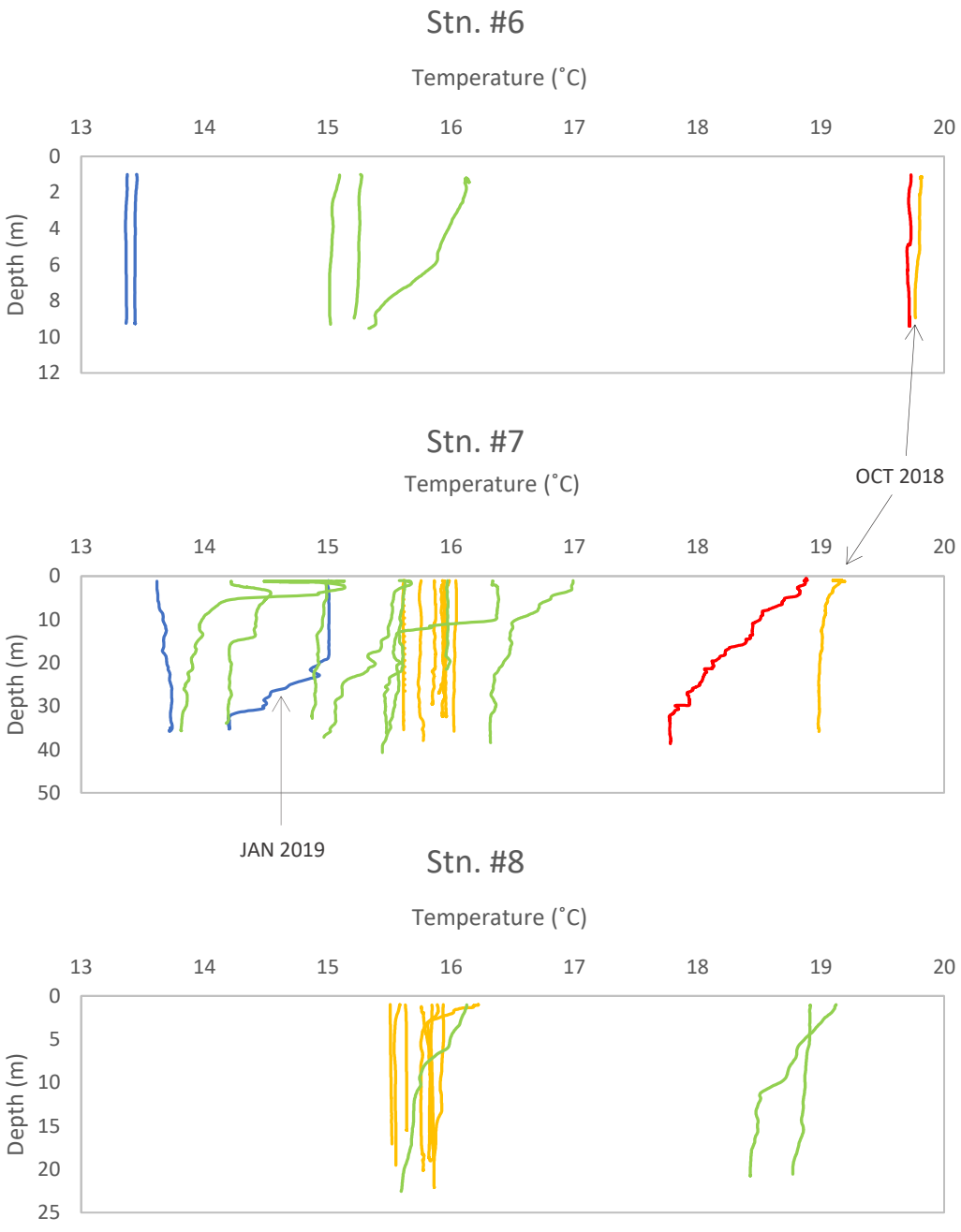

Figure 2.10. Temperature profiles obtained in CTD stns. #6, #7 and #8 (summer campaigns in red, autumn campaigns in orange, winter campaigns in blue and spring campaigns in green).

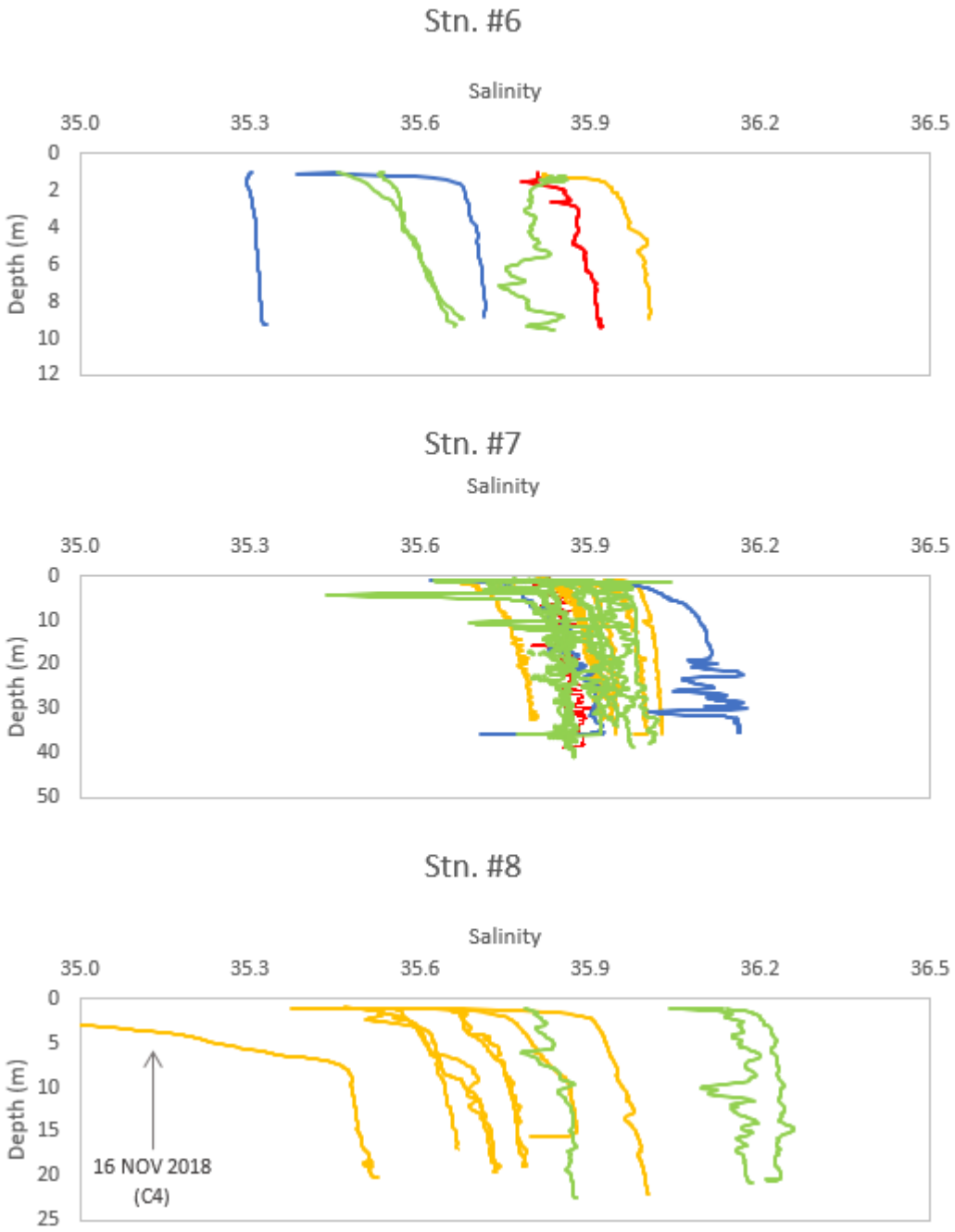

Figure 2.11. Salinity profiles obtained in CTD stns. #6, #7 and #8 (summer campaigns in red, autumn campaigns in orange, winter campaigns in blue and spring campaigns in green). C4 – 4th partial cycle measurement

In stn. #7, the salinities were in the interval 35.5-36.2, while in the other stations there was a greater variation of values. Relevant variations of salinity along the water column were not observed at all stations, which may suggest that the water columns were well mixed during sampling. However, an increase in the salinity was seen at the surface in several profiles, with lower values in the first meters of the water column. This was especially verified in the profiles obtained during winter and autumn. Noteworthy, is the profile C4 obtained in stn. #8 in the campaign of 16 NOV (orange profile with lower values in Figure 2.10), where the surface salinity

was 33.2, reaching a value of 35.0 at ≈ 3 m depth. This profile can be seen in its entirety in Annex II. It is interesting to highlight the tendency for the profiles obtained during ebb (blue profiles in Figure 2.12) to yield the highest variations of salinity at the surface, compared to the profiles obtained during flood (red profiles in Figure 2.12). Once again, in Figure 2.12, the bigger salinity variation was verified on 16 NOV (ebb profile), in the last measurement set (C4), where the first 10 m of the water column show an increase of the salinity.

In the hot months (September and October 2018 and May 2019), the salinity values in stn. #6 were very similar to those observed in stn. #7, for the respective campaigns. During the remaining months, salinities in stn. #6 were 0.5 lower than in stn. #7, for the same campaigns (Annex III). Since the salinity in stn. #7 did not change significantly over time, stn. #6 presented a higher sensitivity to seasonal variability, as described earlier.

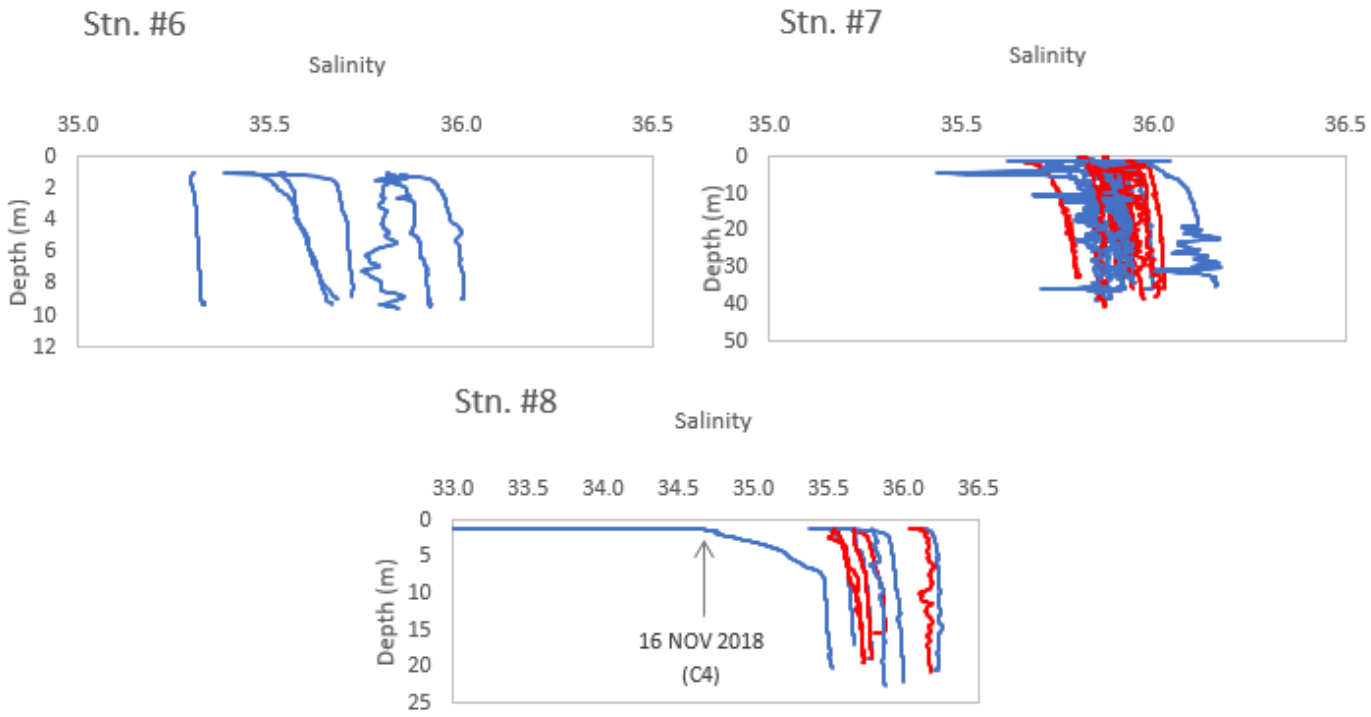

Figure 2.12. Salinity profiles obtain in CTD stns. #6, #7 and #8 related with the tidal regime (flood in red and ebb in blue). C4 – 4th partial cycle measurement

A T/S scatter diagram of the whole set of stations is presented in Figure 2.13, where the color code was kept according the season of the year as before. These results complement well the ones presented previously, as it is clearly shown that the seasonal variability of the temperature is framed in practically unchanging salinity values, throughout the whole year.

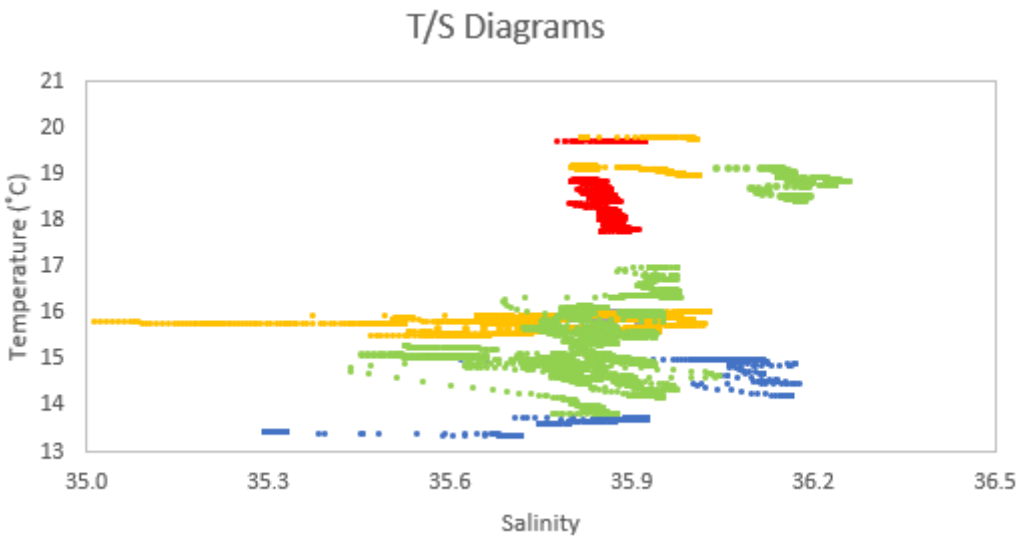

Figure 2.13. T/S scatter diagrams of stns.#6, #7 and #8 (summer campaigns in red, autumn campaigns in orange, winter campaigns in blue and spring campaigns in green).

All the sigma-t values ranged between 25.1 and ≈ 26.9 kg/m^3 (Figure 2.14). Sigma-t values were similar in the three stations. However, a seasonal pattern of sigma-t and, therefore, of the water density, was observed, with denser waters in winter and lighter waters in summer (Figure 2.14; summer campaigns in red, autumn campaigns in orange, winter campaigns in blue and spring campaigns in green). No relevant vertical variation of the sigma-t values was observed. An exception occurred in stn. #7 (SEP 2018), where sigma-t increased with depth throughout the entire water column. This increase is a result of the temperature decrease observed in stn. #7 (red profile in Figure 2.10), which shows a slight stratification in the water column.

Turbidity values collected with the CTD were also analyzed and did not differ significantly in the three stations (Figure 2.15). The values tended to vary between 0.0 and ≈ 7.0 FTU throughout time. However, the profiles collected in 08 NOV (stns. #7 and #8) and 18 JUN (stn. #8), showed values reaching to 13.0 and 24.0 FTU, respectively, variation that appeared to be atypical for the estuary. Also, there was no meaningful variation of the turbidity along the water column during the sampling period, only in the previously mentioned profiles. When the different stations were compared according to the sampling day, it could be verified that, for the same campaign, stn. #6 had slightly higher values of turbidity than stn. #7 (see Annex IV).

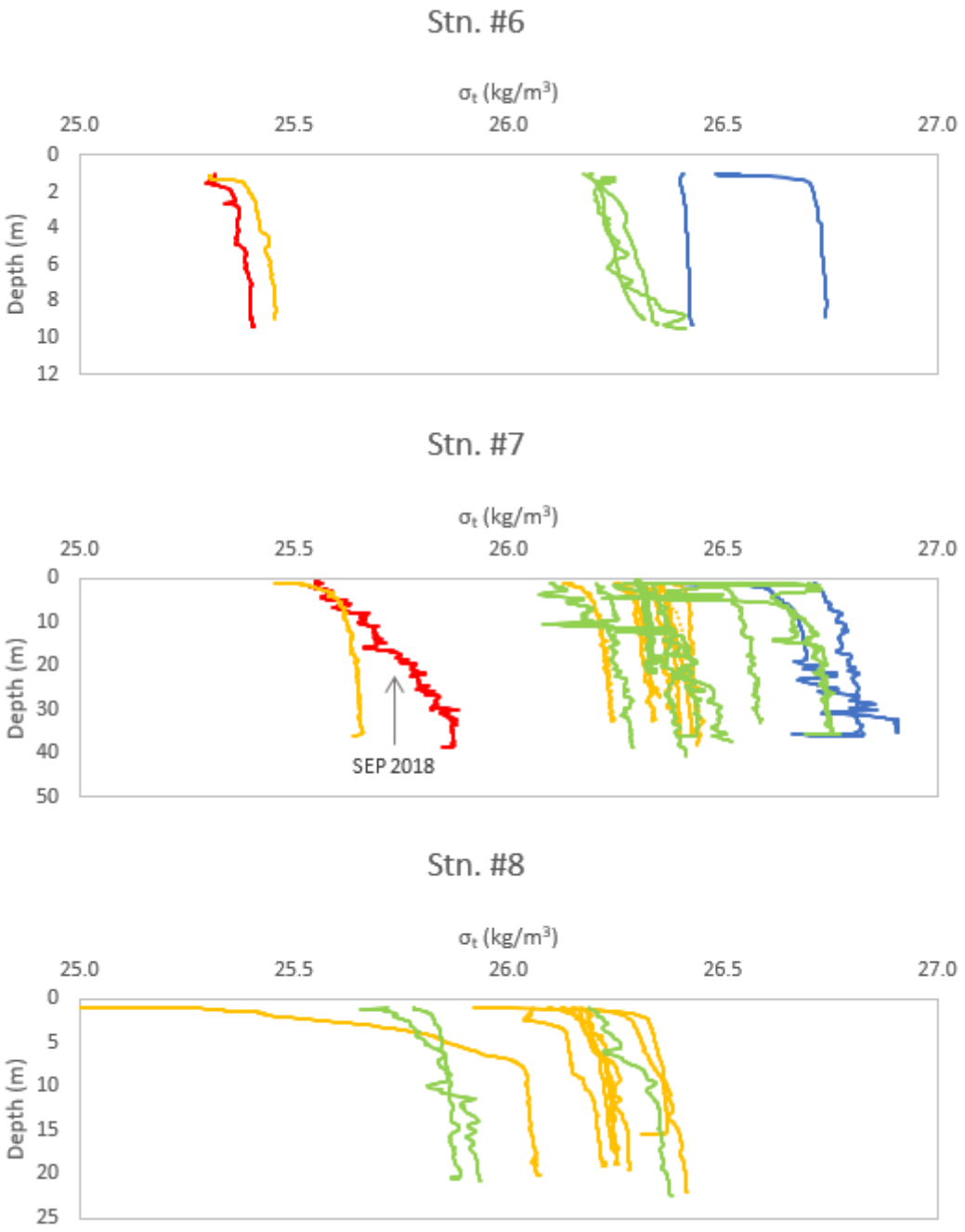

Figure 2.14. Sigma-t profiles obtained in CTD stns. #6, #7 and #8 (summer campaigns in red, autumn campaigns in orange, winter campaigns in blue and spring campaigns in green).

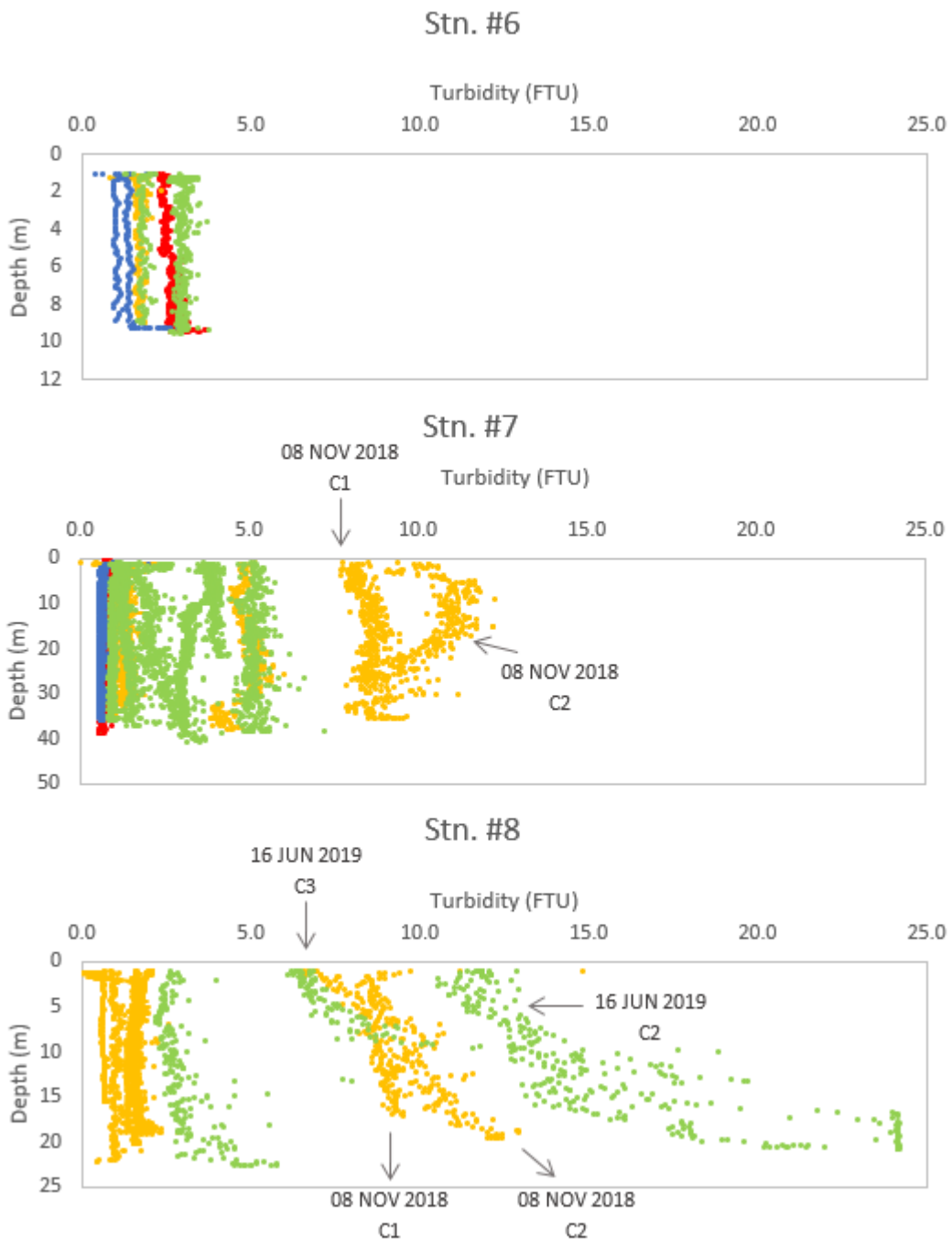

Figure 2.15. Turbidity profiles obtained in CTD stns. #6, #7 and #8 (summer campaigns in red, autumn campaigns in orange, winter campaigns in blue and spring campaigns in green). C - partial cycle measurement.

The data of fluorescence obtained with the CTD (chlorophyll concentration measured by fluorescence) were also analyzed and the results are presented in Figure 2.16. In general terms, the fluorescence data collected seem to indicate no evidence of large variations in the biomass of phytoplankton communities, both vertically (in the water column) and spatially (across the three stations). The values did not exceed 5.0 µg/L throughout the sampling period and most of the profiles were in the range 0.0-3.0 µg/L, without showing a remarkable seasonal variability. However, some profiles showed circumstantial variations with values higher than 3.0 µg/L, being

the profile obtained in stn. #6 in MAR 2019, the one with the increase of fluorescence of higher relevancy (for further detail, see Annex V). In fact, in stn. #6, the profiles appeared to show a maximum of fluorescence between 4 and 6 m (except in September 2018, red profile in Figure 2.16). This behavior could indicate that stn. #6 may show a Deep Chlorophyll Maximum (DCM) at ≈ 5 m. This maximum was not visible in the other stations, probably due to the poor stratification of the estuary waters.

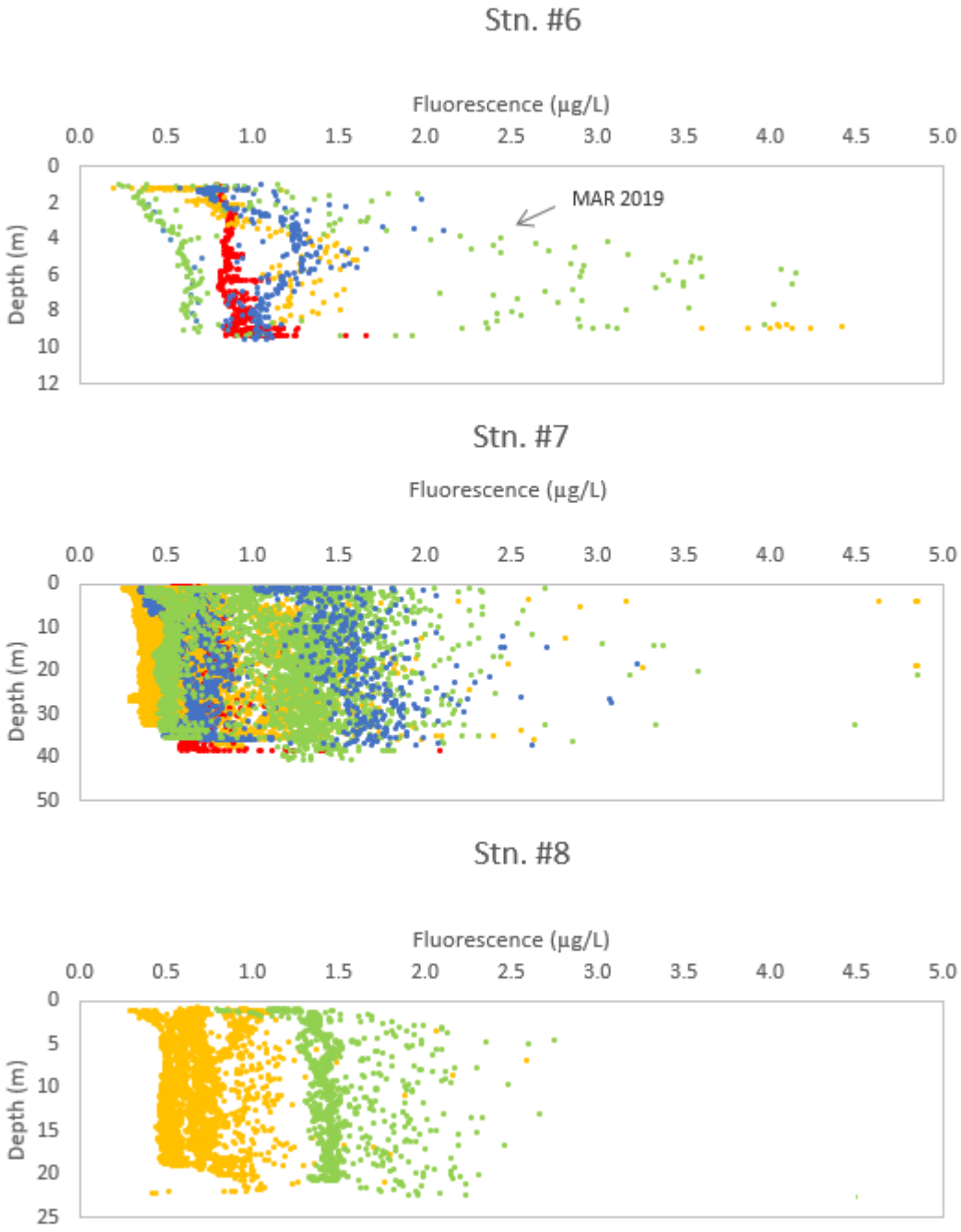

Figure 2.16. Fluorescence profiles obtained in CTD stns. #6, #7 and #8 (summer campaigns in red, autumn campaigns in orange, winter campaigns in blue, spring campaigns in green).

The data collected with the current sensor (CS) during the monthly campaigns were processed in a similar way as the data collected in the cycle campaigns (Stn. #6 - Figure 2.17 and Stn. #8 – Figure 2.18). The direction and the intensity of the current is represented, as well as the time of the measurements relative to high water (HW). The measurements were conducted within the second or third hour after high water in stn. #6, or during slack water in stn. #7.

The currents were consistent with the tidal regime in stn. #6 (see Figure 2.17). During ebb (*e.g.*: 16 JAN 2019, HW+1.6), currents with a strong west component were observed as a sign of water exiting the estuary. However, it is difficult to draw any conclusions regarding the behavior of the current intensity with depth, as there was no similar behavior between campaigns. In stn. #7, there is no evidence of any kind of pattern in the intensity and direction of the current throughout the sampling period or along the water column (Figure 2.18).

Stn. #6

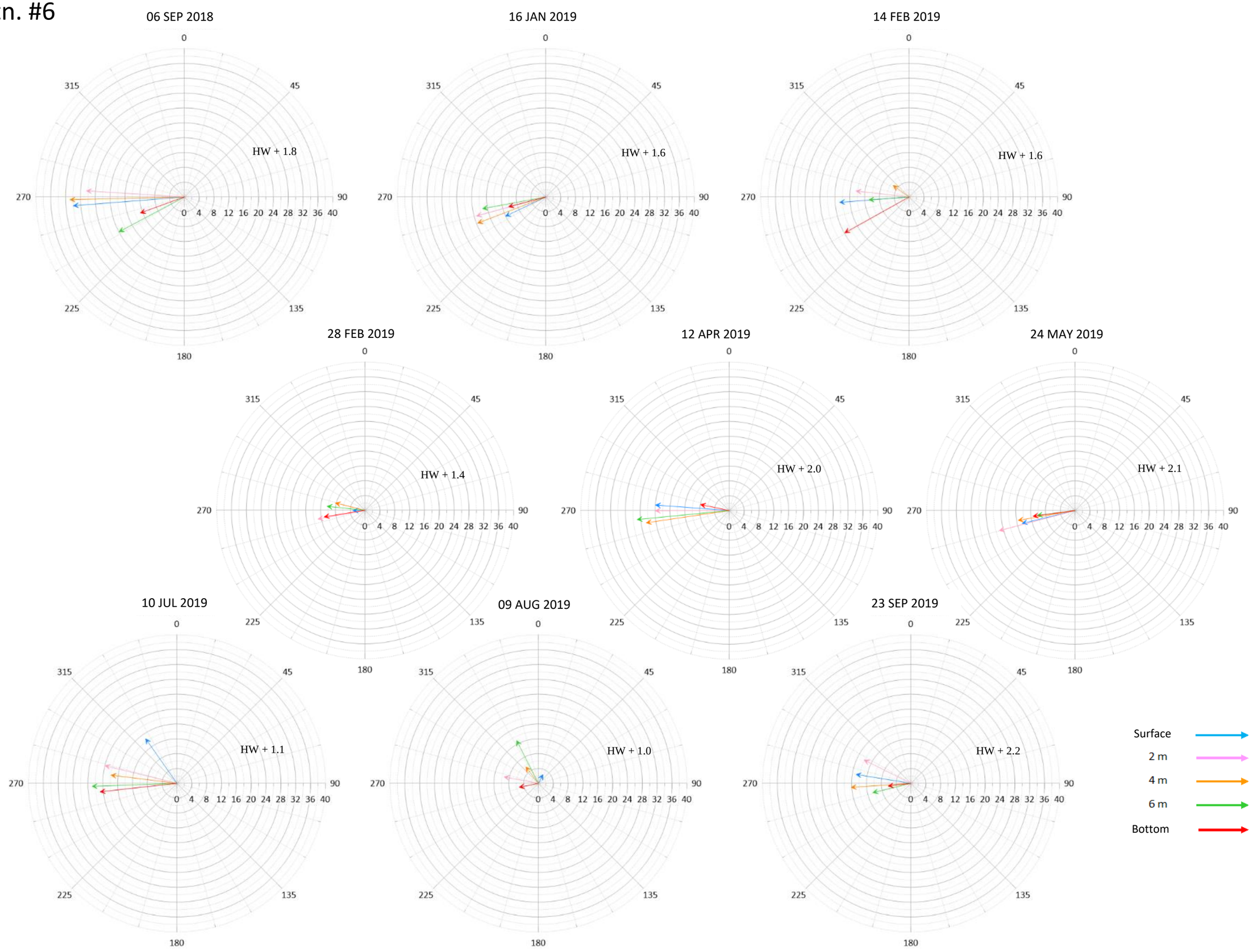

Figure 2.17. Intensity and direction of the current measured in stn. #6, between September 2018 and September 2019, at 5 levels: surface in blue, 2 m in pink, 4 m in orange, 6 m in green and bottom in red. Time of the measurements (given in hours) relative to high water (HW).

Stn. #7

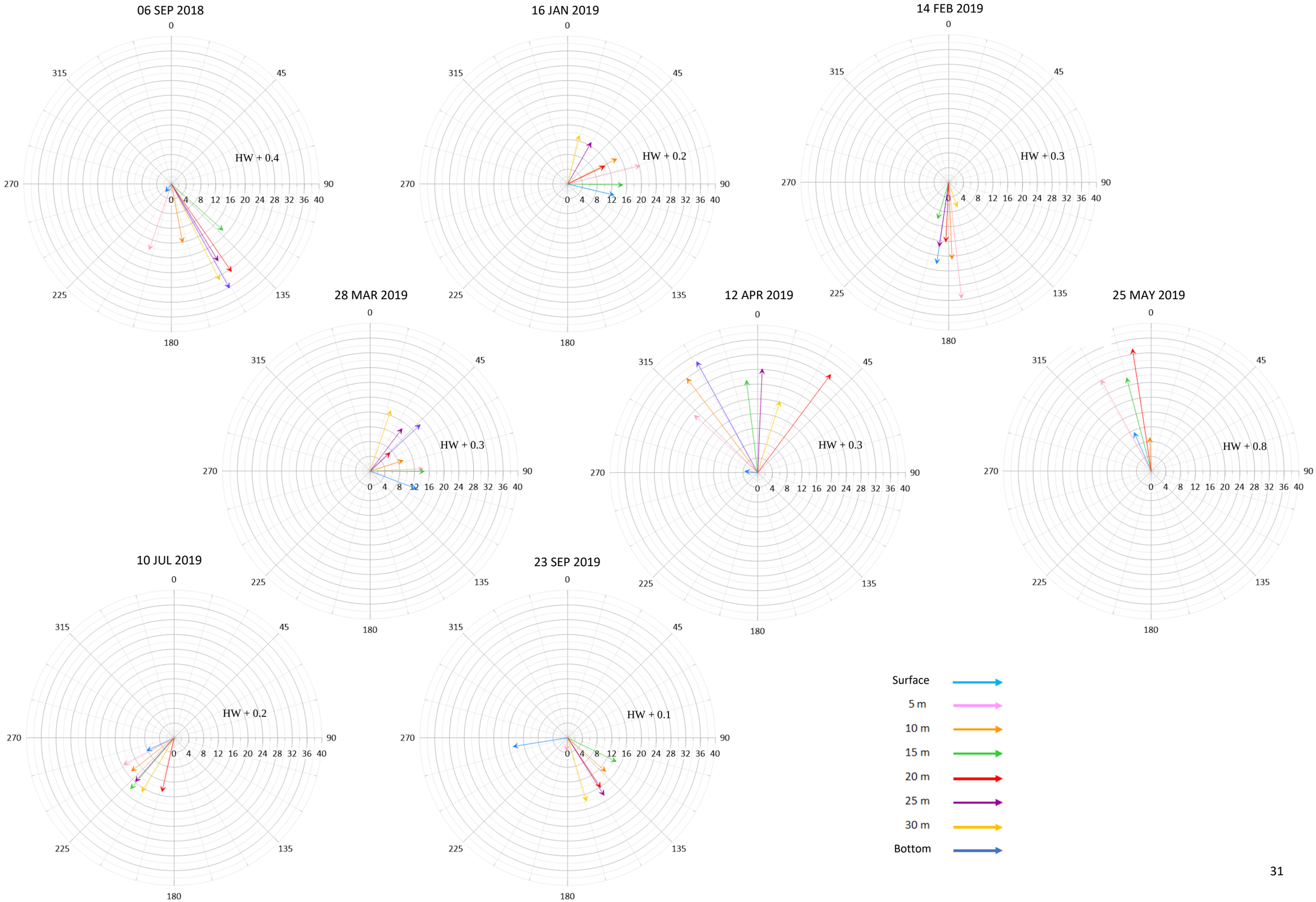

Figure 2.18. Intensity and direction of the current measured in stn. #7, between September 2018 and September 2019, at 8 levels: surface in blue, 5 m in pink, 10 m in orange, 15 m in green, 20 m in red, 25 m in purple, 30 m in yellow and bottom in dark blue. Time of the measurements (given in hours) relative to high water (HW).

2.5 Discussion

From the analysis of the profiles, it was possible to detect a variation in the temperature and turbidity throughout the tidal cycle during the campaign conducted in June, with a thermal amplitude of around 4˚C and a variation of turbidity of 24 FTU. Additionally, during the same campaign, an intrusion of water with lower temperature, salinity and density was observed at 10 m depth (Figure 2.4). The day in which the campaign took place, the sea and weather conditions were adverse, especially during the morning period, when the first measurements took place. The turbulence of the water could justify the range of temperature and turbidity values observed during that day but doesn't justify the water intrusion observed at 10 m depth in stns. #7 and #8, which, should have been mixed, under those turbulent conditions. This intrusion could have been originated by a river discharge but, in that case, it would be observed a signal at the surface too. This occasional variation could also have been a manifestation of a land discharge. According to Rosa (2010), the orthopedic hospital of *Santiago do Outão* has its own waste disposal station that flows into the river. This could be a possible justification for what was observed but, as the first measurement set was taken during the ebb, a hypothetical discharge would flow towards the ocean, not affecting the sampling stations. Therefore, it is more plausible to think in a discharge coming from the interior of the estuary, with capacity to affect stns. #7 and #8, as it happens with Comporta's sewage, that flows directly into the estuary (Dias, 2019). Although the sewage is located ≈ 15 km from stn. #8, it could be the cause of this intrusion. Further studies would be needed to unravel these processes in depth.

A slight salinity increase was observed at the surface layers in some profiles (Figure 2.11). Higher rainfall increases the river flow that, when relevant, can influence the whole estuary, in all its parameters. The analysis of the profiles also revealed that, these low salinity values at the surface layers were obtained during the ebb. The circulation regime in the estuary is strongly dependent on the variation of the tide (Sousa and Lourenço, 1980) and, therefore, any relevant variation in the river flow can affect the entire estuary, mostly during the ebb. This could be the justification for the lower values observed at stn. #8 in November 16, one week after high rainfall.

Despite the influence of the river in some of the profiles analyzed, the mouth of the estuary presented a mean salinity of 35.8, which is in agreement with the values observed in the coastal ocean of Portugal (Marques, 2017). The mouth of the estuary behaved like a coastal lagoon (Ribeiro and Neves, 1982), showing the entrance of seawater into the estuary, with high salinities, along the water column and practically with no temporal variation.

The values of the several parameters matched partly the results presented in previous studies. Sousa and Lourenço (1980) observed, during winter, temperatures of 14 ºC and salinities of 34.0, in the region of stns. #6 and #7, and of ≈ 13 ºC and 32.0 near stn. #8. During summertime, they observed values of 18 ºC (near stns. #6 and #8) and 16 ºC (stn. #7), and salinities ranging between 35.0 and 35.7. In the present study, the profiles obtained during winter showed similar temperatures to those mentioned above, but salinities higher in about 2.0 units. During the summer, the temperature showed to be higher in about 2 or 3 ºC, according to the station, but the salinities were closer to what was measured by Sousa and Lourenço (1980). It seems that, during the sampling period of the present work, there was higher thermal amplitude throughout the year, with temperatures reaching higher values. Also, the influence of the river water in the region of the mouth of the estuary was less than before. These variations could be occasional or be the result of changes in the estuary in recent years. They could be due to variations in the weather conditions and, consequently, of the river flow, which has been decreasing according to Sales (2015) and the Chapter 1 of the present study.

In a more extended temporal analysis, it was possible to see a strong change in the river flow in 1969 (Chapter 1). The *Roxo* dam, placed south of *Moinho da Gamitinha*, built in 1967 and, *Monte da Rocha* dam, built later on, in 1972, constitute two interferences in the river course and probably caused the observed decrease of the Sado river (Sales, 2015). As there are no published oceanographic studies of the estuary prior to the 1970s, it is difficult to verify the influence of the river flow reduction in the estuary dynamic, as well as in the characteristics of the physicochemical parameters. However, it was possible to validate the seasonality of the river flow throughout the year, which can justify some of the observed variations, in the salinity, as mentioned above, and in the turbidity of the water.

The turbidity profiles presented higher values during summer than during winter, which can result from the reduced number of profiles obtained during summer. This evidence can also be justified by the low rainfall observed during winter, that evidenced higher values of turbidity during summer, which may come from the normal increase of productivity observable during that period (ADEC, 2015). However, the turbidity profiles obtained presented low values throughout the sampling period, evidencing the weak interference of the river water in the mouth of the estuary. Some profiles showed turbidity increases but, according to Vale *et al*. (1998), the higher values observed seem to be similar to the ones obtained in other undisturbed estuarine areas (11-20 NTU, Nephelometric Turbidity Unit, directly comparable with FTU, the units used in this work).

There were no significant variations of the parameters in depth, which indicates well mixed waters, with very little stratification and a relatively high vertical homogeneity (Figure 2.5). These results are in agreement with the conclusions of Ambar *et al.* (1982), Ribeiro and Neves (1982), mentioned in Maretec (nd), Coutinho (2003) and Ferreira *et al.* (2005). A note only to the profile obtained at stn. #7 in September, which showed a constant decrease of the temperature in depth, as well as an increase of the density. This behavior is typical of a coastal oceanic station, during the summer. If more data collected in the summer were available, perhaps stn. #7 could be classified as a coastal oceanic station, as it was represented in Sousa and Lourenço (1980). The profiles obtained in January (winter season) suggested the formation of a mixed layer, since in February there was already conformity of the temperature values in the whole water column. In the absence of data collected in December, it is not possible to say if the mixed layer started to form even before January.

The maximum of fluorescence observed in several profiles obtained in stn. #6 at $\approx$ 5 m depth was also corroborated by the data collected with the multiparameter sonde. This suggests the existence of a Deep Chlorophyll Maximum (DCM) that was not observed in the other stations, where a well-mixed water column occurred. This fluorescence maximum could be a result of the coastal influence, since the station was located next to a pier with associated fishing activities, or be a consequence of the influence of the sewers of Setúbal, that flow directly into the river, a few meters apart from the sampling station (Rabaçal, 2018; Goes, 2012). The works to divert the sewers to the Setúbal Wastewater Treatment Plant (WWTP) were not completed by the time the sampling campaigns were finished (Brandão, 2019).

As the profiles obtained in the three stations did not show relevant differences among them, spatial homogeneity can be assumed in the outermost region of the estuary, mainly in stns. #7 and #8. Based on the temperature and salinity distributions, Wollast (1979) divided the estuary into an upper and lower part, being the lower part the area between stn. #7 and the beginning of the Alcácer channel (Sousa and Lourenço, 1980), so the spatial homogeneity mentioned above agrees well with that division. However, stn. #6 slightly diverged from the homogeneity observed between stns. #7 and #8, as the obtained values deviated from the ones observed in the other stations during the same campaigns. That could mainly be due to the lower depth of the water

column and the proximity of stn. #6 to the coast, that also leads to a highest susceptibility to atmospheric variations.

Mainly, it was the variation of the tide that promoted the circulation in the estuary. The campaigns that fully covered the tidal cycle revealed that the water entered the estuary through the 2 channels, with more intensity along the South channel (Figure 2.8). The estuary outflow also occurred through both channels, being the South channel the main one for the water exchange. These results agree with the conclusions of Ambar *et al*. (1982) and Ribeiro and Neves (1982). Maretec (2002a), obtained current intensities similar to the ones observed in this study, with values in the range 50-100 cm/s in the same area.

It was also observed an agreement between the current direction at the surface and at the lowest level across the full cycle. Ambar *et al*. (1982), referred the existence of a two-layer flow in the southern channel - up-estuary near the bottom and seaward at the surface - and currents more consistently up-estuary in the northern channel, which is in opposition with what was observed in the present study. The data collected during this study was not enough to draw conclusions regarding the residual current in the estuary. Ambar *et al*. (1982) and Maretec (2002a) mentioned a circulation model where the water entered the estuary predominantly through the North channel, leaving the estuary mainly through the South channel. This could not be verified with the present work but, possibly due to the lack of information of the interior of the estuary.

The data collected at stn. #7 were illustrative of the difficulties in characterizing the circulation near Outão, as also happened with Sousa and Lourenço (1980). The very complex circulation detected could be explained not only by estuarine water exchange, but also by the strong coastal exposition of the area. A large amount of the observations collected in stn. #7 were carried out during slack water, which also possibly influenced the large variation of the current intensity and direction in the water column and throughout the year. Also, the measurements in that station were made while the boat was drifting and that might have affected the results, making the campaigns hard to be compared.

Based on the results obtained in this study, there could have been a possible change in the circulation regime of the estuary. However, more observations along tidal cycle analysis and in more stations throughout the estuary would be needed to allow conclusions about that possible change. It would be interesting to complement and validate the data obtained during this work extending the tidal cycle analysis to the CTD. That would allow to elaborate a more complete description of the variation of the physicochemical parameters along the tidal cycle and understand whether the observed changes in the salinity and temperature do correspond to the actual behavior of the estuary. In order to fully understand the actual circulation regime in the Sado estuary, a tidal analysis in its interior region and within the river channels would be important.

The Sado estuary is currently undergoing through a dredging process to improve the access of large ships to the port of Setúbal. These works have been removing large amounts of sand from the northern navigation channel (more than 6 million tons of sand (Guimarães, 2019)). Such works can lead to changes in the circulation of the estuary (van Maren, 2015; Conceição, 2016). The change of the circulation regime due to dredging activities was already verified in the Oka Estuary (Spain) by Liria *et al.* (2009). Therefore, it would be very interesting to keep these works monitored in order to see whether there is an anthropogenic modification of the system, and, if so, what kind of repercussions would it have in the future of the estuary.

In conclusion, the outermost area of the estuary can be described as spatially homogeneous, with occasional stratification in the water column. The variations observed in depth and throughout the sampling period were mainly due to environmental and anthropogenic pressures (atmospheric variations, changes of the river flow or land discharges). Also, the

outermost area of the estuary presented salinity values that are typical of coastal oceanic waters, throughout the whole sampling period. Stn. #7 resembled a coastal oceanic station and stn. #6 was the most susceptible station to seasonal variations, showing a possible DCM at ≈5 m. The river flow appears to have been decreasing in the past years and the variation of the tide was the main enhancer of the circulation in the estuary. The circulation was made through the two navigation channels, being the South channel the main route for the estuary water exchange. The intensity of the current decreased in depth and its direction was similar along the water column, according to the tidal regime. Possible changes in the circulation may have occurred in recent years, as some of the results presented here did not agree with the results of previous studies. Currently, dredging works taking place in the estuary can also be threatening the circulation regime and the behavior of the estuary. Therefore, it is important to monitor the estuary and to scientifically follow possible investment activities in the region.

Chapter 3

Seasonal and interannual variability based on satellite data

3.1 Introduction

Remote sensing emerged in the second half of the 20th century in the form of satellite observations of land and ocean (Dassenaki *et al.*, 2012). In the field of oceanographic studies, satellite data are often used to evaluate four sea properties, commonly referred to as primary quantities: sea surface temperature (SST), ocean color, roughness and elevation (Sutcliffe *et al.*, 2016). The study presented herein is focused on these first two properties in a costal environment context, the Sado estuary. However, there are numerous challenges in analyzing this type of environments. Estuaries have strong land-see interactions, as water and sediment inputs or constant coastal erosion, and are exposed to a high anthropogenic forcing, given the man's interest in exploring these environments. Therefore, these factors give a complex and spatially heterogeneous natural condition to the wetlands and land surface characteristics of the estuaries (Chi and Fu, 2018). Despite the constant dynamism that turns estuaries difficult to analyze, their monitoring is extremely important. They are among the most productive ecosystems in the world, are habitat for several species (NOAA, 2020a) and are crucial for the economy.

Measuring sea surface temperature with satellites was one of the first properties to be of interest to the scientific community. Scientists record sea surface temperature (SST) to understand how the ocean interacts with Earth's atmosphere. SST provides fundamental information on the global climate system and is important for the study of marine ecosystems, namely estuaries (NOAA, 2020a). There are now over 40 years of data collected by sensors dedicated to the SST study. With relevance and still in activity are, for example, the Advanced Very High Resolution Radiometer (AVHRR), the Moderate Resolution Imaging Spectroradiometer (MODIS) and the Visible Infrared Imaging Radiometer Suite (VIIRS). The AVHRR is a sensor that records daily images with a spatial resolution of 1 km and was launched by NOAA in 1978 (ESA Earth Online, 2020a). In 1999, NASA launched the MODIS sensor on board Terra satellite and in 2002, on board Aqua satellite. Both sensors have been providing SST products with 1 km resolution with a continuous global coverage every 1 to 2 days (NASA, 2020). The VIIRS was launched by NASA in 2011 to extend and improve the series of measurements initiated by its predecessors, AVHRR and MODIS. It has a spatial resolution of 750 m and a repeat cycle of 16 days (NASA Earth Data, 2020).

Currently, the Group for High Resolution Sea Surface Temperature (GHRSST) is also in action. This is an international and open science group that encourages and promotes the SST monitorization with satellites and allows scientists and entities to collaborate in order to create a global and updated database (GHRSST, 2020). This group's platform contains several products, some of which integrate data from the various sensors described above in a unique product. In the present work, one of the products of the GHRSST database (Multiscale Ultrahigh Resolution (MUR) product – 1 km spatial resolution) was used.

Globally, this platform (GHRSST) has been used for several studies of ocean water monitoring (e.g. Chin *et al.*, 2017; Martin *et al.* 2012) and for product validation. Vazquez-Cuervo *et al.* (2019) proceeded with the validation of SST satellite products, including the MUR GHRSST, with *in situ* data collected with a Saildrone AUV (Autonomous Underwater Vehicle) in the coastal ocean of the California/Baja Coast. This product, according to the authors, appeared to show a good correlation with the AUV data but, the differences observed between the values, were justified by the satellite spatial resolution. However, Crosman *et al.* (2017), studied the use of MUR GHRSST in a lake environment (Lake Michigan – 85 m depth, 190 km wide and 2 600 km long; Lake Okeechobee – 2.7 m depth, 48 km wide and 56 km long; Lake Oneida – 6.7 m depth, 8.0 km wide and 32 km long), useful in this work as it is an environment with shallow waters surrounded by continental landmasses, similar to Sado estuary. These authors concluded that MUR product was a promising tool for providing real-time analyses of surface temperature for lakes larger than a few km in diameter.

In Portugal, the problem of the lack of resolution of SST satellite products was also noticed for the Tagus estuary, the closest estuary to Sado. There are records of applications of the Mediterranean Sea Ultra High Resolution Sea Surface Temperature Analysis from Copernicus, with a resolution of 1 km (Mateus *et al.*, 2013) in Tagus estuary, for forensic sciences purposes (to estimate the accumulated degree days for two drowning accidents). The low precision of this product, when applied to the region, is mentioned by the authors. However, Pablo *et al* (2019) used the products of the GHRSST MUR and achieved a successful validation of the 3D-MOHID Hydrodynamic Model for the Tagus Coastal Area, corroborating the studies of Crosman *et al.* (2017).

Although some problems in the use of products with 1 km spatial resolution in shallow and small areas seem to exist (uncertainties as atmospheric corrections, cloud contamination, water emissivity and shoreline effects (Crosman *et al.*, 2017)), there seems to be a consensus on the use of MUR, which appears to be the most viable product to use in an analysis of the SST at Sado estuary. Therefore, a characterization of the interannual and seasonal variability of the SST in the Sado estuary was made using the GHRSST satellite imagery to study the temporal and spatial variation of the sea surface temperature in the estuary.

Ocean color products, more specifically the ones providing concentrations of surface chlorophyll *a* derived from satellite data also have diverse and important applications. Chlorophyll *a* is the most important light absorbing substance in the open ocean and exists in all photosynthetic microorganism, named phytoplankton, that are at the base of most food chains of aquatic ecosystems. Chlorophyll *a* concentrations can be used as a proxy of phytoplankton biomass, *i.e.*, more phytoplankton in the water, the greener the water is....the less phytoplankton, the bluer it is (Nagaraja, 2019). The development of remote sensing ocean color dates back to 1978 with the launch of the Coastal Zone Color Scanner Experiment (CZCS), the first instrument optimized for water analysis on board of a spacecraft (NASA, 2019). Although CZCS was intended as a one-year proof-of-concept mission, the sensor continued to transmit data over selected oceanic test sites until early 1986 (ESA Earth Online, 2020b). After CZCS, some historically relevant instruments were launched. SeaWiFS was released in 1997 by NASA to

provide useful ocean color data to the Earth science community. It collected data with 1.1 km resolution (Local Area Coverage) until it ended its mission in 2010. With the SeaWiFS instrument, NASA gathered the first record of photosynthetic productivity in the oceans. In 1999, as earlier referred, NASA launched MODIS sensor. Beyond SST, MODIS can measure the photosynthetic activity of land and marine plants (phytoplankton) with a resolution of 1 km (Nagaraja, 2020). Furthermore, in the year of 2002, MERIS sensor was launched by ESA (in ENVISAT satellite) and was the first imaging spectrometer mission with a primary objective for ocean and coastal color remote sensing. MERIS operations were stable with only few interruptions and continuously provided data to its users until 2012 (ESA Earth Online, 2020b). The sensor had a global coverage every 3 days with a spatial resolution of 300 m (ESA Earth Online, 2019a). Lastly, ESA, within the EC Copernicus Program, released the Sentinel program in 2014 to provide continuation of Earth observation missions. In this program, ESA launched several satellites/sensors, each one with specifics purposes. Sentinel-3 has the marine observation as the primary objective and collects data of ocean color with the Ocean and Land Color Instrument (OLCI). Sentinel-3 has a spatial resolution of approximately 300 m and a revisit time of 2 to 3 days (ESA Earth Online, 2019b).

Worldwide, coastal ocean environments have been remotely studied in several disciplinary areas with ocean color products. Cui *et al.* (2010) explored the potential of using MERIS data in the Bohai Sea (78 000 km²) and achieved an overestimation of the satellite-derived chlorophyll *a* in the region regarding the *in situ* data, given the high turbidity of the water. On the other hand, MERIS satellite data have been demonstrated by Palmer *et al.* (2015) to be effective, in accurately retrieving chlorophyll *a* concentrations across the spatial extension of lake Balaton (596 km^2, 3.3 m depth). Abbas *et al.* (2019) tried to use MODIS product in Chesapeake Bay, but the OC3M algorithm used failed to perform well in the coastal water.

In Portugal, Sá *et al.* (2015) conducted a study to investigate the performance of MODIS Aqua OC3M, MERIS OC4Me (algal 1) and MERIS Neural Network (algal 2) chlorophyll data for the Western Iberian coast, and tested as well several chlorophyll products provided by the CoastColour Project and by the Climate Change Initiative (CCI) program, and a regional version of the Multi Layer Perceptron neural network developed within the scope of their study. Their statistical analyses showed that satellite chlorophyll estimates tended to be higher than the *in situ* reference values. However, among standard remote sensing products, MODIS OC3M and MERIS algal 2 yield the best agreement with *in situ* data.

In general terms, the main problem globally observed in remotely quantifying chlorophyll *a* concentrations in shallow and coastal waters is related with the use of operational algorithms that are only suitable for oceanic water bodies (Abbas *et al.*, 2019). The main difficulties to overcome these issues are associated with the presence of highly diffusing suspended mineral particles as well as high concentrations of particulate organic matter, which may bias atmospheric corrections and impact bio-optical algorithms. Additionally, in the presence of highly turbid waters, cloud-free pixels are sometimes erroneously classified as clouds, leading to a loss of data. Also, the crucial and mandatory validation exercises are greatly complicated to perform due to the extreme spatial heterogeneity of these areas (Loisel *et al.*, 2012). Sá *et al.* (2015) also confirmed that a non-uniform chlorophyll distribution in the water column can be a concurring factor to the documented overestimation tendency when considering larger optical depth match-up stations. However, improvements can be achieved by coastal products and through regionalized models developed with *in situ* chlorophyll and concomitant radiometric data. Regional solutions need to be considered when application requirements are not corresponded by standard product accuracy (Sá *et al.*, 2015).

A new era for continuous, high frequency water quality monitoring of coastal waters, was considered to begin in 2016 with the launch of OLCI on board Sentinel-3 (Toming *et al.*, 2017). Lins *et al*. (2017) achieved successful chlorophyll *a* retrievals using Sentinel-3 OLCI data in the Mundaú-Manguaba Estuarine-Lagoon System (Brazil, maximum depth of 3.5 m). Furthermore, the sensor was described as being promising to remotely estimate chlorophyll *a* for coming decades in turbid inland waters (Lins *et al*., 2017).

Therefore, the purpose of this study was to evaluate the performance of several approaches to estimate the chlorophyll *a* in Sado estuary, a region still poorly studied in this matter. Using *in situ* observations, the feasibility of using MODIS Aqua, MERIS and OLCI databases was studied, always considering the spatial resolution of each sensor. The estuary was assessed in terms of temporal and spatial variability of chlorophyll *a*.

3.2 Data and Methodologies

3.2.1 Satellite-derived Sea Surface Temperature (SST)

The SST dataset was gathered from the Global Ocean Data Assimilation Experiment (**G**ODAE) **H**igh-**R**esolution **SST P**ilot **P**roject (GHRSST-PP). These products were produced as a retrospective data set (latency of four days) and of near real time (one day latency) at the Physical Oceanography Distributed Active Archive Center (PO.DAAC) of Jet Propulsion Laboratory (JPL), using wavelets as the basic functions in an optimized interpolation approach with a global grid of 0.01 degrees.

The data version chosen was version 4.1 from the Multiscale Ultrahigh Resolution (MUR) product, based upon nighttime GHRSST L2 sea surface and subsurface temperature data collected by various instruments:

- NASA's Advanced Microwave Scanning Radiometer-EOS (AMSRE)
- Moderate Resolution Imaging Spectroradiometer (MODIS) on NASA's Aqua and Terra platforms
- US Navy WindSat microwave radiometer
- Advanced Very High Resolution Radiometer (AVHRR) on NOAA-n series satellites
- *in situ* observations derived from NOAA's iQuam project

These images are characterized as of level 4 (L4) due the integration of data obtained by different methods, sensors and models. All images had a spatial resolution of 1 km and a temporal resolution of 1 day, and the data set had global records since June 2002 up to the present (data set short name - MUR-JPL-L4-GLOB-v4.1). For the present study, the temporal series used encompassed images from 01 JUN 2002 to 30 SEP 2019, as the measurement of the *in situ* parameters in the Sado estuary ended in September 2019 (dataset available at https://podaac.jpl.nasa.gov/dataset/MUR-JPL-L4-GLOB-v4.1).

All images obtained were processed using SNAP - Sentinel Application Platform satellite data processing and analysis program. In SNAP, the SST information of each image was automatically extracted from the previously established *in situ* stations, using the mean value of a 3x3 pixel grid (3 km x 3 km) centered in the pixel of each station. Additionally, MATLAB software was used to process the monthly, seasonal, annual and interannual average images of SST, from the daily satellite data. Lastly, the annual anomalies (an) presented for each sampling station followed Equation 3.1, where *vo* represents the mean value obtained for each year and *vr* the value of reference.

$$an = vo - vr \quad [3.1]$$

3.2.2 Satellite-derived chlorophyll *a* concentrations

To study the variability of chlorophyll *a* in the estuary, three satellite instruments were considered: MODIS Aqua, MERIS and Sentinel-3 OLCI. The first instrument used in this study was the MODIS Aqua (Moderate Resolution Imaging Spectroradiometer), a satellite of the Earth Observing System project, with data accessible through the Ocean Color Web database of NASA (available at www.oceancolor.gsfc.nasa.gov/cgi/browse.pl? sen=amod). This sensor provided level 2 (L2) global images every 2 days. L2 images result from a data processing step in which the geophysical component is obtained, transforming measurements of electromagnetic radiation to measurements of oceanographic parameters. The sensor acquired data from 2002 to the present, with a spatial resolution of 1 km. However, it had a low spatial resolution when applied to the scale of the Sado estuary (total area of 212.4 km^2 (Neto *et al.*, 2019)). Therefore, additional instruments, such as MERIS and Sentinel-3 were considered. MERIS was an imaging multi-spectral radiometer (Visible/Infrared, vis/IR), with a global coverage every 3 days and a spatial resolution of 300 m (ESA Earth Online, 2019a). Despite the better resolution, MERIS ended its activities in 2012, which made the comparison with the *in situ* data not possible.

In order to be able to proceed with the analysis of the present behavior of the estuary in terms of chlorophyll *a* distribution and validate the products with the *in situ* values collected, a satellite still in activity and with a good spatial resolution had to be chosen. Therefore, there was the attempt to use data of Copernicus Sentinel for the year of 2018 and the days in which the campaigns occurred. Sentinel-3 started its mission in 2016, by ESA and EUMETSAT, with the purpose to deliver operational ocean and land observation services. From the set of sensors that incorporated this mission, the products of Sentinel-3 OLCI (Ocean and Land Colour Instrument) were used for this study. Sentinel-3 has a spatial resolution of ≈ 300 m and a revisit time of 2 to 3 days (ESA Earth Online, 2019b). This is a sensor especially designed to coastal waters and that emerged as a successor of MERIS. For this work, it was used the product provided using the Neural Net algorithm, since it was developed for application to more complex case 2 waters (coastal waters). Sentinel images can be found in EUMETSAT Data Centre (available at https://www.eumetsat.int/website/home/Data/DataDelivery/EUMETSATData Centre/index.html).

Sentinel-3 data was considered ideal for the analysis of the present situation of the Sado estuary. For the long-term analysis, the precursor of Sentinel-3, *i.e.* MERIS, was selected. The bio-optical algorithm applied to MERIS data was OC5, also developed for application to coastal waters (Gohin *et al.*, 2002). MERIS 10-year ocean color data set can be found in the NERC Earth Observation Data Acquisition and Analysis Service (NEODAAS) database.

All the images obtained were processed using SNAP and the chlorophyll *a* values were automatically extracted from the previously established *in situ* stations, using the mean value of a 3x3 pixel grid (900 m x 900 m) centered in the pixel of each station, similar to SST image processing. The Sentinel-3 images available for validation with *in situ* data were filtered following the criteria defined by EUMETSAT: the pixels considered as valid for the analysis were those not flagged as INVALID, CLOUD, CLOUD_AMBIGUOUS, CLOUD_MARGIN, SNOW_ICE, COSMETIC, SUSPECT, HISOLZEN, HIGHGLINT or OCNN_FAIL (EUMETSAT, 2019).

The computation of the monthly, seasonal, annual and interannual averages followed exactly the same procedure as the data of SST, through MATLAB, as described earlier. The annual anomalies presented also followed equation 3.1.

3.2.3 *In situ* dataset

The *in situ* data of sea surface temperature (SST) and chlorophyll *a* were obtained from monthly on-site campaigns that took place between March 2018 and September 2019 in the Sado estuary. These were performed within the scope of the Mar2020 AQUASADO Project. The sampling strategy used consisted in monthly sampling at 7 stations (Figure 3.1 and Table 3.1). In May and November 2018, as well as in June 2019, there were two campaigns instead of one, with measurements at stns. #5, #6, #7 and #8. Stn. #8 was the one with the least information because it has only been monitored in those campaigns.

Figure 3.1. Distribution of the sampling stations in Sado estuary

Table 3.1. Sampling stations: designation and geographical coordinates.

Stations (Stn.)	**Designation**	**Coordinates**	
		Latitude ˚ N	Longitude ˚ W
#1	Rice field - E Channel	38.41522	008.67155
#2	Rice field - W Channel	38.43333	008.73333
#3	Águas de Moura - S Channel	38.50000	008.74833
#4	Águas de Moura - N Channel	38.52187	008.74828
#5	Lisnave	38.47083	008.79389
#6	Setúbal	38.51809	008.89838
#7	Outão	38.48667	008.93000
#8	Troia	38.49278	008.88167

All the monthly campaigns were planned in order to start the measurements in high water and provided a unique sea surface temperature value for station. During the months with 2 campaigns, the observations were made throughout the day in each of the stations analyzed, as already described in the previous chapter. From these campaigns resulted as many temperature values as the number of measurement sets described in Table 3.2. In order to be able to use these data for comparison with the single SST values provided by the GHRSST database for each day, the daily average of the collected values was calculated.

During the different campaigns, water samples were collected for laboratory determination of chlorophyll concentrations and SST data were acquired using a CTD, a Multiparameter Sonde and a Current Sensor. In order to make the reading easier, from now on, the Multiparameter Sonde is referred as MS and the Current Sensor as CS, as in the previous chapter.

As referred, of the data collected with the 3 instruments, only the temperature was analyzed in this chapter. During the campaigns, the 3 instruments were lowered in the water to measure temperature profiles. From these profiles, it was used the temperature values collected between 0.5 and 1 m depth as the sea surface values.

Of the *in situ* chlorophyll *a* data obtained, only the values of some campaigns were used. To proceed with a product validation in a specific region, the *in situ* collections have to be concomitant with the passage of the satellite (match-up). As mentioned earlier, Sentinel-3 does not provide results on a daily basis, so it was not always possible to obtain match-ups, even though the campaigns have been planned in order to optimize the achievement of match-ups. Also, the presence of clouds, problems with atmospheric correction, etc., can compromise the quality of the satellite data, in this case showing invalid values for a region. The days and the sampling stations on which water samples and temperature data were collected are shown in Table 3.2. The total number of SST values (N) collected with the instruments during the sampling period is also presented in the table. The CTD and the CS started collecting data in September 2018 at stn. #6, #7 and #8 and the MS started the collections in May 2018, having an almost total coverage of the estuary stations. Due to logistic constraints, it was not possible to collect data at all sampling occasions and using all the instruments. Also, for the interior and exterior area of the estuary different MS were used.

The water samples were collected and transported to the laboratory as soon as possible. Samples were filtered using GF/F filters with 25 mm diameter and a mesh of 0.7 µm (Whatman). The filters were then wrapped in aluminum and stored at -80 °C to be later analyzed through High Performance Liquid Chromatography (HPLC), in order to allow the extraction and quantification of the different phytoplankton pigments. 3 mL of an extraction solution composed of 95% cold methanol, buffered with 2% of ammonium acetate and containing 0.35 mg/L of trans-β-Apo-8′-carotenal were used. After placing the extraction solution in the sample test tube, the filter was grinded with a glass rod. Then, the tube was placed in the freezer (-20 ºC) for 30 minutes to, later on, be taken to the ultrasound for 5 minutes. The test tube was put back in the freezer (-20 ºC) for 30 minutes and then, the sample was centrifuged for 10-15 min at 4000 RPM (4 ºC). Lastly, the sample was filtered and run in the HPLC machine.

Table 3.2. Sampling dates and the stations at which each instrument made measurements. CS corresponds to the current sensor and MS to the multiparameter sonde. N represents the total number of sea surface temperature values collected during the sampling period with each instrument. Sets - cycles of measurements made.

	Stations with collected data		
Sampling Dates	CTD	CS	MS
27 MAR 2018	-	-	#1, #2, #3, #4, #5, #6, #7
23 APR 2018	-	-	#2, #3, #4, #5, #6, #7
08 MAY 2018	-	-	#1, #2, #3, #4, #5 (8 sets), #6 (7 sets), #7 (8 sets), #8 (7 sets)
15 MAY 2018	-	-	#5 (6 sets), #6 (7 sets), #7 (7 sets), #8 (7 sets)
06 JUN 2018	-	-	#1, #2, #3, #4, #5, #6, #7
06 JUL 2018	-	-	#1, #2, #5, #6, #7
03 AUG 2018	-	-	#1, #2, #6, #7
06 SEP 2018	#6, #7	#6, #7	#1, #2, #6, #7
03 OCT 2018	#6, #7	-	#1, #2, #6, #7
08 NOV 2018	#7 (4 sets), #8 (4 sets)	#7 (4 sets), #8 (4 sets)	#5 (3 sets), #6 (2 sets), #7 (2 sets), #8 (2 sets)
16 NOV 2018	#7 (4 sets), #8 (4 sets)	#7 (4 sets), #8 (4 sets)	#5 (1 set), #6 (1 sets)
19 DEC 2018	-	-	#1, #2, #3, #4, #5, #6, #7
16 JAN 2019	#6, #7	#6, #7	#1, #2, #4, #5, #6, #7
14 FEB 2019	#6, #7	#6, #7	#1, #2, #6, #7
28 MAR 2019	#6, #7	#6, #7	#1, #2, #3, #4, #5, #6, #7
12 APR 2019	#6, #7	#6, #7	#1, #2, #6, #7
24 MAY 2019	#6, #7	#6, #7	#1, #2, #3, #4, #5, #6, #7
18 JUN 2019	#7 (5 sets), #8 (3 sets)	#7 (5 sets), #8 (3 sets)	#7 (5 sets), #8 (3 sets)
26 JUN 2019	-	#7 (7 sets), #8 (5 sets)	#1, #2, #3, #4, #5 (5 sets), #6 (5 sets), #7 (7 sets), #8 (5 sets)
10 JUL 2019	-	#6, #7	#1, #2
09 AUG 2019	-	#6	#1, #2, #3, #4, #5, #6,
23 SEP 2019	-	#6, #7	#1, #2, #6, #7
N	38	53	190

3.3 Results

3.3.1 Satellite-derived Sea Surface Temperature (SST)

3.3.1.1 Data Validation

First, the *in situ* temperature values obtained by the different instruments were compared, in order to understand if there were relevant discrepancies between the instruments used. Figure 3.2 shows the existing correlations between the CTD, the CS and the MS, the linear regression equation obtained as well as the number of inputs considered (N). The red dashed line represents the reference line, with slope 1.

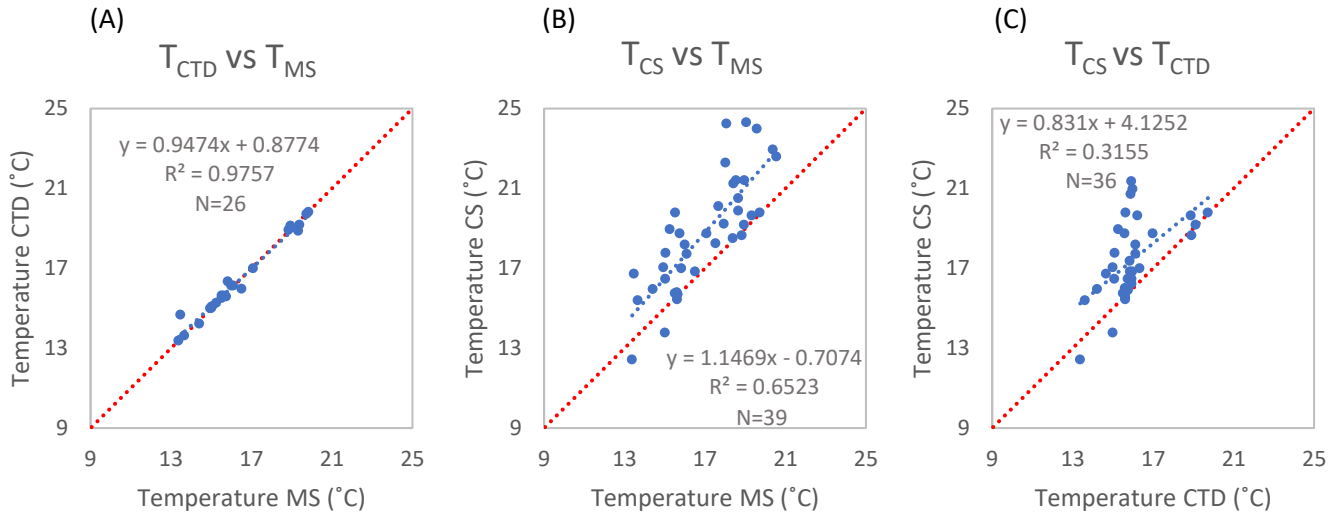

Figure 3.2. Correlation between the sea surface temperature data collected in situ during the campaigns with the CS, the MS and the CTD. The red dashed line represents the slope 1 reference line.

The best existing relationship is the one between the CTD and the MS, exhibiting a great similarity between those values (R^2=0.9757). Additionally, an overestimation of the values measured by the CS was observed. As such, it is acceptable to consider that the CTD and the MS are the most appropriate instruments for this study, given that they provide the most reliable temperature measurements. This was also confirmed by the comparison between *in situ* and satellite (GHRSST) data (Figure 3.3) for the stations located in the outermost area of the estuary (stns. #6, #7 and #8), represented in blue. Of note is that the slope of the relation line was closer to 1 between the CTD/MS and the satellite data, and farther from 1 with the CS, as would be expected.

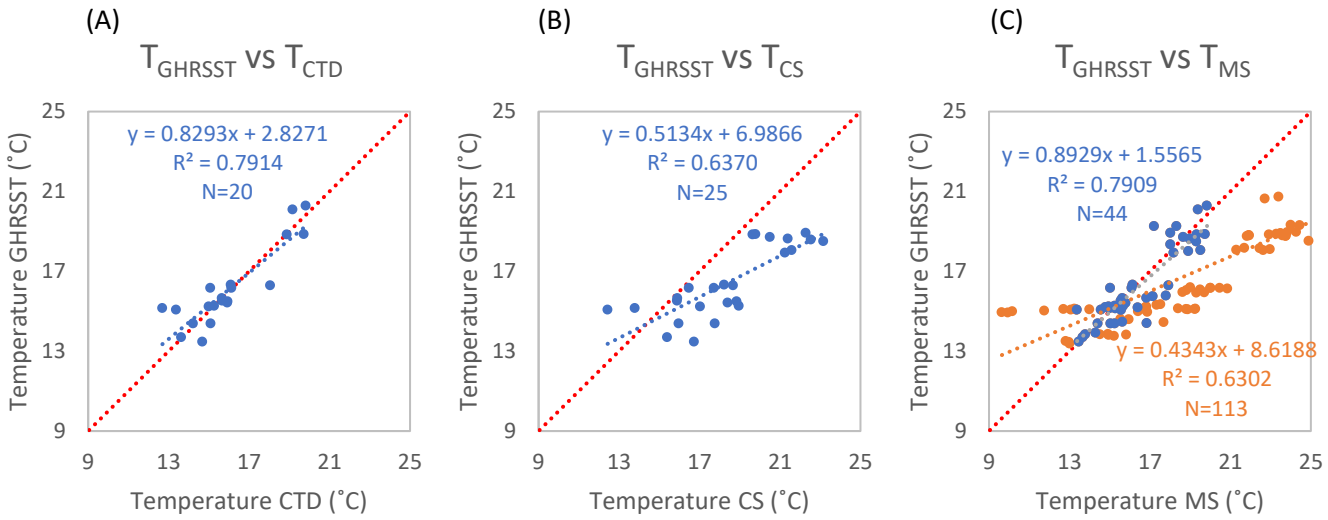

Figure 3.3. Correlation between the sea surface temperature data obtained with the satellite (GHRSST) and collected in situ during the campaigns with the CTD (A), the CS (B) and the MS (C) and considering only the stations located in the outermost area of the estuary (stns. #6, #7 and #8) in blue, and in orange, the set of all the stations. The red dashed line represents the slope 1 reference line.

The validation exercise involved a statistical assessment of the agreement between *in situ* and satellite data (Table 3.3). Therefore, the percentage of underestimated satellite measurements (*in situ* > satellite, %), the average difference of temperature between the equipments (*in situ - satellite*, ΔT) and the respective standard deviation are presented in Table 3.3. Lastly, the mean Relative Percentage Difference (RPD) and the mean Absolute Percentage Difference (APD) were also computed to allow a more intuitively understanding of the relationship between the datasets. RPD and APD were calculated according to equations 3.2 and 3.3.

Table 3.3. Relation between the temperature measured in situ and the satellite data, considering only stns. #6, #7 and #8 and the all set. % - percentage of underestimated satellite measurement (in situ>satellite); ΔT - average difference of temperature between the equipments (in situ-satellite); STD – ΔT Standard Deviation; RPD - mean Relative Percentage Difference; APD - mean Absolute Percentage Difference; N – number of inputs considered.

	Stns. #6, #7 and #8			**All the stations**
	CTD vs Satellite	CS vs Satellite	MS vs Satellite	MS vs Satellite
%	38.9	91.7	54.5	70.5
ΔT (˚C)	0.65	2.27	0.68	2.09
ΔT STD (˚C)	0.73	1.26	0.63	1.73
RPD (%)	0.93	-9.75	-1.14	-5.54
APD (%)	4.28	12.26	4.01	11.31
N	20	25	44	113

$$\mathrm{RPD} = \frac{1}{N}\sum_{i=1}^{N}\frac{[Sat]_i - [in\ situ]_i}{[in\ situ]_i} \times 100 \qquad [3.2]$$

$$\text{APD} = \frac{1}{N}\sum_{i=1}^{N}\frac{|[Sat]_i - [in\ situ]_i|}{[in\ situ]_i} \times 100 \quad [3.3]$$

In general terms, a good approximation between the values measured by these *in situ* instruments and those collected by the satellite was obtained. The best relation was found between the satellite and the CTD and the MS for stns. #6, #7 and #8 (the outermost stations of the estuary), with the RPD closer to 1 and -1 % for the CTD and MS, respectively, and the APD close to 4 % for both instruments. The RPD of the MS was negative because 54.5 % of the MS values were higher than the satellite. When considering the values obtained with the MS for all the sampling stations, a greater dispersion of the results and a lower agreement between the values can be seen. Therefore, it seems that the satellite provides more appropriate readings in the outermost region of the estuary, being less suitable for the interior area.

To confirm if there was any variation in the relationship between the temperature of the *in situ* instruments and the satellite along the estuary, the relation between the temperature data obtained by the MS with the values of the satellite was analyzed, since it had a greater spatial coverage than the other instruments, for each sampling station (Table 3.4).

Table 3.4. Correlation between the satellite and the MS data for each station, with the respective slope value and intersection of the linear regression line, the coefficient of determination (R^2) and the number of points used in the analysis (N).

MS vs Satellite

Station	Slope	Intersection	R^2	N
#1	0.4106	8.8829	0.7500	17
#2	0.4411	8.3891	0.7891	18
#3	0.5229	5.8211	0.8779	9
#4	0.0787	13.8080	0.1794	10
#5	0.3509	9.5358	0.5347	14
#6	0.9172	1.1779	0.8543	20
#7	1.0222	0.2404	0.8614	19
#8	0.7260	3.2966	0.6256	5

Based on the results presented in Table 3.4, the relationship between the satellite and the *in situ* values was better at stns. #6 and #7. When compared with the other stations, these two presented a higher R^2 and a better approximation to the reference line (slope of 1). This indicates a better approximation of the satellite values to the *in situ* ones of the outermost stations of the estuary, as stated before, through Figure 3.3. This behavior was also verified when the temporal variation of this parameter was analyzed at every station.

The temporal variation of *in situ* and satellite temperature values from March 2018 to September 2019 is presented in Figure 3.4. Only two stations (#1 and #7) were selected as examples. Stn. #1 is located in the inner zone of the estuary and stn. #7 is located in the outermost

area, representing two extremes of the estuary. The temporal variation of the temperature in the other sampling stations can be found in Annex VI.

For all the sampling stations, the *in situ* data followed the behavior of satellite data but with a difference in terms of absolute values. This difference seemed to decrease with the approach to the estuary mouth, given that for stns. #6 and #7, the temperature of the different instruments was similar through the sampling period, showing a very good agreement between the values. Also, through the example of stn. #1, it can be seen that the satellite's accuracy appears to be limited - during the months in which extreme temperatures are reached, the satellite values were more different in relation to the *in situ* ones, contrary to the verified during the rest of the months.

Therefore, it seems adequate to assume that the GHRSST dataset is acceptable for a thorough temporal analysis of the temperatures in the estuary, especially for the outermost part of the system.

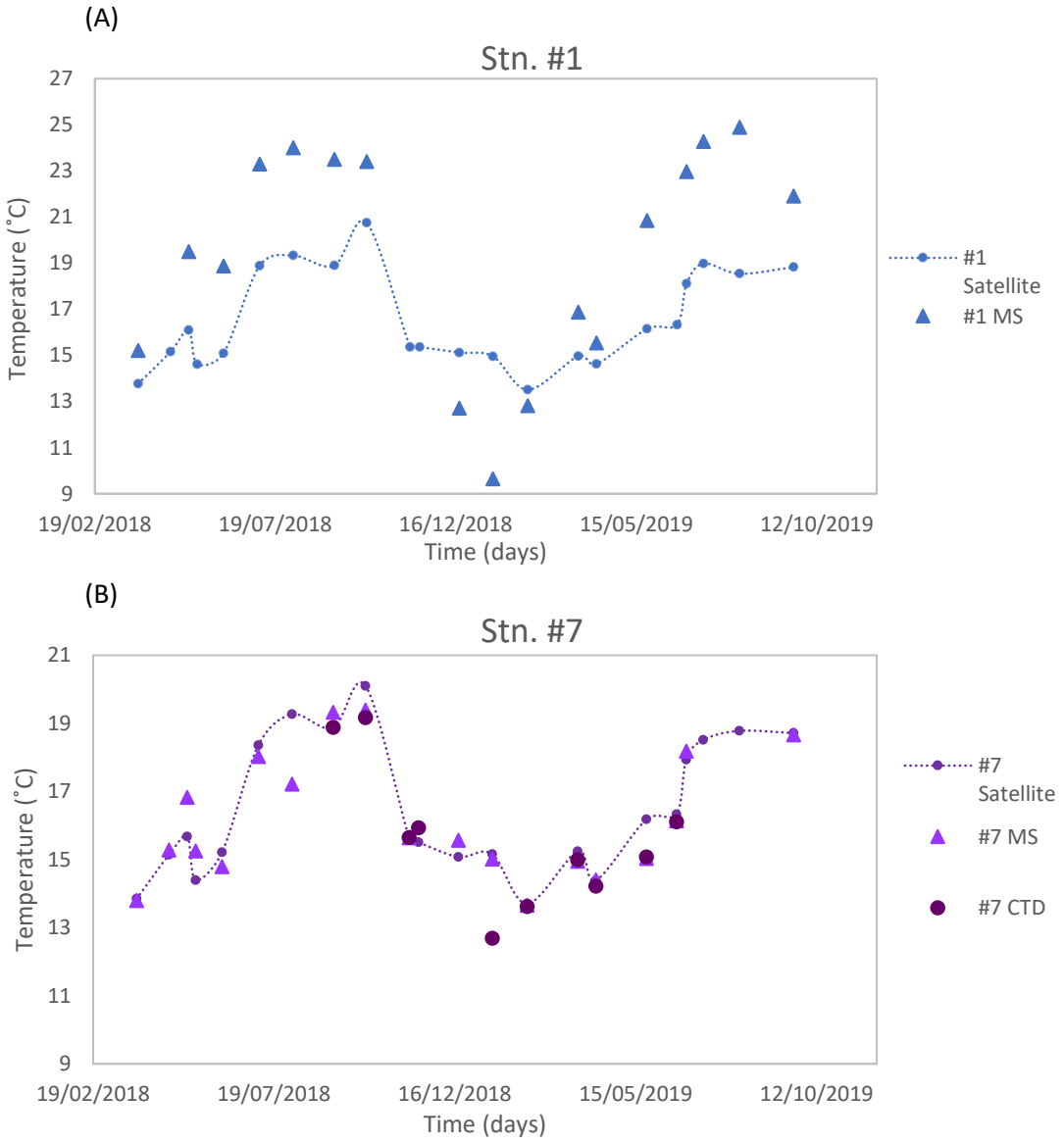

Figure 3.4. Temporal variation of the temperature data obtained with the CTD, the MS and satellite during the sampling campaigns in stns. #1 and #7.

3.3.1.2 Seasonal Variation

A seasonal evaluation of the SST in the Sado estuary was made through the mean SST value obtained for each season, at each sampling station (Table 3.5). The spatial mean, with the associated standard deviation, was also calculated for each season. Seasonally, as expected, summer and winter had the highest and lowest SST values, respectively.

Table 3.5. Average SST values (˚C) obtained for each season, every sampling station and the mean value for the set of stations with the respective standard deviation.

	Stations									
	#1	#2	#3	#4	#5	#6	#7	#8	**Mean**	**Standard Deviation**
Winter	14.48	14.51	14.46	14.44	14.51	14.48	14.49	14.51	14.48	0.88
Spring	16.31	16.32	16.32	16.32	16.32	16.25	16.17	16.24	16.28	1.07
Summer	18.89	18.90	18.89	18.89	18.90	18.85	18.79	18.86	18.87	1.62
Autumn	17.68	17.70	17.67	17.66	17.71	17.64	17.60	17.66	17.66	1.63

These seasonal variations are also represented in Figure 3.5, where it is possible to compare the temperature values obtained for the estuary with the temperature measured outside.

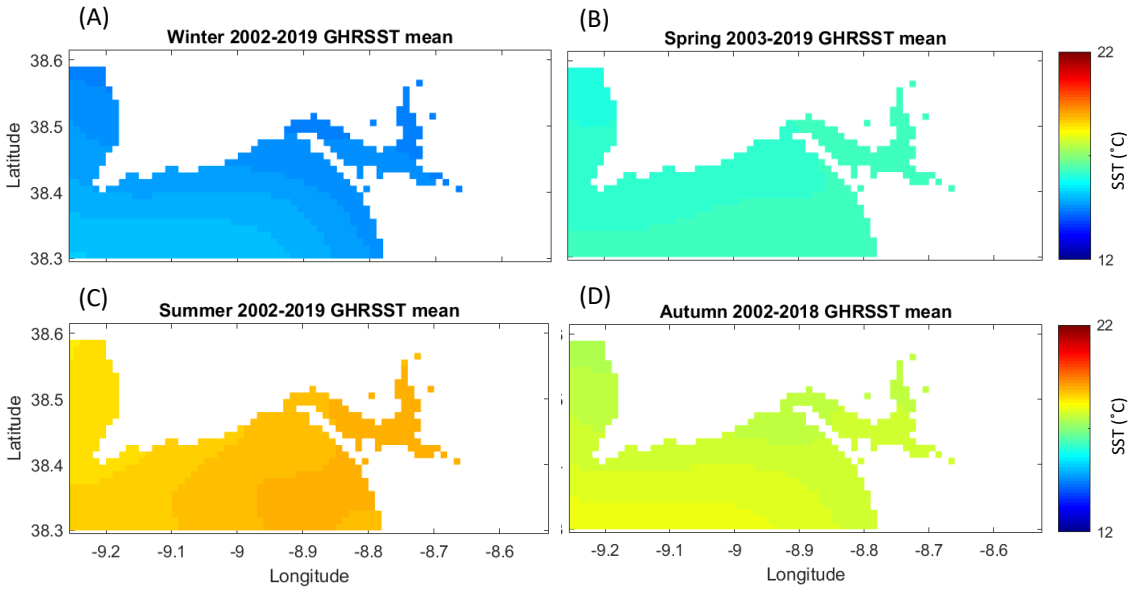

Figure 3.5. Distribution of the average sea surface temperature for each season, with data from 2002 to 2019 (GHRSST).

A gradient in the SST between the inner and outer zone of the estuary is noticeable in the GHRSST images used, although with a low thermic amplitude. During summer, the inner waters of the estuary presented higher SST values than the outermost zone of the estuary, and during

winter, the opposite seemed to be verified. However, this variation only occurred from 2008 onwards (except 2010). An example can be seen in Annex VII, where it is observable the SST variation throughout the year of 2008, 2010 and 2018, in one station from the inner area of the estuary (#1) and another from the outermost zone (#7), smoothed with a moving mean filter with a 15-day window. A clear thermal difference between the stations of the outermost zone and the inner zone of the estuary was also seen in 2010 (Annex VII), unlike the remaining years, when the values were observed to be similar.

In summary, a monthly analysis was performed considering the SST average estimated for the whole estuary (average of the 8 sampling stations), for each month from June 2002 to September 2019 (Figure 3.6). Figure 3.7 shows the intra-annual variation of the monthly SST variation in the estuary and the surrounding region. Monthly, the highest temperatures were verified in August and the lowest in February and, on average, there was a thermal amplitude of ≈ 5 ˚C over the annual period.

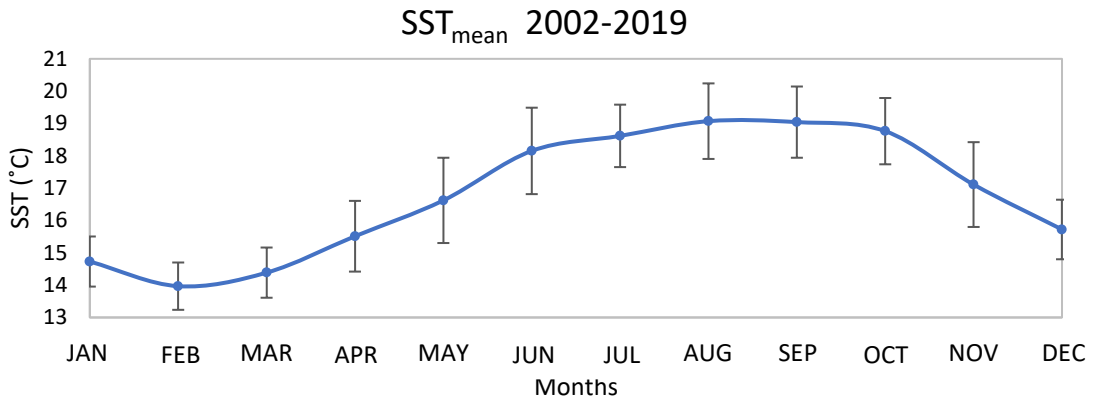

Figure 3.6. Mean SST values obtained for every month and the respective standard deviation, considering the data from June 2002 to September 2019.

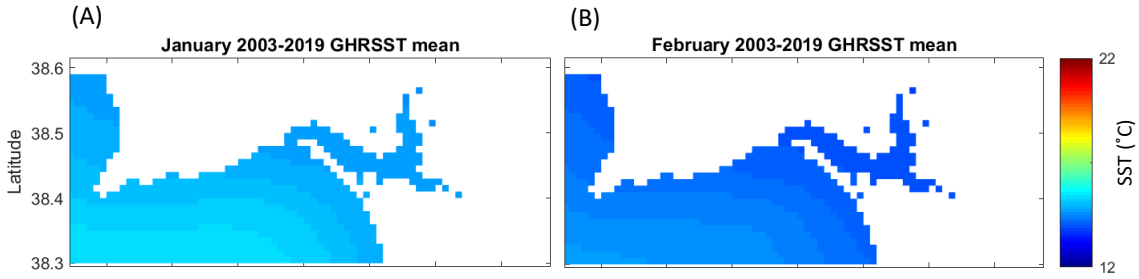

Figure 3.7. Distribution of the average sea surface temperature for each month with data from 2002 to 2019 (GHRSST).

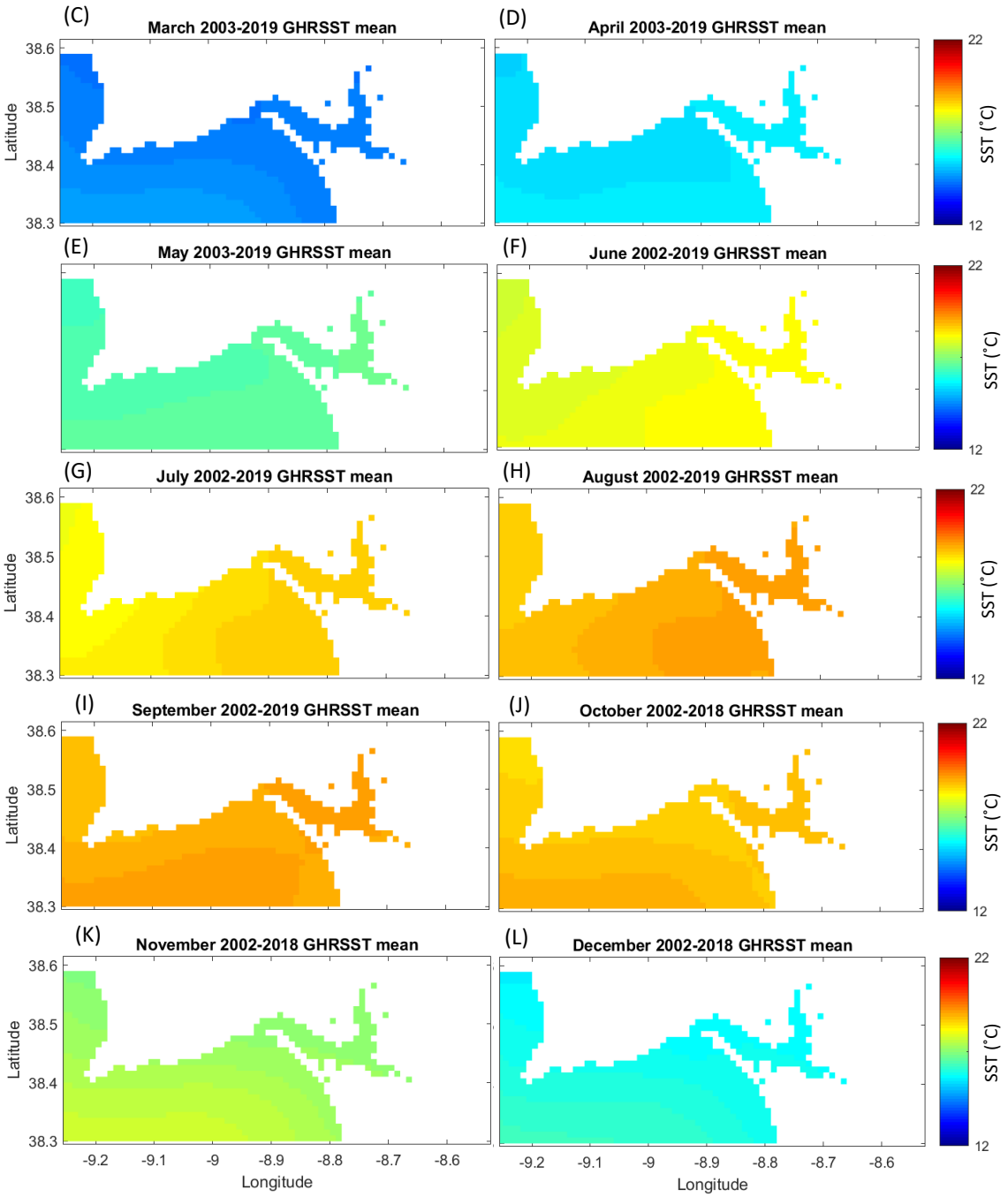

Figure 3.7 (continued).

3.3.1.3 Interannual Variation

All satellite-derived SST data were used to evaluate its interannual variation and possible anomalies. This analysis considers data from June 2002 to September 2019 (Figure 3.8).

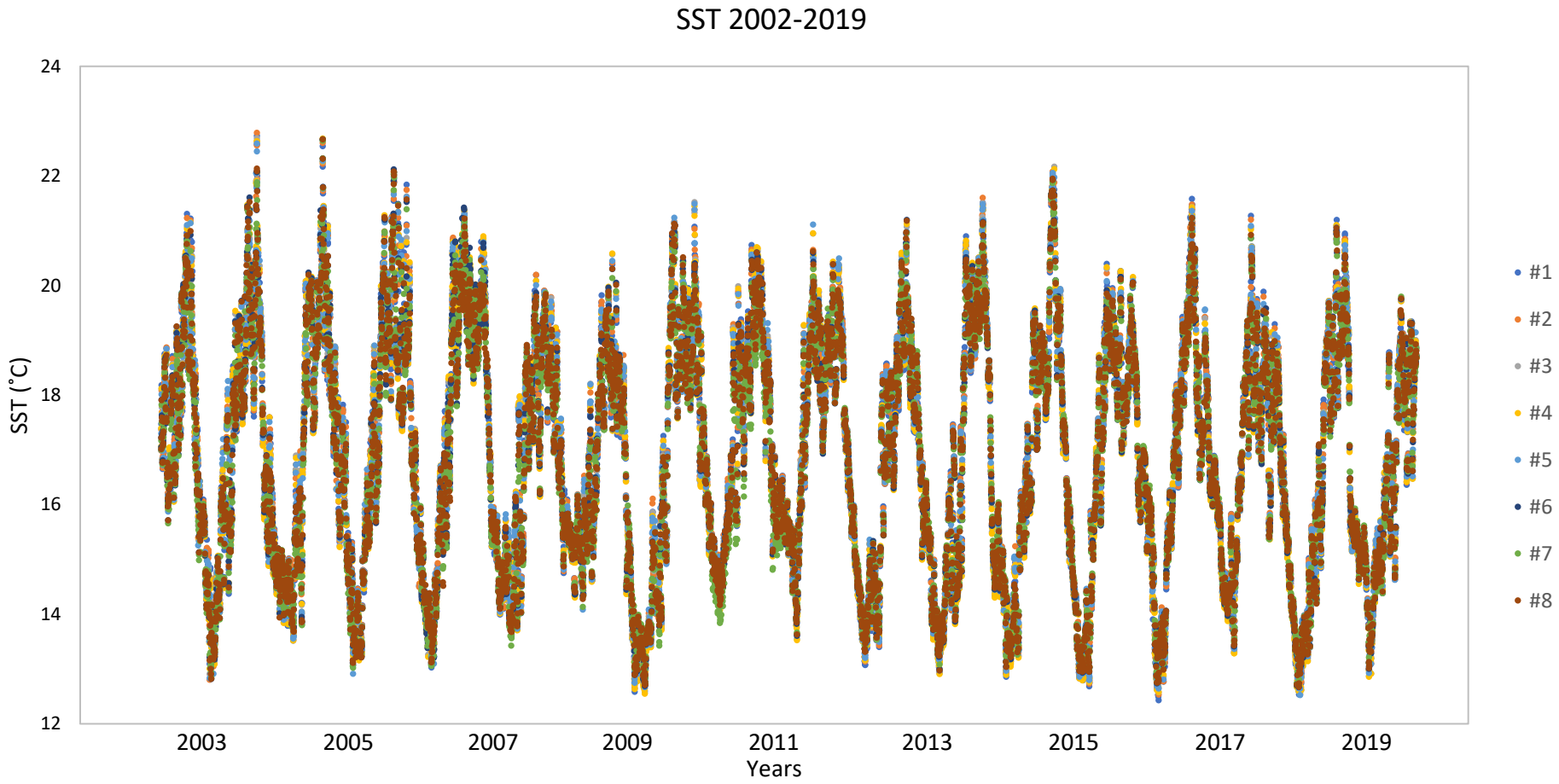

Figure 3.8. Temporal variation of the SST data (GHRSST) over the period considered (June 2002 - September 2019).

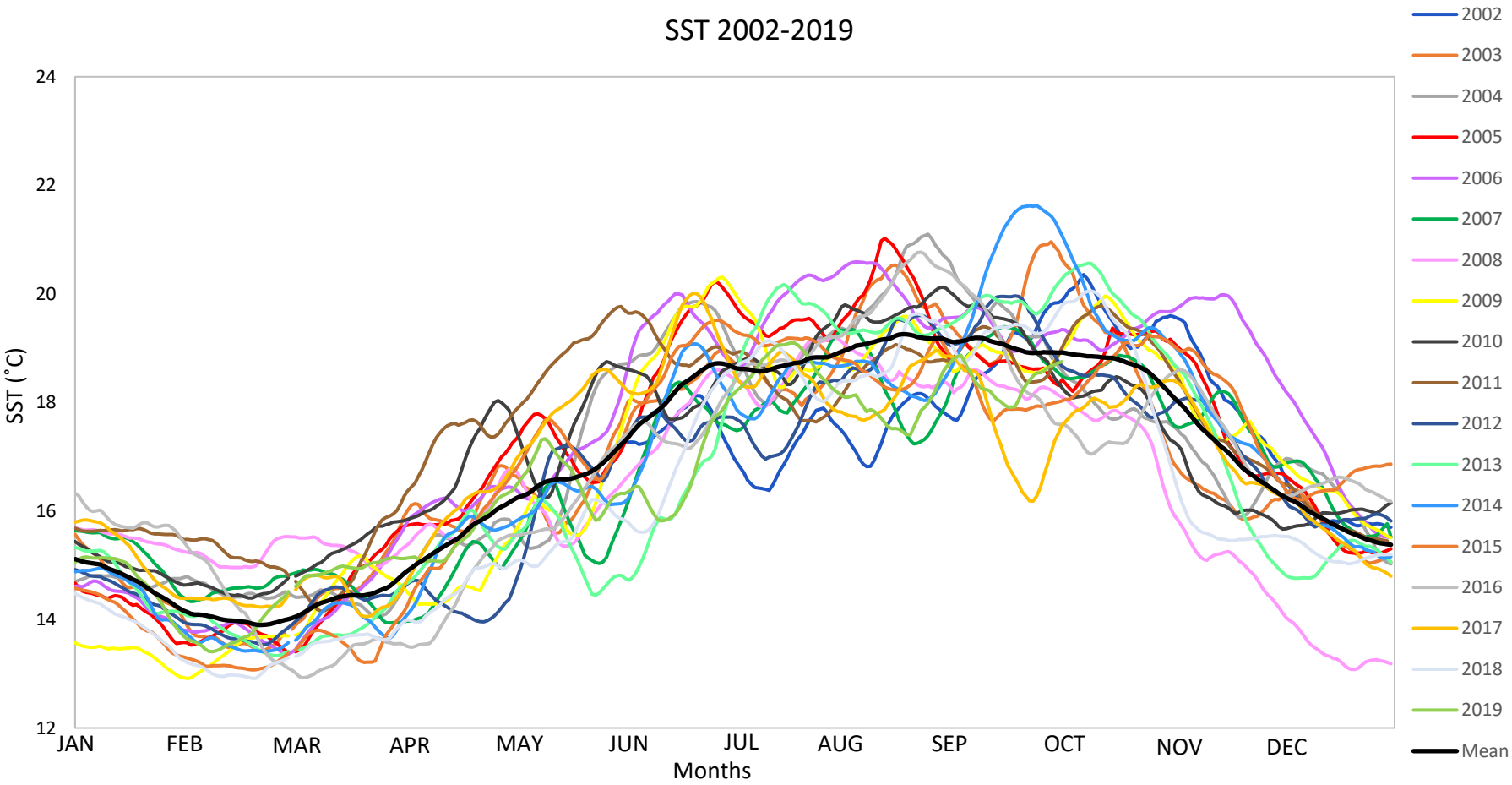

Figure 3.9. Temporal variation of the annual sets of SST data (GHRSST) obtained from June 2002 to September 2019, smoothed with a moving mean filter with a 15-day window.

The 18-year analysis made, detected annual cycles with bigger temperatures observed during summertime and minimum temperature values during winter. Over time, some relevant oscillations could be observed. Of note are the maximum temperatures that occurred in 2003 and 2014 (≈ 23 ºC), years with the biggest thermic amplitudes, and the highest minimum temperatures observed in 2007, 2008 and 2010, characterized by having much lower maximum temperatures as well.

The difference of the values between the stations is very low, on average 0.31 ˚C between the station with the maximum and the minimum value (Figure 3.8). Therefore, this low spatial variability of the satellite-measured SST, makes appropriate to consider the average of the stations as the value of the whole estuary (although it was observed a seasonal change of the behavior between the inner and outermost stations of the estuary, as mentioned in the previous section). Therefore, the estuary is considered as a whole from this point forward.

Also, as there were several years of data being analyzed, there was an interest in overlapping the different annual series and compare the variation of the SST values over the course of each year (Figure 3.9). Figure 3.9 was obtained by filtering the data using a moving mean with a 15-day window, to remove the irregular oscillations present in every annual series, that is, the frequent fluctuation of the values that appeared to have a frequency of about 7 days. Also, the background noise was removed and the clarity of the seasonal pattern was improved. This window was chosen because it is the period between spring and neap tides and to allow a greater attenuation of the oscillation observed.

With the overlap of the different annual series observable in Figure 3.9, it can be concluded that through the period of study, the temperature behavior was similar. However, some irregularities stood out. An example was the autumn and winter of 2008, with much lower SST values than the other years, achieving almost less 2º C than the second year with lower temperatures. On the other hand, the winter of 2015/2016 had the highest temperature values. During spring 2011 is worth mentioning the high temperatures that were recorded and, of note, is also the high STT values obtained for the summer of 2006, that continued to stand out throughout the autumn. 2002 was presented as the year with the lowest temperatures during summer.

The spatial variation of the SST in the estuary throughout the years, from 2003 to 2018 is presented in Figure 3.10. The data from 2002 and 2019 were not considered in this analysis because they did not consider entire years.

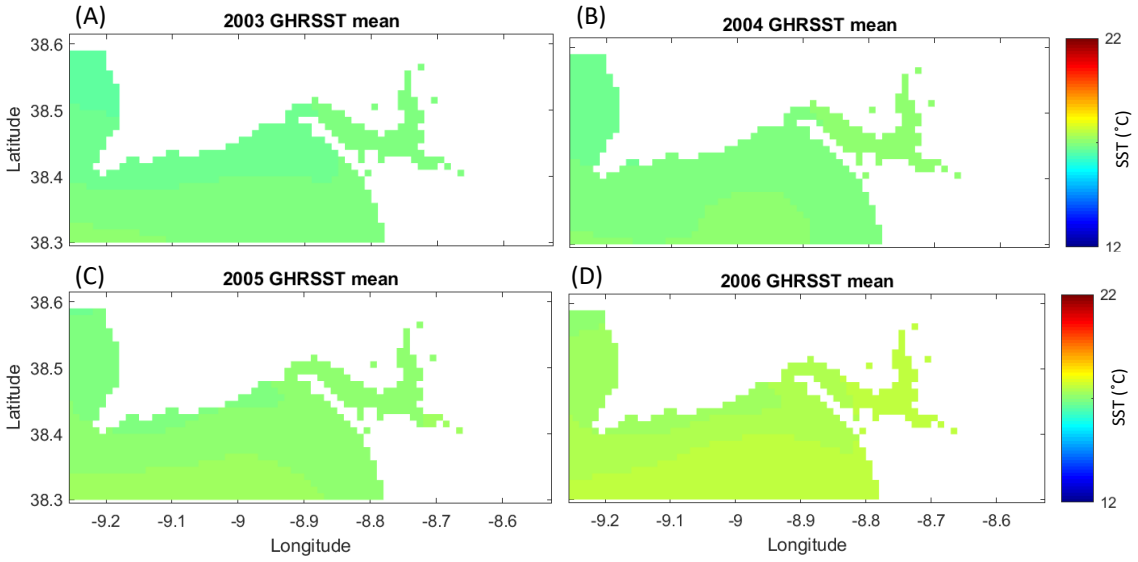

Figure 3.10. Distribution of the average sea surface temperature for each year, from 2003 to 2018 (GHRSST).

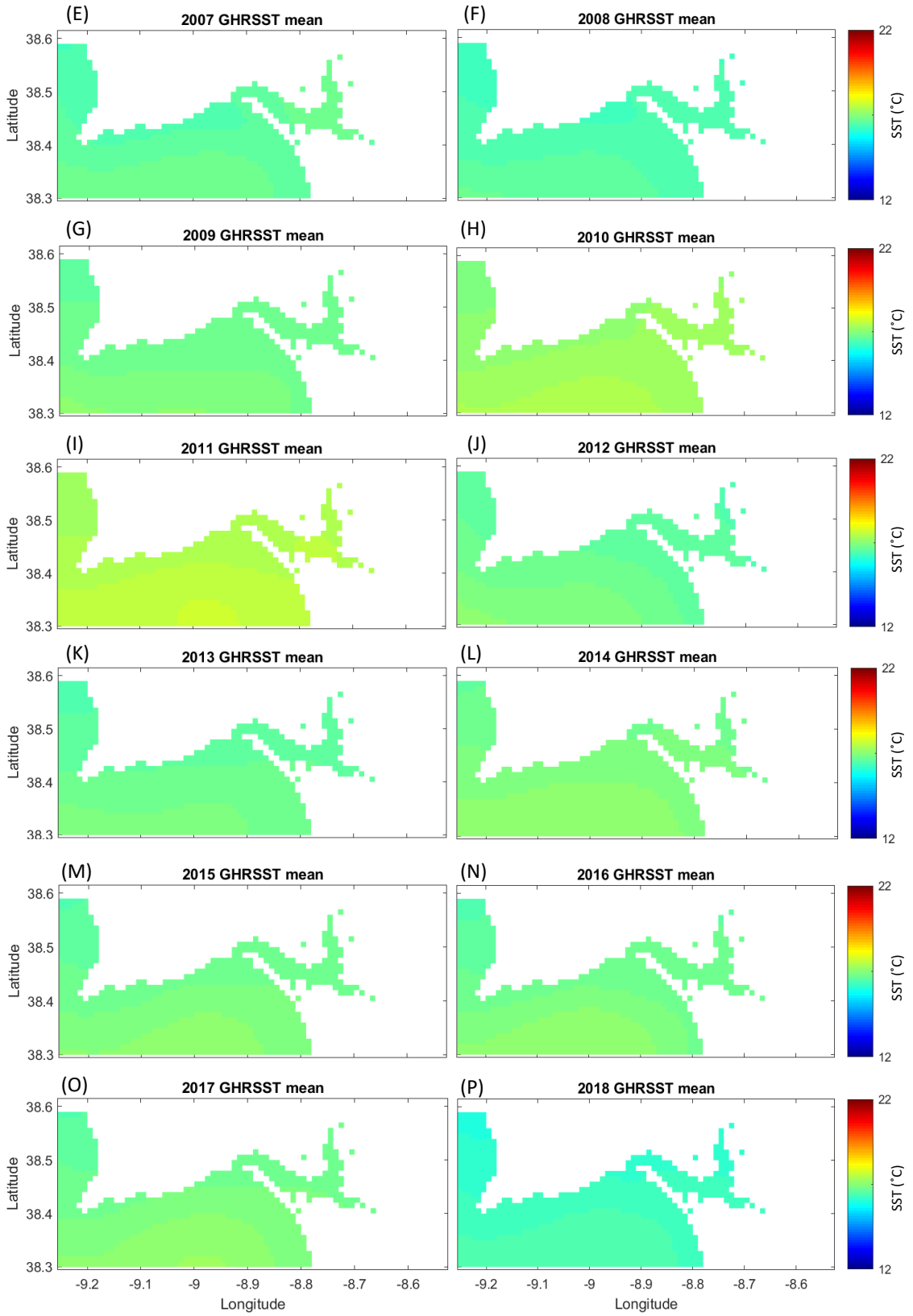

Figure 3.10 (continued).

The representation of Figure 3.10 allows the comparison between the values observed inside the estuary with the ones obtained for the adjacent region, the coastal zone. Is possible to observe that there are no relevant differences between the temperature inside and outside the estuary (Figure 3.10). Furthermore, within the estuary itself, it is difficult to observe a spatial variation of the SST. However, it is possible to see that 2006, 2010 and 2011 were the years with the highest temperature values recorded. Also, it is noticeable that the temperature in the interior of the estuary had lower values than the surrounding region particularly in 2008 and 2012.

The annual temperatures inside the estuary ranged between 16 and 18 ºC, being, usually, close 17 ºC, between 2003 to 2018 (Figure 3.11). The years with higher and lower values of SST according to the figure, agree with what was observed in Figure 3.10. Also, it is possible to see a trend towards a decrease of the temperature of the estuary in the past years.

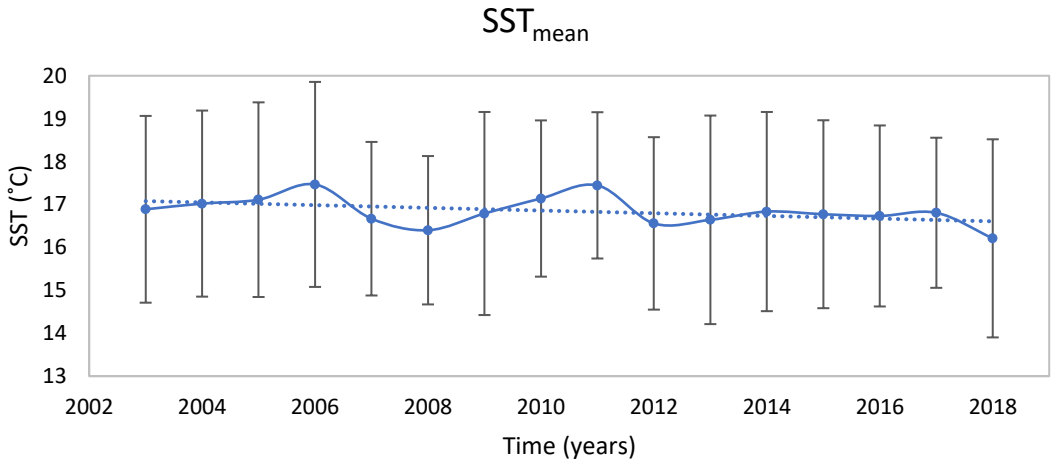

Figure 3.11. Annual SST values obtained for the estuary (from the average of the sampling stations), since 2003 to 2018.

Figure 3.12 shows the SST annual anomalies obtained for every sampling stations between 2003 to 2018. Higher temperature anomalies were observed in the years of 2006 and 2011 (Figure 3.12) for all stations evaluated in the Sado estuary. This is in agreement with the analysis of the annual averages (Figure 3.9). 2006 was a year with high temperatures across several months. However, 2011 yielded higher temperatures especially during the first part of the year, until the summer, which was not particularly hot. On the other hand, the year with the strongest negative anomaly was 2018 (Figure 3.12). However, while until 2011 the signal of the anomalies tended to vary, from 2012 onwards a negative anomaly in almost the entire estuary was registered. Spatially, it appears that in some years, like 2003 or 2006, there was a slight differentiation in the anomalies of the outermost stations of the estuary (stns. #6, #7 and #8) when compared with the others, but in general, there was a uniform behavior along the estuary.

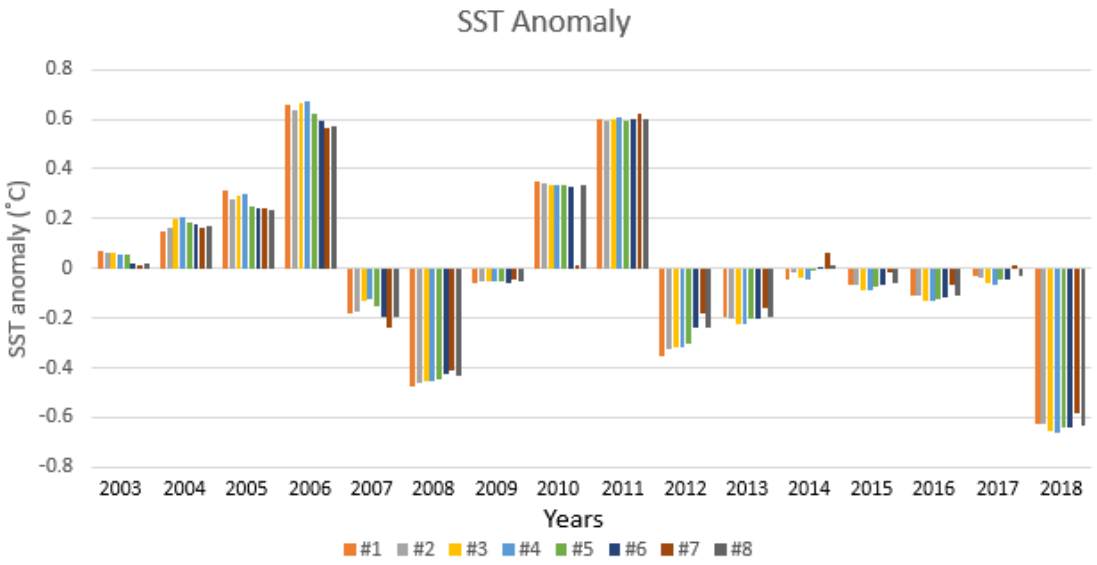

Figure 3.12. Annual SST anomalies verified since 2003 to 2018, for every sampling station, considering the reference for each one of the stations as the mean of the SST obtained for each station between 2003-2018.

From the data gathered (June 2002 - September 2019), an average value for the SST of 16.86 ˚C for the Sado estuary was obtained. Figure 3.13. represents this result and the engaging area.

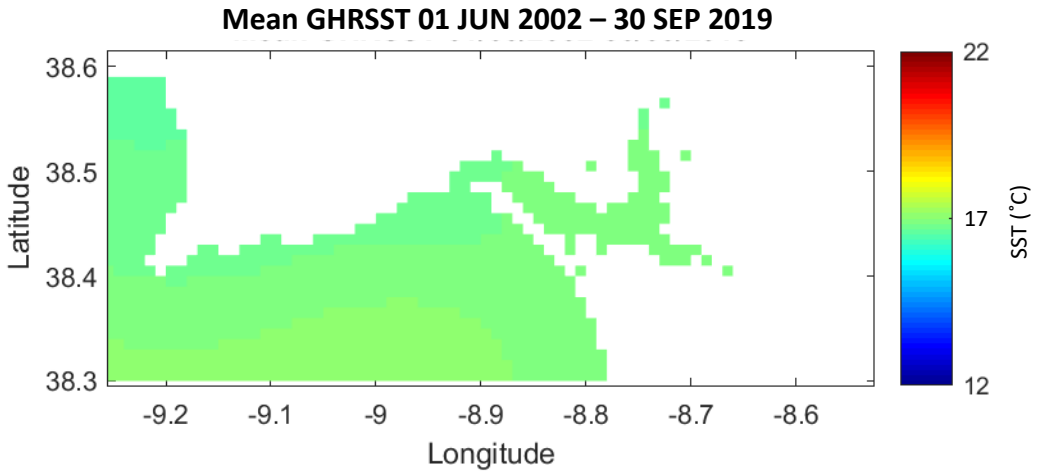

Figure 3.13. Distribution of the average sea surface temperature considering the data from June 2002 to September 2019 (GHRSST).

3.3.2 Satellite-derived Chlorophyll *a* concentrations

The MERIS database, has a better spatial resolution for the area of Sado estuary than other sensors such as MODIS, as already mentioned. However, it only presented 802 valid daily images, of a set of 2,607, from September 2002 to April 2012 (Table 3.6). Sentinel-3 OLCI collected 304 images of the estuary throughout the year of 2018 but only 159 were considered valid (Table 3.6). These images were assumed as invalid when they did not present values in any of the 8 sampling stations or if there were several records for the same day (overlap of satellite passage). In this last case, the image with more stations with data was considered the valid one for the day. The validation of the Sentinel-3 data was made using the 18 chlorophyll *a* values obtained after applying the flag filter in the images corresponding to the days the sampling campaigns occurred, as previously specified in section 3.2.2 (Table 3.7).

Therefore, these databases allowed performing a temporal analysis of the chlorophyll concentrations throughout the estuary considering the number (N) of valid images described in Table 3.6 for each period.

Table 3.6. Number of MERIS and Sentinel-3 images (N) used in the different periodic analyzes.

MERIS

Month	N
January	61
February	61
March	57
April	47
May	52
June	59
July	83
August	92
September	71
October	75
November	67
December	77
	802

Year	N
2002	7
2003	50
2004	65
2005	56
2006	86
2007	118
2008	104
2009	109
2010	88
2011	83
2012	36
	802

Season	N
Winter	244
Spring	209
Summer	193
Autumn	156
	802

Sentinel-3 (2018)

Month	N
January	11
February	12
March	7
April	11
May	16
June	15
July	13
August	14
September	16
October	16
November	13
December	15
	159

Season	N
Winter	31
Spring	42
Summer	43
Autumn	43
	159

Table 3.7. Sampling dates and respective stations in which valid chlorophyll a data was obtained.

Sampling Dates	Stations
08 NOV 2018	#5, #6, #7, #8
16 NOV 2018	#3, #5, #6, #8
14 FEB 2019	#3, #5, #6
28 MAR 2019	#3, #5, #6, #7
12 APR 2019	#3, #5, #7

3.3.2.1 Data Validation

Sentinel-3 OLCI data were validated to understand the viability of these data for current studies and to be able to proceed with a more consistent characterization of the chlorophyll *a* distribution along the estuary.

Therefore, satellite-derived chlorophyll *a* concentrations (Neural Net algorithm, Chla NN) were compared with the *in situ* values (Chla *in situ*). A low agreement between the datasets was observed (Figure 3.14 – A). This comparison seems to indicate a tendency to an overestimation of the concentrations derived from the satellite, when compared with the *in situ* data. Also, the values obtained during the campaign conducted in November 8 were evidenced by their deviation from the slope line and, when removed, it could be seen that they badly affected the relation between the data series (Figure 3.14 – B). Although it is still observable the satellite overestimation, the datasets seem to maintain a more consistent relationship, with less dispersion of the values.

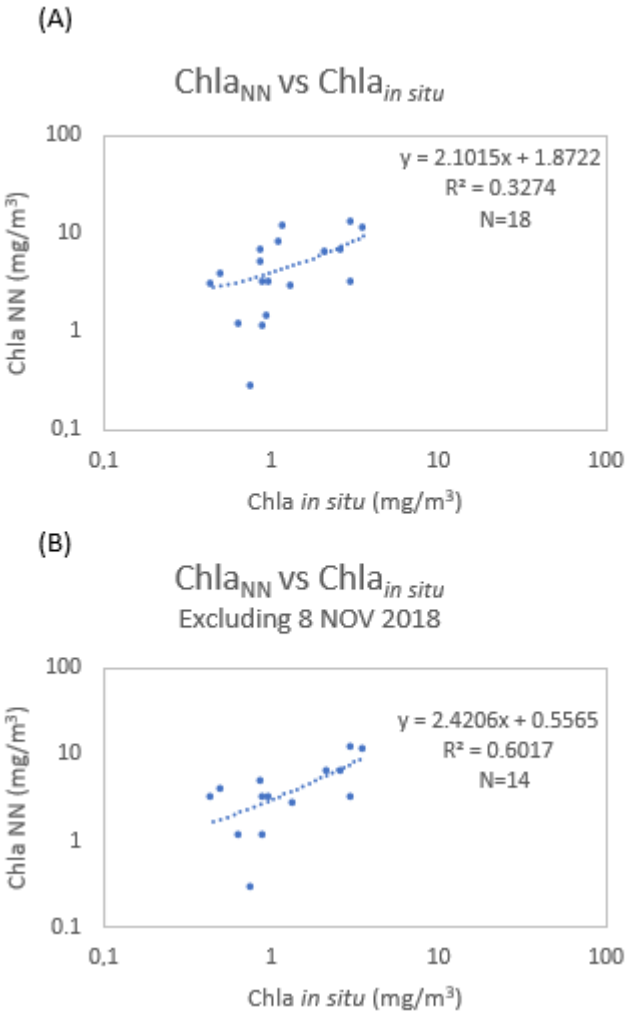

Figure 3.14. Correlation between the chlorophyll a concentration obtained with the satellite and in situ. In A is considered the whole set of data and in B the set containing data from November 16, February, March and April.

Interestingly, it was observed that the 8 of November was a day with increased values of suspended particle matter (SPM) in the Sado estuary. As this could affect the signal in the visible spectra, and, therefore, affect the overall estimation of chlorophyll *a*, SPM data was gathered from AQUASADO project to investigate its influence in the satellite-derived chlorophyll *a* concentrations. So, the relation between the absolute chlorophyll error (|Chla NN – Chla *in situ*|) and the SPM obtained during the *in situ* campaigns is presented in Figure 3.15. Although not high, it is possible to find a relation between these two parameters: bigger differences between the chlorophyll values seem to be associated with higher SPM values. Also, for equal error values, higher SPM values were obtained during the campaign of 8 of November (represented in Figure 3.15 in orange). These values were particularly high, possibly due to high levels of precipitation and of river runoff that may have occurred during that period. Additionally, it was not found any relation between the SPM and the *in situ* chlorophyll *a* concentrations. This gives a preliminary indication that SPM could play a relevant role in the chlorophyll *a* estimation from satellite.

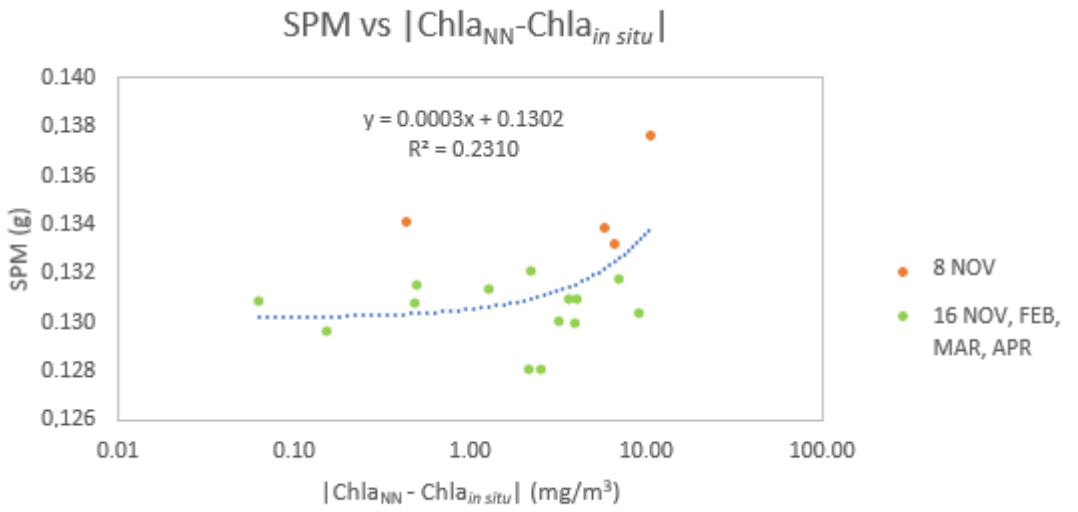

Figure 3.15. Relation between the in situ SPM and the absolute chlorophyll error (|Chla $_{NN}$ – Chla $_{in\ situ}$|). The set containing data from November 16, February, March and April is represented in green and November 8 in orange.

Additionally, when these Sentinel-3 images were projected, the data presented the spatial distribution that can be observed in Figure 3.16. In light grey are the pixels covered by the flag filter and in dark grey the land pixels.

By observing the results obtained with Sentinel-3 (Figure 3.16), it was possible to see that the data presented a good spatial resolution, allowing to conclude about the distribution of chlorophyll along the estuary. From Figure 3.16, it was possible to observe that the channels of Marateca and Comporta tended to present a higher concentration of chlorophyll *a* than the rest of the estuary. In the first campaign of November, high values of chlorophyll were observed in the estuary, but they seemed to be abnormally high for the time of year. The large portion of land covered by grey pixels in this day may also be an indication of atmospheric problems. In fact, the previous validation analysis, showed a low agreement between the satellite and the *in situ* values obtained during this campaign (Figure 3.14).

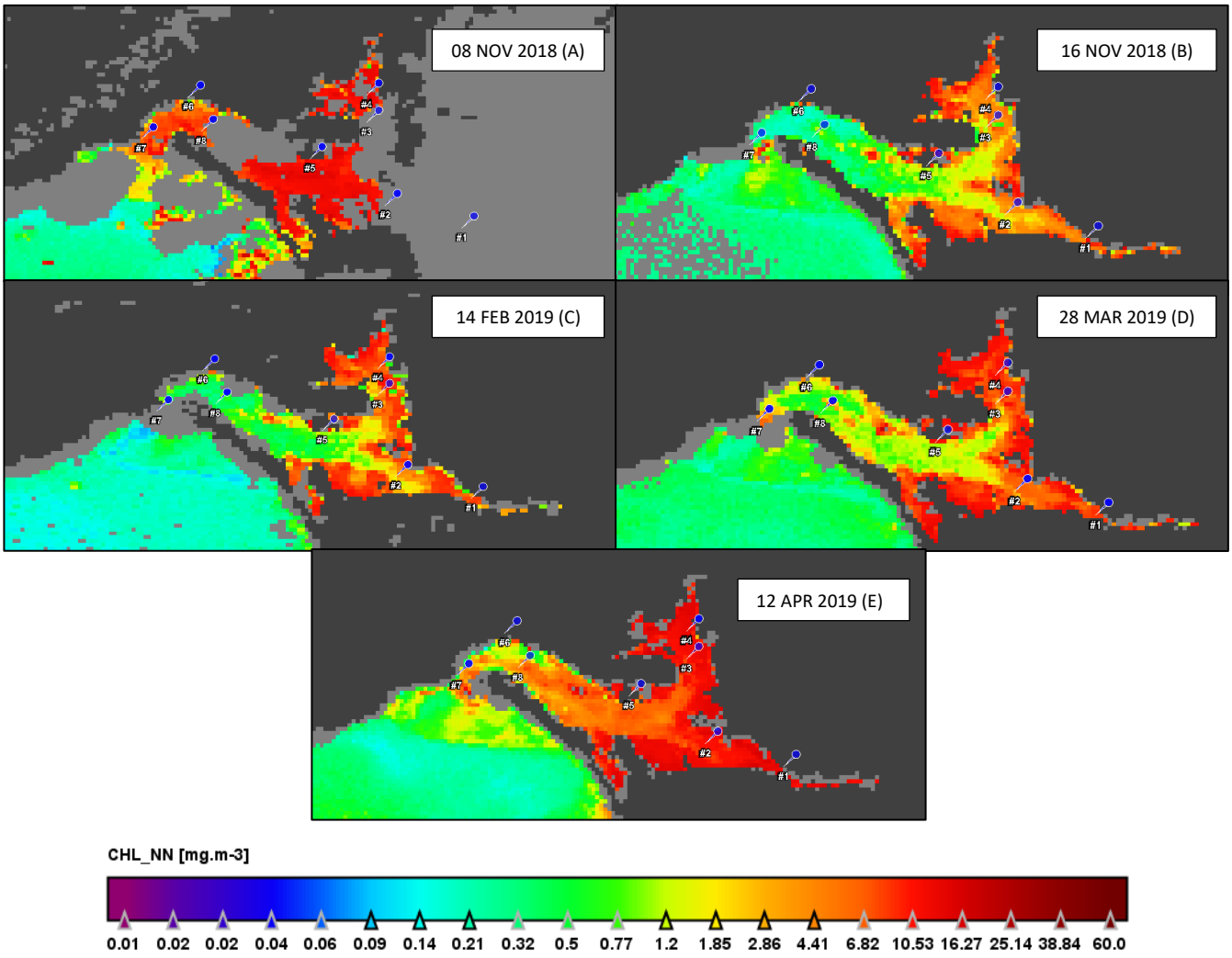

Figure 3.16. Distribution of the chlorophyll a concentration in the Sentinel-3 images that were considered acceptable for validation with in situ data.

3.3.2.2 Seasonal Variation

In this section, the results obtained with MERIS and OLCI on the seasonality of the chlorophyll *a* in the estuary are presented following a chronological approach.

Regarding MERIS, the concentration of chlorophyll *a* (Chla: mg/m^3) obtained for each season and at each station is shown in Table 3.8, where is mentioned the number of images with valid values that were considered (N). In addition, the seasonal average for the whole estuary and the respective standard deviation are also presented (Table 3.8). Stns. #1 and #6 were not considered in MERIS seasonal analysis, as they were located very close to the coast. High concentrations of chlorophyll *a* were observed during spring. Interestingly, concentrations observed during winter were also high (Table 3.8 and Figure 3.17). It is also possible to highlight higher values of chlorophyll *a* at stns. #2, #3 and #4, compared to the other stations. On the other hand, the highest concentrations of chlorophyll *a* were observed during spring and summer in the coastal zone (Figure 3.17).

Table 3.8. Average chlorophyll a values (mg/m^3) obtained for each season, every sampling station and the mean value for the set of stations, with the respective standard deviation (MERIS). N is the number of images considered.

	Stations													
	#2		#3		#4		#5		#7		#8			
	Chla	N	Chla	N	Chla	N	Chla	N	Chla	N	Chla	N	**Mean**	**Standard Deviation**
Winter	4.57	153	4.36	145	4.87	124	2.58	4	2.27	140	3.19	172	3.64	3.19
Spring	4.74	104	4.43	89	4.57	83	5.78	1	3.27	82	3.69	118	4.41	3.19
Summer	4.42	182	4.09	158	4.10	131	3.35	3	2.05	161	2.81	203	3.47	3.56
Autumn	3.98	161	4.18	141	4.14	131	3.25	3	2.09	145	2.87	167	3.42	2.80

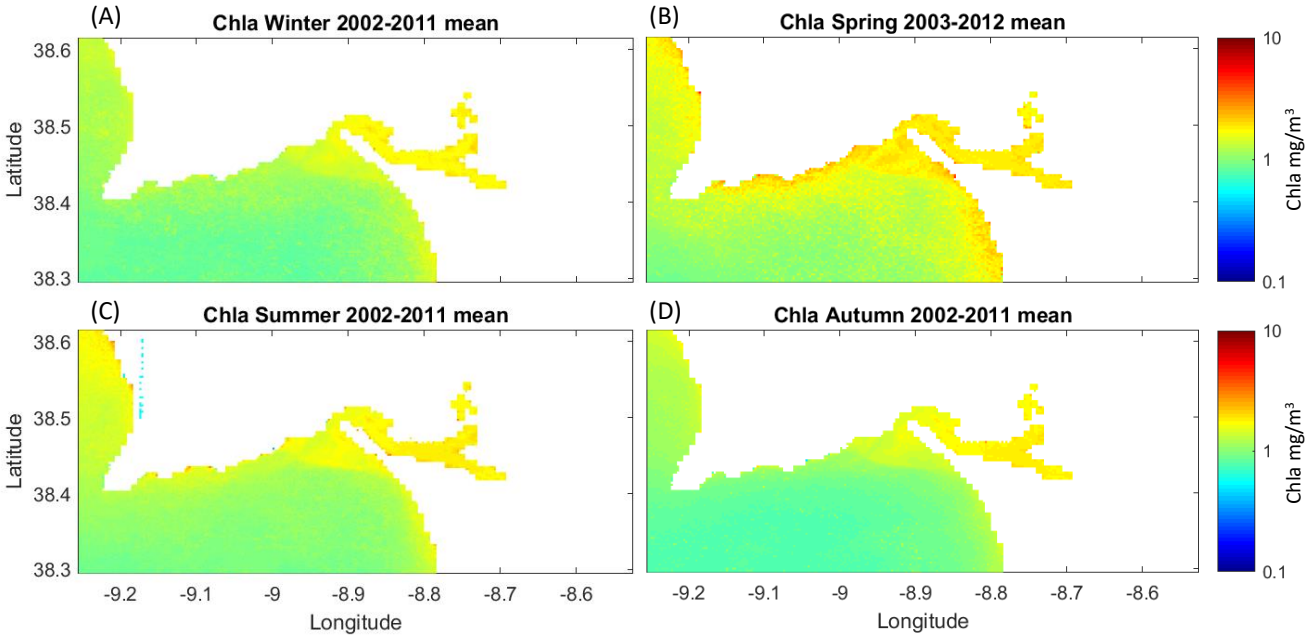

Figure 3.17. Distribution of the average chlorophyll a concentration obtained for each season (MERIS).

The variation of the chlorophyll *a* distribution in the estuary throughout the year and considering the monthly averages obtained for the estuary (through the average of the 8 sampling stations) is shown in Figures 3.18 and 3.19. The results showed in these images display similarities with the previous ones (Table 3.8 and Figure 3.17). There were low values in the estuary during the summer months comparing with spring and winter, unexpectedly, as summer is generally a season of high productivity in estuaries. In the coastal ocean, it was during the winter months that the chlorophyll *a* concentrations were the lowest and during spring and summer that they were the highest (Figure 3.19).

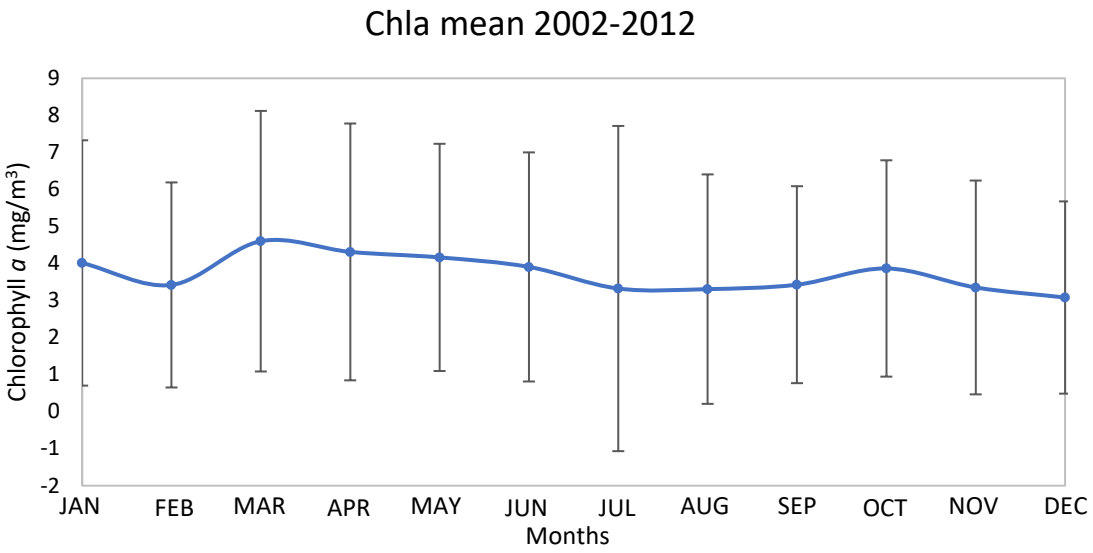

Figure 3.18. Distribution of the average chlorophyll a concentration obtained for each month (MERIS).

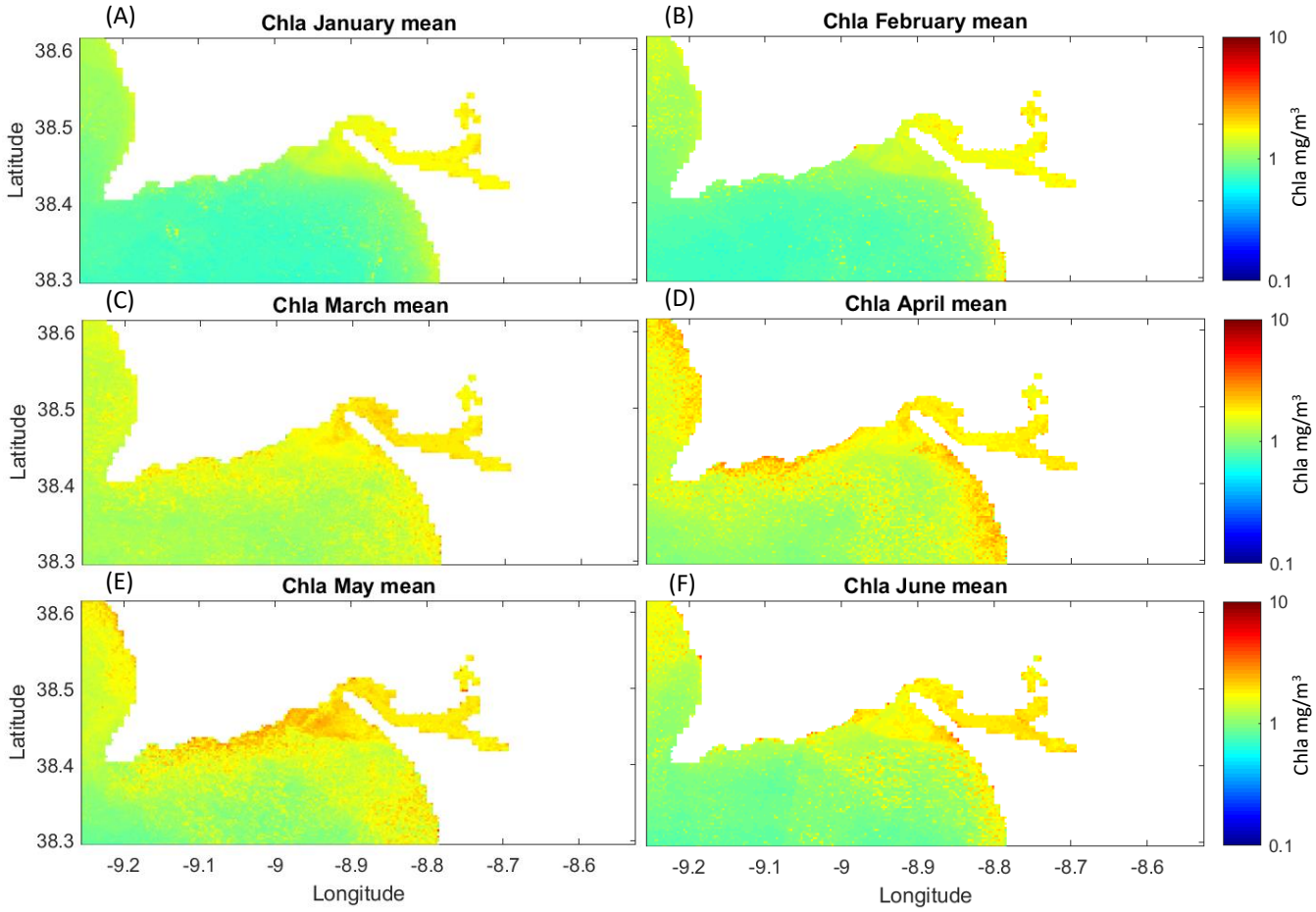

Figure 3.19. Distribution of the average chlorophyll a concentration obtained for every month (MERIS).

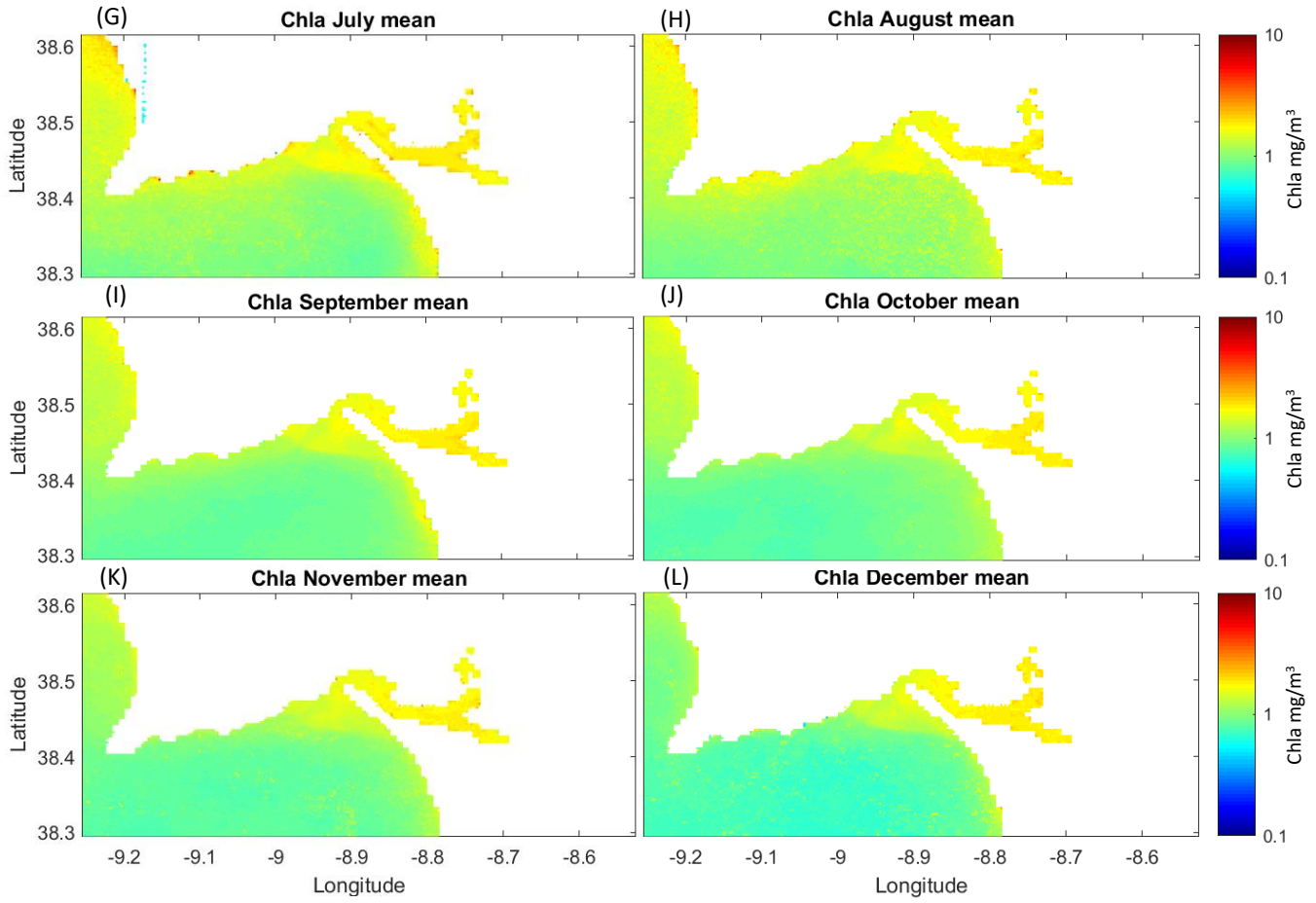

Figure 3.19 (continued).

In order to give continuity to the time series obtained with MERIS that covers the years 2002-2012, a temporal characterization of the chlorophyll *a* for the year of 2018 was also performed with OLCI data (Sentinel-3) (Figure 3.20). The chlorophyll *a* concentrations obtained for the period between January and December 2018 ranged between 0 and 21 mg/m^3 and tended to vary a lot (Figure 3.20). However, the data seemed to present a slight sign of seasonality, with higher values emerging in April. From Figure 3.20, it is possible to observe a spatial differentiation of the chlorophyll values over the year, given the clear difference existing between the stations of the inner region of the estuary (represented in orange) and those in the outermost area (represented in blue). The mean value obtained from the set of stations is also represented in Figure 3.20 and appears to delimit the two regions of the estuary. This spatial variability is more evident in Table 3.9, where the average values obtained for the year 2018 at each station are presented. This estuarine area appeared to yield increasing values of chlorophyll *a* from the mouth of the estuary towards its interior and seemed to present a clear separation of the outermost region (#7 and #8) and the area of the interior of the channels (#1, #2, #3 and #4), as already observed in Figure 3.20.

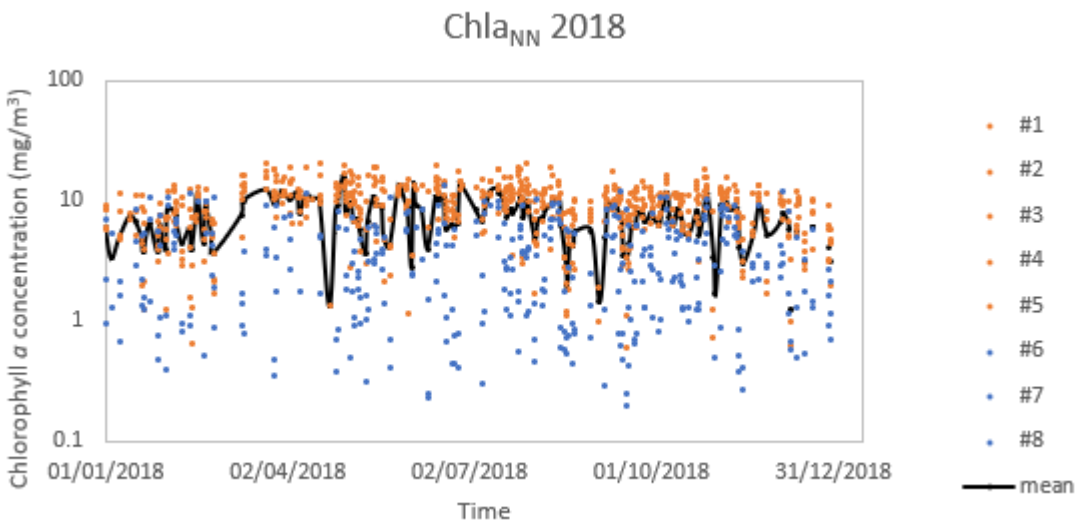

Figure 3.20. Temporal variation of chlorophyll a concentration at the 8 sampling stations using Sentinel-3 data (Neural Net algorithm) for the year of 2018. In orange are represented the stations of the inner zone of the estuary (#1, #2, #3, #4 and #5) and in blue the stations of the outermost region (#6, #7 and #8).

Table 3.9. Spatial variation of chlorophyll a concentration obtained at the 8 sampling stations using Sentinel-3 data (Neural Net algorithm) considering the mean value for 2018 at each station.

Stations	**Mean chlorophyll *a* concentration (mg/m^3) 2018**
#1	9.74
#2	9.94
#3	8.67
#4	10.22
#5	8.13
#6	5.68
#7	3.02
#8	2.87

The apparent seasonality shown in Figure 3.20, was studied following an integrated approach in order to visualize the patterns more clearly (Table 3.10). The average chlorophyll values (Chla) obtained at each sampling station every season, with the reference to the respective number of images used (N), is presented in Table 3.10. Also, in Table 3.10 is the mean seasonal value for the set of stations and its respective standard deviation. Is possible to see a seasonal variation of the chlorophyll concentration in the estuary for the year of 2018, with a great variability in the region of the most interior stations (Table 3.10). Additionally, winter is the season of the year with the lowest chlorophyll values along the estuary, while spring and summer

are the seasons with the most chlorophyll concentration. This behavior is also observed in the monthly averages presented in Figure 3.21. The winter months were those characterized by lower chlorophyll values. These results were different from the results obtained with the study of MERIS database. The monthly disparity between the two datasets (MERIS vs OLCI) can be easily observable (Figure 3.22) and is statistically significant (based on a paired t-test).

Table 3.10. Average chlorophyll a values (mg/m^3) obtained for each season, every sampling station and the mean value for the set of stations, with the respective standard deviation (data from Sentinel-3 for 2018). N is the number of images considered.

	Stations																	
	#1		#2		#3		#4		#5		#6		#7		#8			
	Chla	N	Chla	N	Chla	N	Chla	N	Chla	N	Chla	N	Chla	N	Chla	N	**Mean**	**Standard Deviation**
Winter	7.46	25	6.92	25	6.08	23	7.63	23	7.31	21	6.00	22	3.16	23	2.19	21	6.00	2.15
Spring	12.63	37	12.82	32	10.78	31	11.28	32	9.06	24	5.61	27	3.27	28	2.89	28	8.95	3.05
Summer	8.42	39	9.65	41	9.20	39	11.26	39	8.20	35	5.60	35	2.67	39	3.05	38	7.44	2.87
Autumn	9.77	33	9.81	35	7.92	36	9.78	34	7.90	32	5.62	32	3.10	38	3.07	37	6.92	2.41

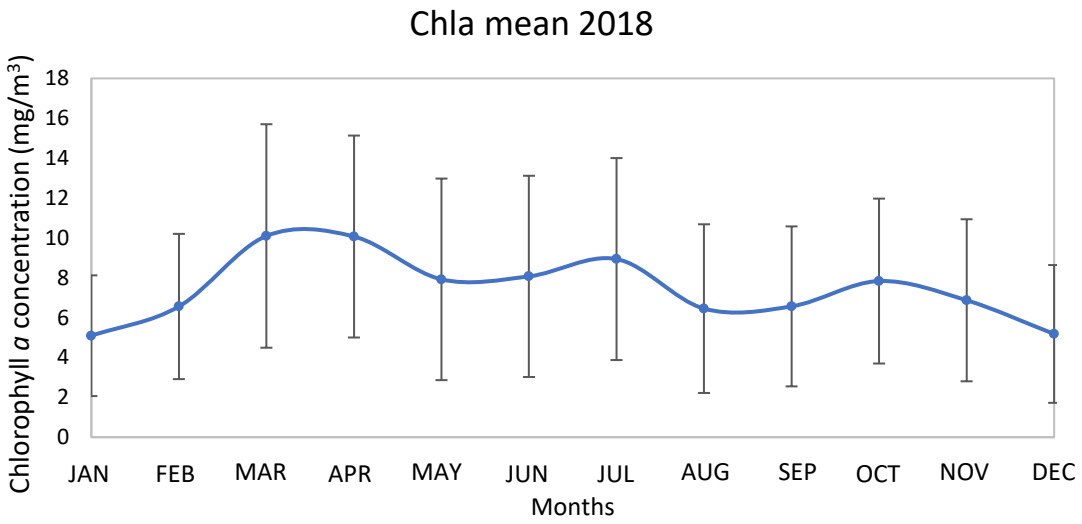

Figure 3.21. Distribution of the average chlorophyll a concentration obtained for each month (Sentinel-3) with the respective standard deviation.

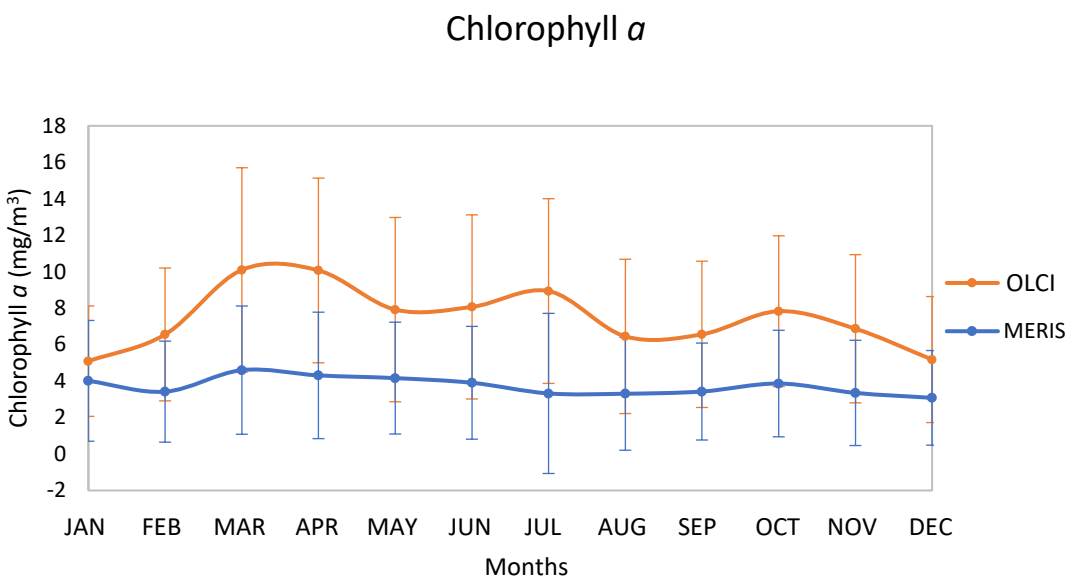

Figure 3.22. Distribution of the average chlorophyll a concentration obtained for each month (MERIS and Sentinel-3) with the respective standard deviation.

3.3.2.3 Interannual Variation

The temporal variation of chlorophyll *a* concentrations for each sampling station, since SEP 2002 to APR 2012, using MERIS database (OC5 algorithm) is represented in Figure 3.23. Stns. #1 and #6 were not considered in this interannual analysis, as they were located very close to the coast. This analysis showed average chlorophyll values of 3.66 µg/L with a mean daily maximum and minimum of 5.06 µg/L and 2.32 µg/L, respectively. Also, it was not easy to detect a seasonal pattern. The mean values presented in Figure 3.23 were calculated after the application of a moving mean filter with a 15-day window (chosen because it is the interval between spring and neap tides) to allow a greater attenuation of the oscillations that would be verified without the filter. According to that average series, it may be possible to assume that 2003, 2007 and 2009 were years characterized by having higher chlorophyll *a* concentrations inside the estuary (Figure 3.23).

An annual analysis, presenting the spatial distribution of chlorophyll inside and outside the estuary for each year of data considered, showed the estuary with a major concentration of chlorophyll than the coastal ocean. Also, the innermost region of the estuary, had higher values of chlorophyll *a* than the area of the bay and mouth (Figure 3.24). The years of 2003, 2007 and 2009 were highlighted by the high concentration of chlorophyll in the region outside the estuary, being this variation coincident with the one observed inside the estuary in Figure 3.23. The years 2002 and 2012 were not included in the analysis since they only had data from September onwards or until April, respectively.

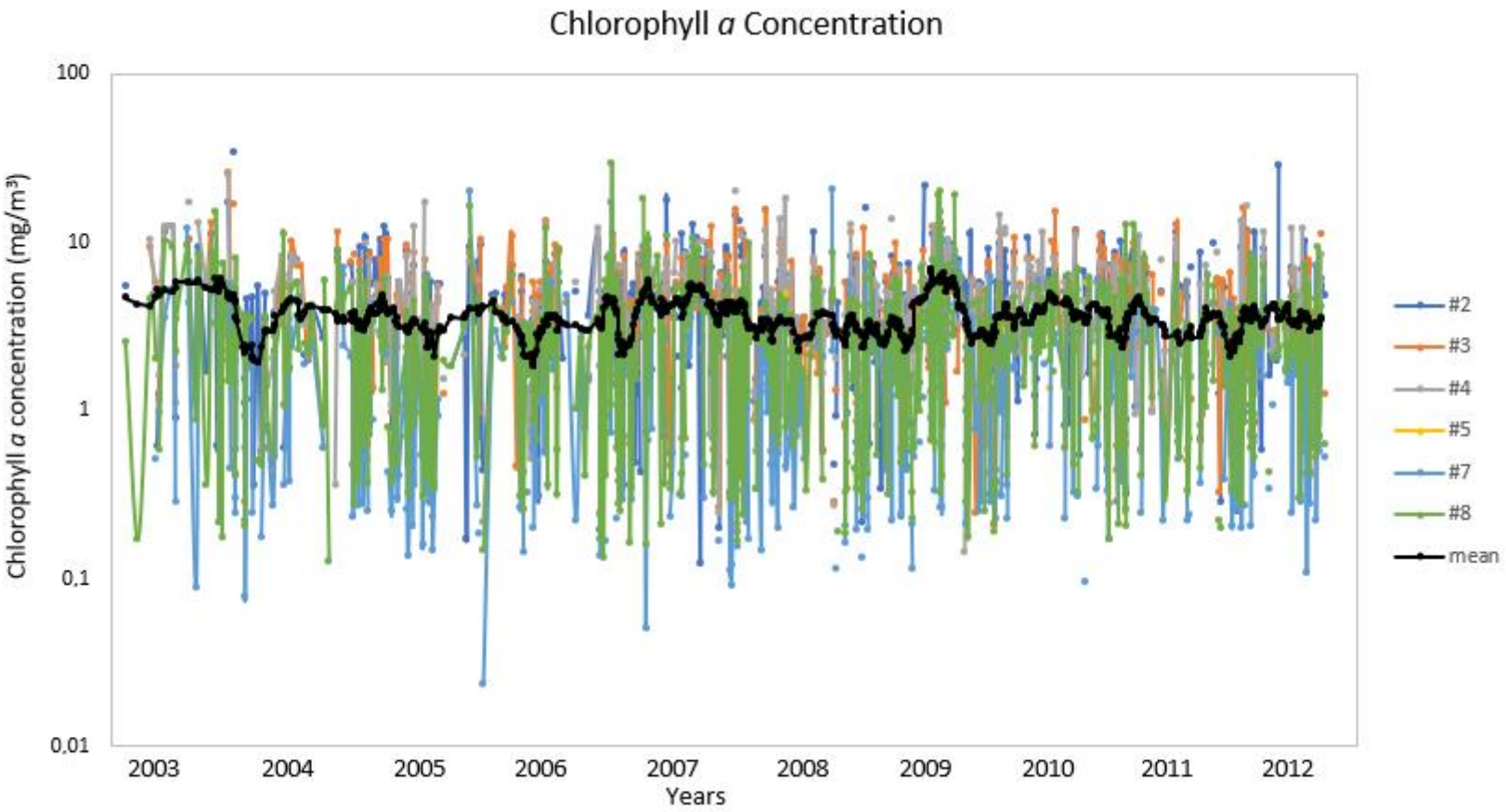

Figure 3.23. Temporal variation of chlorophyll a concentration using MERIS data (OC5 algorithm) in stns. #2, #3, #4, #6, #7 and #8, from SEP 2002 to APR 2012.

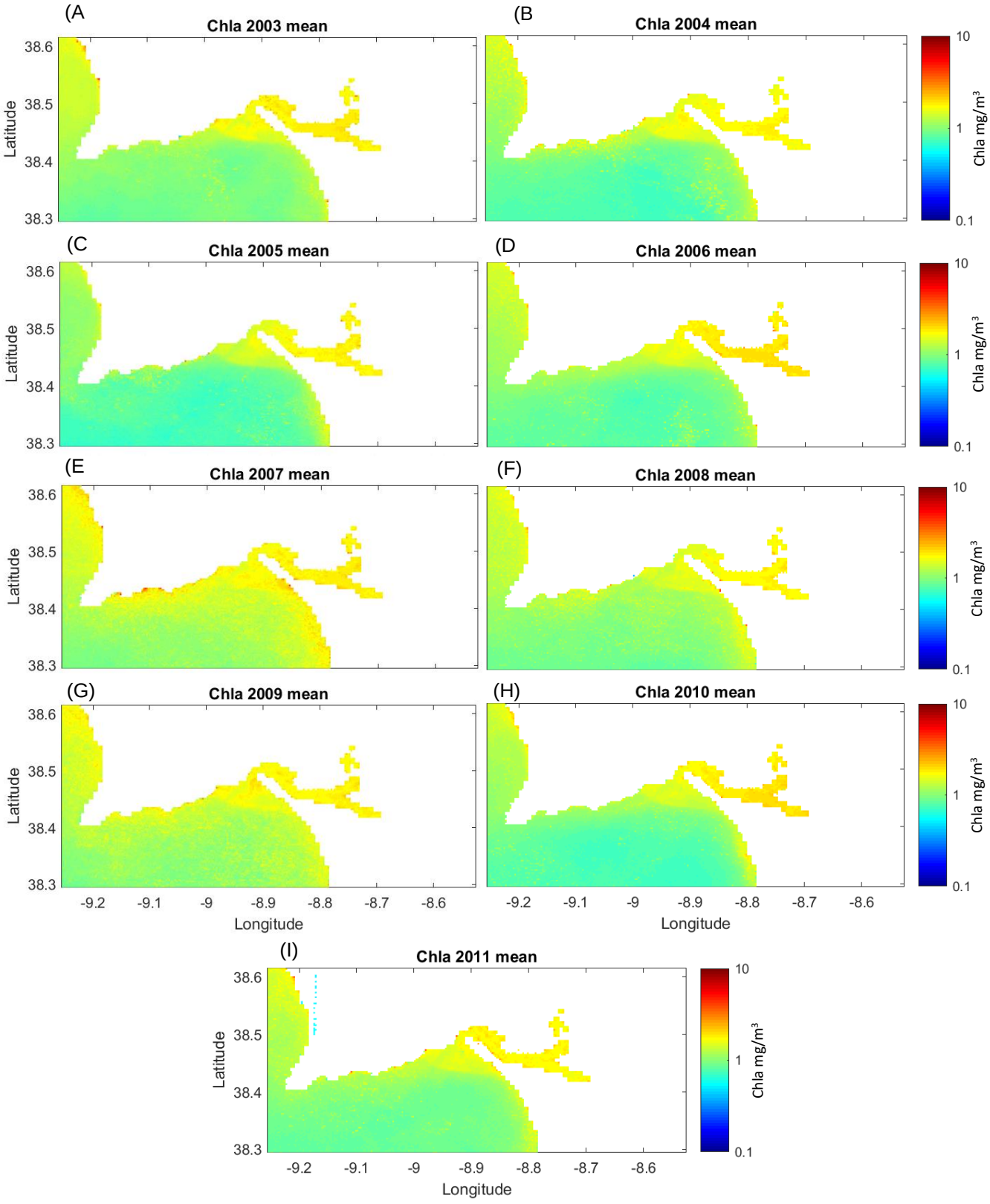

Figure 3.24. Mean chlorophyll a concentration obtained for each year between 2003 and 2011 (MERIS).

The annual averages of chlorophyll concentrations considering all stations, are presented in Figure 3.25. The respective standard deviation is also presented. Similarly to what was previously mentioned, 2003, 2007 and 2009 were the years with higher values of chlorophyll. The average values were almost constant throughout time, with a variation of 0.98 mg/m^3.

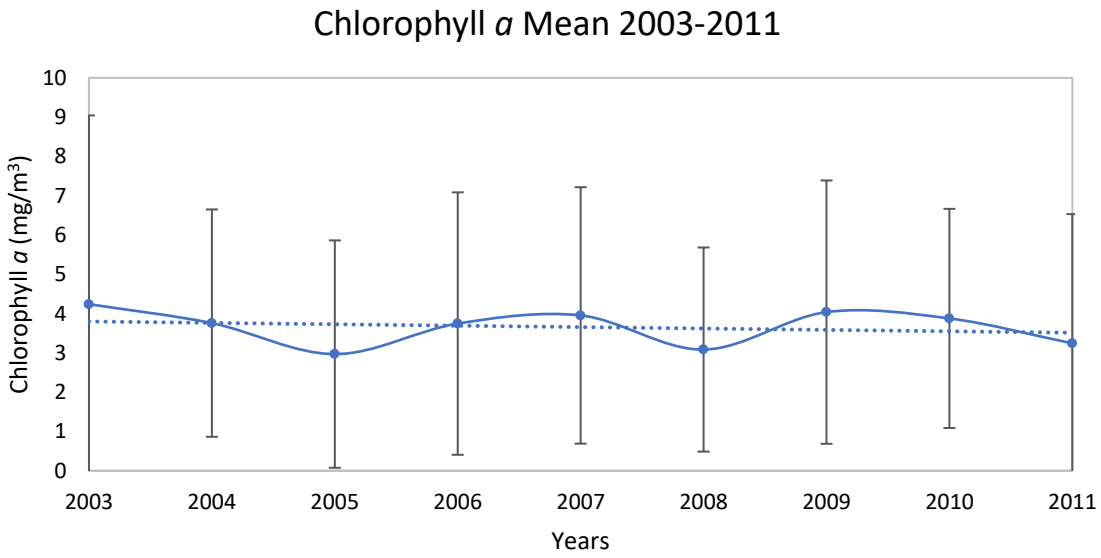

Figure 3.25. Distribution of the average chlorophyll a concentration for each year (MERIS) and the respective standard deviation.

The anomalies of the distribution of chlorophyll *a* in the estuary for each station, every year, are represented in Figure 3.26. The reference value for each one of the stations was the mean of the chlorophyll *a* obtained for each station between 2003-2011.

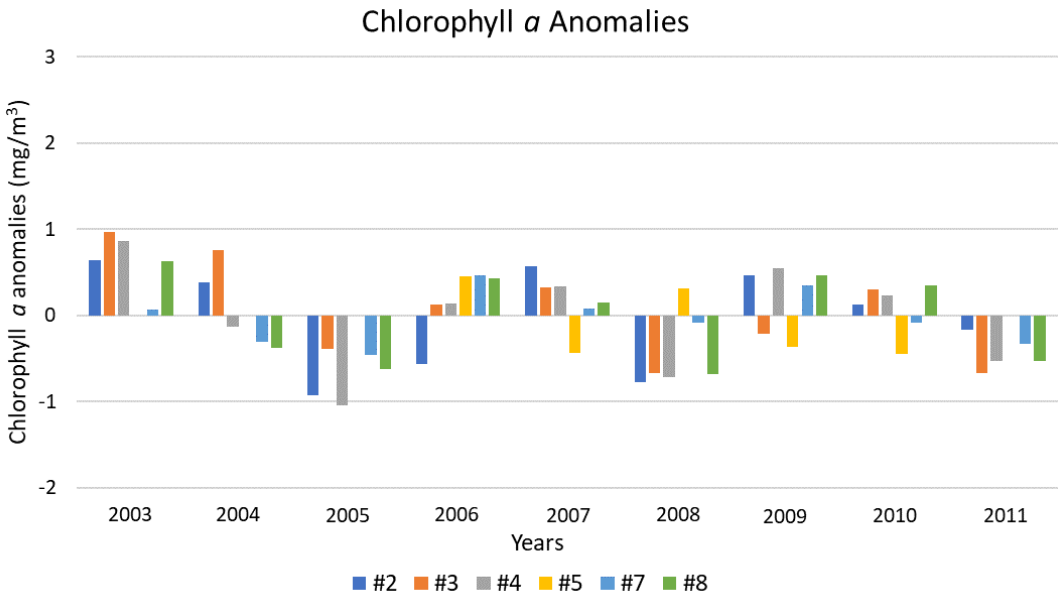

Figure 3.26. Anomalies of the chlorophyll a concentration in the sampling stations of Sado estuary every year, considering the reference for each one of the stations as the mean of the chlorophyll obtained for each station between 2003-2011.

The variation of the anomalies (Figure 3.26) seemed to follow the variation of the annual averages observed in the Figure 3.25. In addition, there appears to have been a trend towards a decrease in chlorophyll between 2003 and 2011, despite being within the standard deviation.

When considering all the images of the database, a spatial climatological average for this region was obtained (Figure 3.27). The value obtained for chlorophyll *a* concentration in the estuary from 2002 to 2012 was 3.66 mg/m^3.

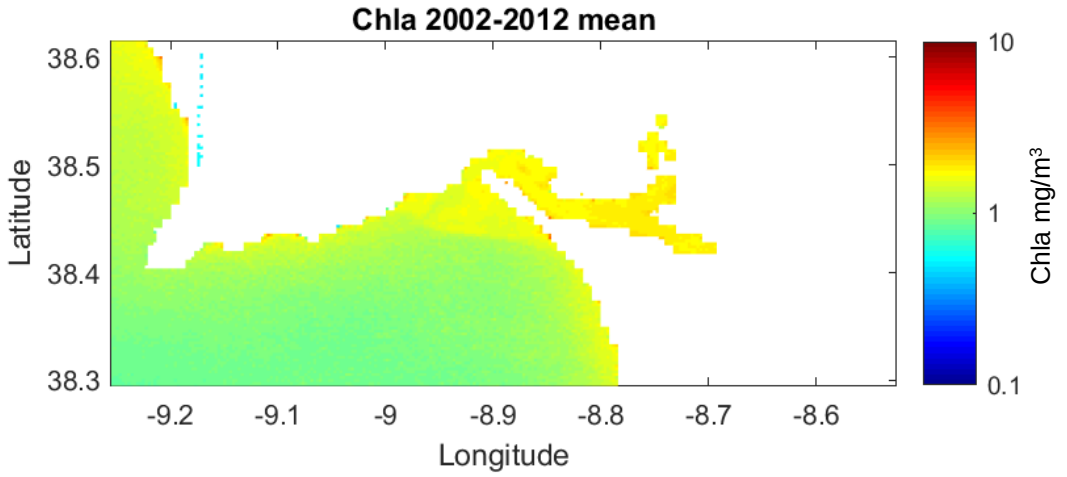

Figure 3.27. Distribution of the average chlorophyll a concentration resulting from the set of all the images from 2002 to 2012 (MERIS).

3.4 Discussion

The satellite showed a small spatial variability of the SST when comparing the data of the 8 stations, making it suitable to consider the estuary as a whole. Nevertheless, the performance of MUR (GHRSST) seemed to be particularly better at stns. #6 and #7, the stations of the outermost region of the estuary (Figure 3.3 and Table 3.4). The database analyzed in this study was also studied by Cadima (2020) in a project that showed the MUR product as the most suitable to characterize the Portuguese coast, from the analyzed possibilities. As stns. #6 and #7 are closer to the ocean than the other sampling stations, the good relation verified is consistent with the work of Cadima (2020). However, in the present study, the satellite did not succeed in detecting reliable temperatures at the inner zone of estuary. This could be justified by the sensor's low spatial resolution or due to the greater spatial variation that occurs in the innermost areas of the estuary, areas with shallow water columns (Loisel *et al.*, 2012). Nevertheless, the product proved to be sensitive to temporal variations in that region of the estuary, as the stations of the inner zone, during winter, registered lower temperatures than the outermost stations, and during summer, reversed this behavior.

A relevant difference between the SST in the inner and the outermost region of the estuary was only detected in 2010. When the river flow anomalies obtained for the period between 1941 and 2019 were analyzed, it was detected a high positive anomaly for 2010, which stood out from the remaining years. 2009/2010 was also characterized by a strong negative NAO, the strongest of the last decades (Climate4you, 2020). The North Atlantic Oscillation (NAO) is the dominant pattern of atmospheric circulation variability in the North Atlantic region ranging from central North America to Europe (a seesaw in atmospheric mass between the subtropical high and the polar low) (Climate4you, 2020). The negative phase of NAO is associated with wet winters

in Southern Europe. This can be a justification for the increase of the river flow in the region in the winter 2009-10. Therefore, it is possible that a strong river flow caused the increase of the thermal amplitude that was verified in that year along the estuary. As the outermost region of the estuary is shown as the coolest, the temperature of the water that flows from the river was higher than the ocean water, contrary to what was published by Ambar *et al.* (1982). Nevertheless, it would be important to have the river flow data for all the years of the studied period to be able to further analyze these findings.

The 18-year analysis using GHRSST dataset showed that the satellite detected annual temperature variation cycles and suggested an oscillatory behavior of the SST over time. The years of 2006 and 2011 presented the higher positive anomalies and 2008 and 2018 showed SST values lower in about 0.4 and 0.6 ˚C relatively to the reference, respectively (Figure 3.12). These variations were apparently strongly related to the weather conditions observed in that period of time, which is suggested by a detailed analysis of the seasonal and annual weather reports prepared by IPMA (available online) and the river flow annual time series (Chapter 1). Years with lower SST values (larger negative SST anomalies) corresponded to the years that registered lower river flow (greater negative flow anomaly), due to lower precipitation levels. Also, these years were of positive NAO index (2007/08 and 2017/18), factor that, again, can justify the climatic variations observed in those years (Climate4you, 2020). Aravena *et al.* (2008) studied the influence of NAO on climatic factors and estuarine water temperature on the Basque coast, in Spain (estuaries of Bilbao and of Urdaibai) and achieved similar results: NAO played a noticeable role in the water temperature variations that occur in those estuaries through its effect on the air temperature (positive phases of NAO resulted in decreased air temperature and, therefore, decreased SST). Also, during part of the studied period, NAO indices were high and seemed to produce a slight decrease of both rainfall and river discharge (despite no significant relationships between the parameters were obtained). In the present study, for 2008 and 2018, as it was verified a lower river flow, it can be assumed that there was a greater influence of ocean water in the estuary. Therefore, the assumption that the river water had higher temperatures than the oceanic water is corroborated. It appears that the precipitation does in fact influence the SST on a large scale, but as for the air temperature, its influence can only be concluded with the seasonal analysis of SST. Establishing an interannual relationship between the parameters was difficult, as the annual mean air temperature values available online are presented at a national and not a regional level, making it difficult to further discuss this topic. However, an attempt was made in order to understand if days of abnormal increases of the air temperature (heat waves) affected the daily values of the SST. Interestingly, it was not observed any relevant sign of those increases at this scale. The small temporal extension of these periods or a possible coincidence with occasional variations of the temperature of the adjacent coastal ocean, may justify the absence or attenuation of the influence of this type of phenomena in the daily values of SST.

Moreover, through the interannual analysis made, a decrease of the sea surface temperature in the past years was identified. According to IPMA, since 1956, there has been a rise in the sea temperature off the west coast of Portugal. Specifically, near the Tagus estuary, in Cascais, a rise as also been verified between 2000 and 2010 (Santos *et al.*, 2012). Therefore, considering the present study, the Sado estuary seems not to show the same trend as the one identified in other regions of Portugal. Also, this contradicts the trend of an increasing water temperature already verified in the oceans of the world, as one of the consequences of the climatic changes that planet is currently facing (Bindoff *et al.*, 2019). However, a statistical test to analyze the significance of this trend would be needed. Also, it would be good to have a time series of SST from this and other estuaries in the country, with a better spatial coverage, to allow a better understanding of the evolution of this variable in the past years and to try to predict the future.

Regarding the recurrent fluctuations with a few days of frequency that were verified in the SST time series, they may likely occur due to atmospheric forcing and may correspond to the impact of weakly atmospheric variations (Laux and Kunstmann, 2008).

In addition to the annual signal, the satellite was able to detect a seasonal signal (Figure 3.6). The water temperature was higher in the warmer months, and cooler in the winter months, inside and outside the estuary. Therefore, the temperature of the air, in fact influences the water temperature (Ocean Health Index, 2020). This is clearer in the inner areas of the estuary, probably due to shallow water columns. The same was verified in the Tagus estuary in Gonçalves and Brogueira (2010), when the inner region of the estuary showed to be more susceptible to seasonal variations of the air temperature than the outermost region.

In the outer region of the estuary, the isotherms presented different orientations in summer and winter (Figure 3.5), which suggests that during summer, occurred the transport of warmer waters from the south of the country to Troia peninsula. These observations indicate that the estuary and the adjacent area were not affected by the typical seasonal upwelling that characterizes the coastal region of Portugal (Coutinho, 2003). This may be due to the fact that Setúbal Peninsula interrupts the North-South coastal drift current originated by the dominant Northerly winds, and creates a shelter situation throughout the sector of Troia to Carvalhal Beach, which turns the seawater temperatures higher than those that characterize the western coast during the summer (Neto, 2000).

On the other hand, the relationship between the water temperature and the chlorophyll distribution appeared to follow a different behavior. In the area of costal ocean, it was possible to see that, when the SST was higher (higher air temperature), there were lower values of chlorophyll *a* in the region (MERIS database). However, the values obtained for the estuary were not entirely in agreement with that. These results showed that summer was a season with lower productivity than winter, which was not in agreement with what was already known about the seasonal variability of the chlorophyll concentration and with what was mentioned by Coutinho (2003) for the Sado estuary. In her study, Coutinho characterized the phytoplankton community of the Sado estuary in its structure, dynamics and ecological aspects, and indicated maxima and minima of chlorophyll *a* concentrations (used as a proxy of phytoplankton biomass) in three regions, the outer (equivalent to stns. #6, #7 and #8), middle (area encompassing stns. #2, #3, #4 and #5) and innermost areas of the estuary (where stn. #1 is located), between 1990 and 1993. During that period, the maxima were obtained between June and August (summer) and the minima between November and March (autumn/winter). Also, over the years, she verified an increase of the chlorophyll *a* concentrations from the outermost region of the estuary to its innermost region. Thus, the higher winter values obtained with MERIS for the estuary may have been influenced by some environmental events such as precipitation, surface runoff or higher river flow. These events tend to increase the suspended matter in the estuary and can possibly influence the estimation of the satellite chlorophyll *a* concentrations. Since the determination of this parameter is based on an analysis of the visible spectrum, the suspended matter as well as the colored dissolved organic matter (CDOM) can change the color of the water, disturb the signal released from the water column and unable the efficient quantification of chlorophyll *a* (Sutcliffe *et al.*, 2016). Therefore, it is necessary to develop algorithms specially dedicated to shallow transitional areas, given their optical complexity.

However, the range of chlorophyll *a* concentrations obtained for the interior of the estuary does not appear to be very different from what was presented in previous works. According to Lemaire *et al.* (2002), the distribution of chlorophyll *a* in the Sado estuary was between 0.2 and 4.0 µg/L. Also, the work conducted by Marectec (2002b) presented an average value for the chlorophyll in the estuary during summertime of 5 µg/L, indicating no sign of eutrophication in

the region, as referred also by Ferreira *et al*. (2003). In those works, it was reported that, although the estuary is homogeneous in its major area, it has higher concentrations of chlorophyll *a* in the channels of Marateca, Comporta and Alcácer, the inner areas of the estuary (Coutinho, 2013). This was also observed with MERIS data.

With the annual anomalies obtained with MERIS database, it was possible to see that there was a tendency of a decrease in the chlorophyll *a* concentration inside the estuary between 2002 to 2012. According to Ferreira *et al*. (2019), the chlorophyll *a* variability in the western coast of the Iberian Peninsula is highly dependent on river discharges and coastal upwelling. Although the authors mentioned some chlorophyll hotspots along the coast (Northern and Central Portuguese coast and mouth of Tagus estuary) and identified the northwestern Iberia with a positive trend for chlorophyll *a*, the coastal region of Sado estuary was compassed in an area of low productivity. Therefore, the decreasing trend observed in this study, if it continues to be verified, can be justified by the decrease of the river flow observed in the past years (Sales, 2015) and because the Sado estuary is not influenced by the seasonal upwelling characteristic of the coast of Portugal, as already mentioned. Such a tendency follows the trend observed globally and already confirmed by NASA with a study that suggested a decline of the oceanic phytoplankton in the northern hemisphere (Rousseaux, 2015).

Interestingly, between the chlorophyll *a* anomalies (MERIS) and the SST anomalies obtained, it was not observed any relevant relationship (neither by comparing each station separately, nor by comparing the average of the stations). Also, the daily Sentinel-3 chlorophyll *a* data was compared with the SST values for the year of 2018 and no association between the datasets was found.

The analysis of chlorophyll *a* estimated from Sentinel-3 OLCI gave a clear indication that these data were more appropriate for this study area, due to the sensor's spatial resolution. More clearly, it was possible to see the inner channels of the estuary with the highest concentration of chlorophyll *a*. Also, it was during spring that was achieved the maximum production of chlorophyll *a* throughout the estuary, as would be expected. However, the correlation between the satellite values and those collected *in situ* was low (R^2 = 0.33). One of the error sources associated with the Sentinel-3 data may be the presence of suspended matter that appears to have interfered with the quantification of chlorophyll *a*, especially during the campaign of 8 November 2018. Low correlations between Sentinel-3 products and *in situ* data have also been verified by other authors, as in the study conducted by Moutzouris-Sidiris *et al*. (2019) where no correlation was observed between the chlorophyll *a* calculated from the neural nets and the *in situ* data collected in the Mediterranean Sea. Given the complexity of coastal environments, the algorithms available are not yet fully efficient and the optically active components can interfere with the estimations of chlorophyll *a* concentrations. However, in the present work, when MERIS and OLCI databases were analyzed and the algorithms developed for coastal waters were used, a quality increase in the satellite products was observed. Therefore, it is important to continue to try to produce new algorithms suitable for shallow transitional waters, using as a base the results obtained by the products validation exercises already performed by several authors in different areas of the world. Improvements can be achieved by coastal products and through regionalized models developed with *in situ* chlorophyll and concomitant radiometric data (Sá *et al.*, 2015).

Chapter 4

General Discussion

The data obtained with the CTD revealed a low variation of all the parameters studied along the tidal cycle. These observations were corroborated by the study of Moreira (1987). Although it was an expected result, it would be interesting to perform additional campaigns to follow complete tidal cycles, given the importance of the tide in the estuary circulation. This study revealed that the water influx and outflux in the region is generally made through the two navigation channels (North and South channels), according to the tide, with more intense currents in the South channel. In the two channels, more intense currents were observed during the ebb than during the flood. The current intensity appeared to decrease with depth and an agreement between the direction of the surface current and the current at the lowest level was also verified (see the schema of the circulation regime in Figure 4.1). This last result deviated from the observed in previous studies, so it is possible that the estuary had gone through a change in the circulation regime in the last years. These changes could have been originated by several factors: they could derive from the decrease of the river flow in the past years, from changes in the morphology of the estuary (natural or anthropogenic) (Neto *et al*., 2019) or even come from the differences between the sampling procedures.

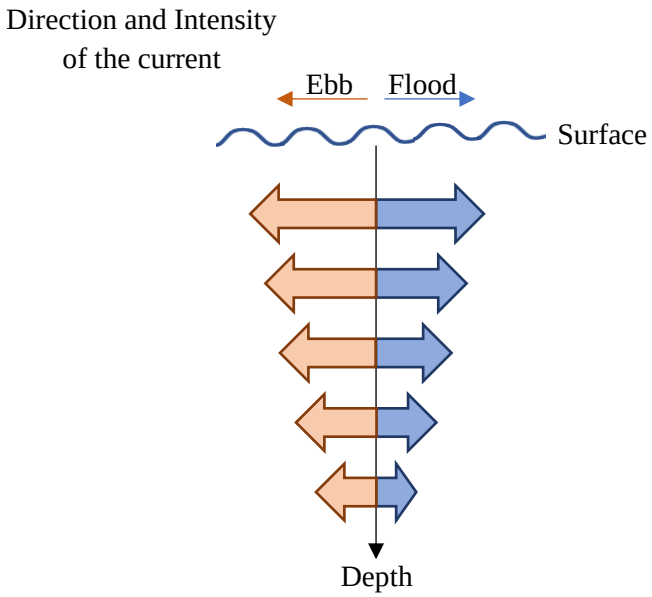

Figure 4.1. Schematic representation of the direction and intensity of the current (not to scale) observed in depth, in the two navigation channels, during flood and ebb.

The variation in the tide and, therefore, in the circulation regime in the estuary, was not observed through the analysis of the studied satellite datasets. However, the utility of using SST products to study circulation patterns in open ocean and coastal regions is recognized worldwide (NOAA, 2020d). In the present study, it was possible to see the circulation pattern of the regional coastal ocean with the Multiscale Ultrahigh Resolution (MUR) product and it was observed that during the summer months, occurred the transport of warmer waters from the south of the country to Troia peninsula. Therefore, the region of the Sado estuary and the adjacent area does not seem to be affected by the seasonal upwelling that influences the west coast of Portugal (Coutinho, 2003).

The influence of the circulation was also not observed in the satellite-derived chlorophyll *a* data, although the cycle of spring/neap tide can influence the distribution of chlorophyll in an estuary (Roegner *et al,* 2010). However, the flow of the river appeared to have influenced the estimation of the satellite chlorophyll *a* concentrations, by increasing the suspended matter in the estuary (Loisel *et al.*, 2012). The influence of the river flow was observed not only in the analysis of the satellite data but also in the *in situ* observations, more evidently in the salinity profiles, which occasionally showed lower salinity values at the surface of the water column.

Based on the data collected during the sampling campaigns, the outermost area of the estuary can be described as spatially homogeneous, with occasional stratification of the water column (Sousa and Lourenço, 1980; Ambar *et al.*, 1982). The same spatial homogeneity was observed in the analysis of GHRSST MUR product, that included data from the whole set of stations distributed along the estuary. However, the satellite presented more realistic results for the outermost region of the estuary, possibly due to the low resolution of the product used. Likewise, these results can be justified by the greater variability of temperatures verified in the inner region of the estuary, due to shallow water columns that turns the region more susceptible to environmental changes (Loisel *et al*., 2012). Nevertheless, the sensor proved to be sensitive to temporal variations in the whole estuary. By the analysis of both the *in situ* observations and the satellite-derived SST, this region showed to be susceptible to the seasonal variation of the weather conditions and, consequently, influenceable by the changes of the river flow. On the other hand, the satellite-derived chlorophyll *a* data, more specifically Sentinel-3 data, showed that the estuary cannot be considered spatially homogeneous for its chlorophyll *a* distribution. Although the agreement between the Sentinel-3 data and the *in situ* values was low, it was observed by the two approaches that the most interior region of the estuary is characterized by having higher concentrations of chlorophyll *a* and that the higher values were obtained during spring. The validation exercises of chlorophyll *a* data are greatly complicated to perform. However, improvements can be achieved if considered regional solutions (coastal products and regionalized models developed with *in situ* chlorophyll and concomitant radiometric data) when application requirements are not corresponded by standard product accuracy (Sá *et al.*, 2015).

All things considered, the integration of both the *in situ* observations and the satellite data in this study led to a more robust analysis of the physicochemical parameters. The *in situ* data allowed assessing the usefulness of specific satellite products that have high spatial and temporal coverage of the Sado estuary. It was through remote sensing that the best temporal and spatial coverage was achieved, but this approach did not allow to observe variations in depth or throughout the tidal cycle, as it was possible to see with the *in situ* observations. The integration of these two methods contributed for a better understanding of the physicochemical processes in the Sado estuary, for which each approach provided a key contribution (Figure 4.2).

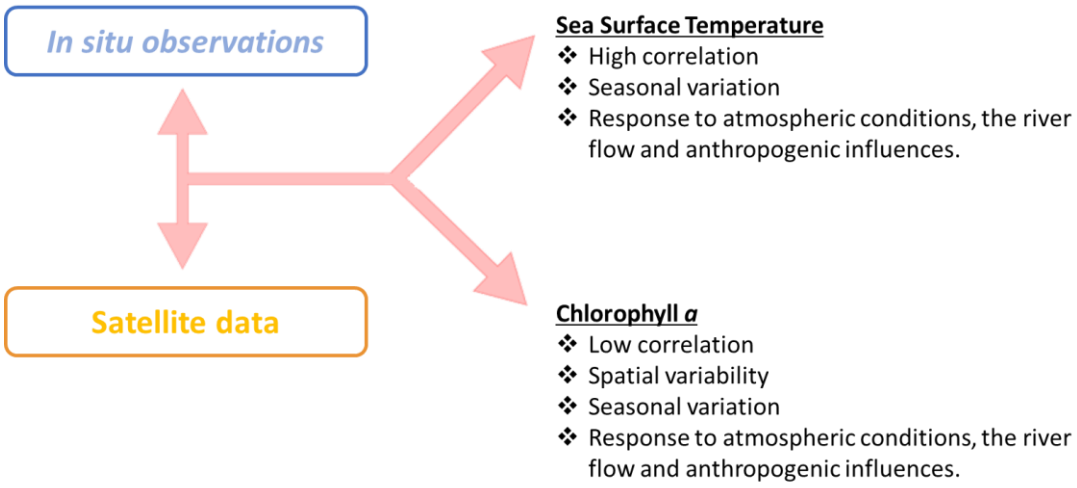

Figure 4.2. Integration of the results obtained with the in situ observations and the satellite data.

Chapter 5

Final Remarks

The Sado estuary has been the subject of several oceanographic studies in the past years. However, currently, it is still a challenge to fully understand the dynamics of this estuary. After the integration of *in situ* observations (with frequent sampling, in depth and throughout the tidal cycle) with satellite data, as performed in the present study, an extended understanding of the temporal and spatial patterns of the Sado estuary was achieved. It was investigated the estuary relatively to the variability of its physicochemical parameters (temperature, salinity, density, turbidity, fluorescence and direction and intensity of the currents), studying seasonal patterns and their variation along the tidal cycle. Also, it was evaluated the use of SST and chlorophyll *a* satellite products in the estuary and accomplished a historical description of the distribution of these parameters throughout the region since 2002, as well as a description of their inter and intra-annual variability.

In the future, it would be interesting to carry out a more extensive analysis of the estuary, both *in situ* and remotely. In the campaigns that followed the partial tidal cycles, some logistical constraints conditioned the sampling, leading to the reduction of the amount of data collected (availability of the boats, number of available light hours to do the measurements, instruments that got damaged, …). It was observed that the campaigns that covered entire tidal cycles were the ideal to do a reliable study about the circulation regime inside the estuary. Therefore, it would be essential to increase the robustness of the results obtained extending the monitoring of complete tidal cycles with frequent sampling to the CTD. Also, expand the use of the CTD and the current meter sensor to several sampling points distributed throughout the estuary would be important. Perhaps the best way to continuously obtain physicochemical data would be by deploying *in situ* buoys equipped with multiparametric sondes in the estuary. A frequent monitoring would also be important to enable an interannual analysis based on *in situ* data, that would allow to complement the existing satellite databases. In the analysis of the satellite-derived data, limitations of spatial resolution were detected in the SST product and problems of atmospheric correction and in the determination of the variables were observed in the chlorophyll products. It became clear that it is still challenging to study estuarine areas, in particular the Sado estuary, using satellite remote sensing data but, based on the results of this work, there is an indication of a relevant improvement in the quality and accuracy of the products generated over the last years. Therefore, it is important to continue to work on the development of new algorithms that are suitable for coastal environments. In the future it would be relevant to perform radiometry measurements to improve algorithms and the feasibility of using satellite data in such areas.

The Sado estuary has been increasingly considered as an area of high economic potential but, simultaneously, and interestingly, as a region that urgently needs to be protected. It is important to sustainably invest in the estuary and, to do so, it is necessary to fully understand the dynamics of the area in the various scientific aspects and monitor possible investment activities (*e.g.*: dredging works). The present study allowed to complement the oceanographic analysis previously carried out in the estuary and raised some questions that are possible to be answered with future studies. Also, shows the potential in exploring the area through satellite remote sensing and works as a consistent study capable of enrich further analysis in a field still underexplored in this estuary.

Bibliography

Abbas, M., Melesse, A., Scinto, L. and Rehage, J. (2019). Satellite Estimation of Chlorophyll-a Using Moderate Resolution Imaging Spectroradiometer (MODIS) Sensor in Shallow Coastal Water Bodies: Validation and Improvement. *In* Water 11(1621), DOI:10.3390/w11081621.

ADEC – Alaska Department of Environmental Conservation (2015). Fact Sheet: Turbidity in Surface Waters. Available at: https://dec.alaska.gov/

Agência Portuguesa do Ambiente, Administração da Região Hidrográfica do Alentejo, Instituto da Conservação da Natureza e da Biodiversidade, Instituto de Gestão do Património Arquitectónico e Arqueológico, Comissão de Coordenação e Desenvolvimento Regional do Alentejo (2009). Remodelação da Estação de Tratamento de Águas Residuais de Tróia. Projeto de Execução. Parecer da Comissão de Avaliação.

Ambar, I., Fiúza, A., Sousa, F. and Lourenço, I. (1982). General Circulation in Lower Sado River Estuary under Drought Conditions. *In* Actual Problems of Oceanography in Portugal, 97-107, JNICT, Lisboa.

Aravena, G., Villate, F., Iriarte, A., Uriarte, I., Ibáñez, B. (2008). Influence of the Northe Atlantic Oscillation (NAO) on climatic factors and estuarine water temperature on the Basque coast (Bay of Biscay): Comparative analysis of three seasonal NAO indices. *In* Elsevier Continental Shel Research 29(4):750-758, DOI: 10.1016/j.csr.2008.12.001.

Benali, A. (2009). Monitoring Chlorophyll-a with remote sensing techniques in the Tagus Estuary. Geophysical Research Abstracts 11(1000). EGU General Assembly.

Bindoff, N., Cheung, W., Kairo, J., Arístegui, J., Guinder, V., Hallberg, R., Hilmi, N., Jiao, N., Karim, M., Levin, L., O'Donoghue, S., Cuicapusa, S., Rinkevich, B., Suga, T., Tagliabue, A., and Williamson, P. (2019). Changing Ocean, Marine Ecosystems, and Dependent Communities. *In* IPCC Special Report on the Ocean and Cryosphere in a Changing Climate.

Brandão, A. (2019). Setúbal quer deixar de despejar esgotos no rio Sado no Verão. Available at: https://www.rtp.pt/noticias/pais/setubal-quer-deixar-de-despejar-esgotos-no-rio-sado-no-verao_a1130613

Brito, P., Amorim, A., Andrade, C., Freitas, M. C. and Monteiro, J. (2003). Assessment of morphological change in estuarine systems – a tool to evaluate responses to future sea level rise. The case of the Sado Estuary (Portugal). II Congresso sobre Planejamento e Gestão da Zonas Costeiras dos Países de Expressão Portuguesa, IX Congresso da Associação Brasileira de Estudos do Quaternário, II Congresso do Quaternário dos Países de Língua Ibéricas.

Cadima, M. (2020). Validação de produtos de satélite de temperatura da superfície do oceano (SST). Relatórios Científicos Técnicos. IPMA.

Caeiro, S. (2004). Environmental data management in Sado estuary: Weight of evidence to assess sediment quality. Thesis to obtain the degree of Doctor of Philosophy in Environmental Engineering. Faculdade de Ciências e Tecnologia, Universidade Nova de Lisboa.

Chi, Y. and Fu, Z. (2018). Spatial heterogeneity of estuarine wetland ecosystem health influenced by complex natural and anthropogenic factors. *In* Science of The Total Environment 634:1445-1462, DOI:10.1016/j.scitotenv.2018.04.085.

Chin, T., Vazquez-Cuervo, J. and Armstrong, E. (2017). A multi-scale high-resolution analysis of global sea surface temperature. *In* Remote Sensing of Environment 200:154-169, DOI:10.1016/j.rse.2017.07.029.

Climate4you (2020). NAO and AO. Available at: http://www.climate4you.com/NAOandAO.htm #List%20of%20contents

Conceição, R. (2016). Gestão de dragagens portuárias – alguns aspectos geotécnicos e geoambientais. Dissertation to obtain the master's degree in Geologic Engineering. Faculdade de Ciências e Tecnologia, Universidade Nova de Lisboa.

Costa, M. (2015). Estudo da utilização espácio-temporal do estuário do Sado pela população residente de roazes (*Tursiops truncatus*), com recurso a um método goniométrico. Dissertation to obtain the master's degree in Conservation Biology. Faculdade de Ciências, Universidade de Lisboa.

Coutinho, M. (2003). Comunidade fitoplanctónica do Estuário do Sado: Estrutura, dinâmica e aspetos ecológicos. Instituto Nacional de Investigação Agrária e das Pescas IPIMAR.

Crosman, R., Vazquez-Cuervo, J. and Chin, T. (2017). Evaluation of the Multi-Scale Ultra-High Resolution (MUR) Analysis of Lake Surface Temperature. *In* Remote Sensing 9(7):723, DOI:10.3390/rs9070723.

Cui, T., Zhang, J., Groom, S., Sun, L., Smyth, T. and Sathyendranath, S. (2010). Validation of MERIS ocean-color products in the Bohai Sea: A case study for turbid coastal waters. *In* Remote Sensing of Environment 114(10):2326-2336, DOI:10.1016/j.rse.2010.05.009.

Cunha, A., Assis, J. and Serrão, E. (2009). Estimation of available seagrass meadow area in Portugal for transplanting purposes. *In* Journal of Coastal Research, Special Issue 56.

Dassenaki, M., Paraskevopoulou, V., Cartalis, C., Adaktilou, N. and Katsiabani, K. (2012). Remote sensing in coastal water monitoring: Applications in the eastern Mediterranean Sea (IUPAC Technical Report). *In* Pure and Applied Chemistry 84(2):335–375, DOI:10.1351/PAC-REP-11-01-11.

Day, J., Crump, B., Kemp, W. and Yáñez-Arancibia, A. (2012). Estuarine Ecology, Second Edition. John Wiley & Sons Ltd. ISBN: 978-0-471-75567-8.

Dias, C. (2019). Promessas têm anos mas esgotos da Comporta continuam a poluir o Sado. Available at: https://www.publico.pt/2019/11/25/local/noticia/etar-comporta-estar-construcao-nao-sabe-arrancam-obras-1895008

EES Group (2018). Threats to estuaries. Department of Planning, Industry and Environment of New South Wales Government. Available at: https://www.environment.nsw.gov.au/about-us/who-we-are

ESA Earth Online (2019a). MERIS. Available at: https://earth.esa.int/web/guest/missions/esa-operational-eo-missions/envisat/instruments/meris

ESA Earth Online (2019b). Sentinel-3. Available at: https://sentinel.esa.int/web/sentinel/missions/sentinel-3

ESA Earth Online (2020a). NOAA AVHRR. Available at: https://earth.esa.int/web/guest/missions/3rd-party-missions/current-missions/noaa-avhrr

ESA Earth Online (2020b). Applications. Available at: https://earth.esa.int/web/guest/missions/esa-operational-eo-missions/envisat/instruments/meris/applications

EUMETSAT (2019). Recommendations for Sentinel-3 OLCI Ocean Colour product validations in comparison with *in situ* measurements – Matchup Protocols. EUM/SEN3/DOC/19/1092968 v5B.

Ferreira, A., Garrido-Amador, P. and Brito, A. C. (2019). Disentangling Environmental Drivers of Phytoplankton Biomass off Western Iberia. *In* Frontiers in Marine Science, https://doi.org/10.3389/fmars.2019.00044.

Ferreira, J., Simas, T., Nobre, A., Silva, M., Shifferegger, K. and Lencart e Silva, J. (2003). Identification of sensitive areas and vulnerable zones in transitional and coastal Portuguese systems. Application of the United States National Estuarine Eutrophication Assessment to the Minho, Lima, Douro, Ria de Aveiro, Mondego, Tagus, Sado, Mira, Ria Formosa and Guadiana systems. INAG/IMAR, ISBN 972-9412-66-9.

Ferreira, J., Bettencourt, A., Bricker, S., Marques, J., Meirinho, A., Newton, A., Nobre, A., Salas, F., Silva, M., Simas, T., Soares, C., Stacey, P., Vale, C. and Wolff, W. (2005). Water Framework Directive – Transitional and Coastal Waters. Proposal for the definition of water bodies. MONAE.

Franz, B. (2007). Satellite Remote Sensing of Ocean Color and Temperature. NASA Ocean Biology Processing Group. University of Queensland, Brisbane.

Gameiro, C. and Brotas, V. (2010). Patterns of Phytoplankton Variability in Tagus Estuary (Portugal). *In* Estuaries and Coasts 33(2):311-323, DOI:10.1007/s12237-009-9194-4.

GHRSST (2020). Overview. Available at: https://www.ghrsst.org/about-ghrsst/overview/

Goes, I. (2012). De espaço rural agrícola a espaço público urbano: A várzea de Setúbal. Dissertation to obtain the master's degree in Landscape Architecture. Instituto Superior de Agronomia, Universidade de Lisboa.

Gohin, F., Druon, J., and Lampert, L. (2002). A five channel chlorophyll concentration algorithm applied to SeaWiFS data processed by SeaDAS in coastal waters. *In* International Journal of Remote Sensing 23(8):1639–1661, DOI:10.1080/01431160110071879.

Gonçalves, C. and Brogueira, M. (2010). Seasonal and tidal influence on the variability of nitrous oxide in the Tagus estuary, Portugal. *In* Scientia Marina 74(S1), DOI:10.3989/scimar.2010.74s1057.

Guimarães, L. (2019). Tribunal suspende dragagens no rio Sado. Available at: https://www.rtp.pt/noticias/pais/tribunal-suspende-dragagens-no-rio-sado_v1191320

ICNF – Instituto de Conservação da Natureza e das Florestas (2020). Reserva Natural do Estuário do Sado – Informação. Available at: http://www2.icnf.pt/portal/ap/resource/ap/rnes/rnes-net-final.pdf

IPMA (2019a). Normais Climatológicas 1971-2000. Available at: https://www.ipma.pt/en/oclima/normais.clima/1971-2000/#170

IPMA (2019b). Boletim Climático Sazonal e Mensal. Available at: http://www.ipma.pt/pt/publicacoes/boletins.jsp?cmbDep=cli&cmbTema=pcl&idDep=cli&idTema=pcl&curAno=-1

IPMA (2019c). E em Portugal? O clima está a mudar?. FAQ's – Climatologia. Available at: https://www.ipma.pt/pt/educativa/faq/climatologia/faqdetail.html?f=/pt/educativa/faq/climatologia/faq_0004.html

JPL MUR MEaSUREs Project (2015). GHRSST Level 4 MUR Global Foundation Sea Surface Temperature Analysis (v4.1). Version 4.1, https://doi.org/10.5067/GHGMR-4FJ04. PO.DAAC, CA, USA.

Kennish, M., Livingston, R., Raffaelli, D. and Reise, K. (2008). Environmental future of estuaries. *In* Aquatic Ecosystems: Trends and Global Prospects 1st Edition, 13:188-208, DOI:10.1017/CBO9780511751790.018. Cambridge University Press. N. V. C. Polunin.

Laux, P. and Kunstmann, H. (2008). Detection of regional weekly weather cycles across Europe. *In* Environmental Research Letters 3(4):044005, DOI:10.1088/1748-9326/3/4/044005.

Lemaire, E., Abril, G., De Wit, R. and Etcheber, H. (2002). Distribution of phytoplankton pigments in nine European estuaries and implications for an estuarine typology. *In* Biogeochemistry 59: 5-23. Kluwer Academic Publishers.

Lins, R., Martinez, J., Marques, D., Cirilo, J. and Fragoso Jr., C. (2017). Assessment of Chlorophyll-a Remote Sensing Algorithms in a Productive Tropical Estuarine-Lagoon System. *In* Remote Sensing 2017(9):1-19, DOI:10.3390/rs9060516.

Liria, P., Garel, E. and Uriarte, A. (2009). The effects of dredging operations on the hydrodynamics of an ebb tidal delta: Oka Estuary, northern Spain. *In* Continental Shelf Research 29(16):1983-1994, DOI: 10.1016/j.csr.2009.01.014.

Loisel, H., Vantrepotte, V., Jamet, C. and Dat, D. (2012). Challenges and New Advances in Ocean Color Remote Sensing of Coastal Waters. *In* IntechOpen Topics in Oceanography, DOI: 10.5772/56414.

Magnetic-Declination.com, (2020). Find the magnetic declination at your location. Available at: www.magnetic-declination.com/

Maretec (nd). Descrição – Sado. Morfologia. Available at: http://maretec.mohid.com/Estuarios/MenusEstuarios/Descri%C3%A7%C3%A3o/descricao_Sado.htm

Maretec (2000a). Sistema de Modelação MOHID 2000. Available at: http://maretec.mohid.com/Estuarios/Inicio/Mohid2000.htm#_Toc518564872

Maretec (2000b). Definição do Limite de Jusante dos Estuários Portugueses. Available at: http://maretec.mohid.com/Estuarios/Inicio/Introducao.htm

Maretec (2002a). Water Quality in Portuguese Estuaries: Tejo – Sado - Mondego. Instituto da Água. Directiva do Tratamento de Águas Residuais Urbanas (91/271/CEE). Directiva dos Nitratos de Origem Agrícola (91/676/CEE).

Maretec (2002b). OSPAR Convention for the Protection of the Marine Environment of the North East Atlantic – Mondego, Tagus and Sado Estuaries. Instituto da Água, Instituto do Ambiente. Ministério das Cidades, Ordenamento do Território e Ambiente.

Marques, N. (2017). Dinâmica oceânica no espaço marítimo português: Caraterização de massas de água e circulação oceânica. Dissertation to obtain the master's degree in Naval Military Sciences. Marinha Portuguesa.

Martin, M., Dash, P., Ignatov, A., Banzon, V., Helen, B., Brasnett, B., Cayula, J., Cummings, J., Donlon, D., Gentemann, C., Grumbine, R., Ishizaki, S., Maturi, E., Reynolds, R. and Roberts-Jones, J. (2012). Group for high resolution sea surface temperature (GHRSST) analysis fields inter-comparisons: Part 1. A GHRSST multi-product ensemble (GMPE). Deep-Sea Research II, DOI:10.1016/j.dsr2.2012.04.013.

Martins, F., Leitão, P. and Neves, R. (2002). Simulating vertical water mixing in homogeneous estuaries: the SADO Estuary case. *In* Hydrobiologia 475/476:221–227, DOI:10.1023/A:1020369431924.

Mateus, M., Mateus, S. and Baretta, J. (2008). Basic concepts of estuarine ecology. *In* Perspectives on Integrated Coastal Zone Management in South America. IST Press, pp.3-14, DOI:10.13140/2.1.4497.0562.

Mateus, M., Pablo, H. and Vaz, N. (2013). An investigation on body displacement after two drowning accidents. *In* Forensic Science International 229(1), DOI:10.1016/j.forsciint. 2013.03.010.

McDougall, T. and Barker, P. (2011). Getting started with TEOS-10 and the Gibbs Seawater (GSW) Oceanographic Toolbox, 28pp. SCOR/IAPSO WG127, ISBN 978-0-646-55621-5.

Moreira, M. (1987). Estudo fitogeográfico do ecossistema de sapal do estuário do Sado. *In* Finisterra XXII(44):247-296.

Moutzouris-Sidiris, I., Topouzelis, K. and Konstantinidou, E. (2019). Assessment of chlorophyll-a concentration derived from Sentinel-3 satellite images using open source data. Proceedings 11174, https://doi.org/10.1117/12.2535591. Seventh International Conference on Remote Sensing and Geoinformation of the Environment (RSCy2019).

Nagaraja, M. (2019). Ocean Color. NASA SCIENCE. Available at: https://science.nasa.gov/earth-science/oceanography/living-ocean/ocean-color

Nagaraja, M. (2020). Remote Sensing. NASA SCIENCE. Available at: https://science.nasa.gov/earth-science/oceanography/living-ocean/remote-sensing

NASA (2019). CZCS. Available at: https://oceancolor.gsfc.nasa.gov/data/czcs/

NASA (2020). MODIS. Available at: https://aqua.nasa.gov/modis

NASA Earth Data (2020). Visible Infrared Imaging Radiometer Suite (VIIRS). Available at: https://ladsweb.modaps.eosdis.nasa.gov/missions-and-measurements/viirs/

Neto, C. (2000). A Circulação do ar na península de Troia e na costa da Galé. *In* Finisterra XXXV(70):41-55, https://doi.org/10.18055/Finis1658.

Neto, J., Caçador, I., Caetano, M., Chaínho, P., Costa, L., Gonçalves, A., Pereira, L., Pinto, L., Ramos, J. and Seixas, S. (2019). Estuários (Capítulo 16). *In* Rios de Portugal – Comunidades, Processos e Alterações. Coimbra University Press, pp.381-421, https://doi.org/10.14195/978-989-26-1624-7_16.

Neves, R. (1985). Étude expérimentale et modélisation mathématique des circulations transitoire et résiduelle dans l'estuaire du Sado. Thesis to obtain the degree of Doctor of Philosophy. Université de Liège, Liège.

Neves, R., Chambel-Leitão, P., Leitão, P. (2000). Modelação numérica da circulação da água no solo – o modelo MOHID. *In* Pedologia 28:46-55.

NOAA (2020a). Why do scientists measure sea surface temperature? National Ocean Service website. Available at: https://oceanservice.noaa.gov/facts/sea-surface-temperature.html

NOAA (2020b). Estuaries: Classifying Estuaries - By Water Circulation. National Ocean Service website. Available at: https://oceanservice.noaa.gov/education/kits/estuaries/estuaries05_circulation.html

NOAA (2020c). Estuaries: What is an estuary? National Ocean Service website. Available at: https://oceanservice.noaa.gov/education/kits /estuaries/estuaries01_whatis.html

NOAA (2020d). How are satellites used to observe the ocean? National Ocean Service website. Available at: https://oceanservice.noaa.gov/facts/satellites-ocean.html

Ocean Health Index (2020). Sea Surface Temperature. Available at: http://www.oceanhealthindex.org/methodology/components/sea-surface-temperature

Pablo, H., Sobrinho, J., Garcia, M., Campuzano, F., Juliano, M. and Neves, R. (2019). Validation of 3D-MOHID Hydrodynamic Model for the Tagus Coastal Area. *In* Water 11(8):1713, DOI: 10.3390/w11081713.

Palmer, S., Hunter, P., Lankester, T., Hubbard, S., Spyrakos, E., Tyler, A., Présing, M., Horváth, H., Lamb, A., Balzter, H. and Tóth, V. (2015). Validation of Envisat MERIS algorithms for chlorophyll retrieval in a large, turbid and optically-complex shallow lake. *In* Remote Sensing of Environment 157:158-169, https://doi.org/10.1016/j.rse.2014.07.024.

Rabaçal, C. (2018). Setúbal inicia construção de estação elevatória que vai acabar com esgotos despejados no Sado. Interview for Agência Lusa. Available at: https://24.sapo.pt/atualidade/artigos/setubal-inicia-construcao-de-estacao-elevatoria-que-vai-acabar-com-esgotos-despejados-no-sado

Ribeiro, M. and Neves, R. (1982). Caracterização Hidrográfica do Estuário do Sado. Serviço de Estudos do Ambiente e Instituto Superior Técnico, Lisboa.

Roegner, G., Seaton, C. and Baptista, A. (2010). Climatic and Tidal Forcing of Hydrography and Chlorophyll Concentrations in the Columbia River Estuary. *In* Estuaries and Coasts 34(2):281-296, DOI: 10.1007/s12237-010-9340-z.

Rosa, M. (2010). Hydrodynamical and Biogeochemical modeling study of Sado Estuary. Dissertation to obtain the master's degree in Marine Sciences and Coastal Zones. Departamento de Ambiente, Universidade de Aveiro.

Rousseaux, C., and Gregg, W. (2015). Recent decadal trends in global phytoplankton composition. *In* Global Biogeochem Cycles 29(10):1674–1688, DOI:10.1002/2015GB005139.

Sá, C., D'Alimonte, D., Brito, A. C., Kajiyama, T., Mendes, C., Vitorino, J., Oliveira, P., Silva, J., Brotas, V. (2015). Validation of standard and alternative satellite ocean-color chlorophyll products off Western Iberia. *In* Remote Sensing of Environment 168:403-419, https://doi.org/10.1016/j.rse.2015.07.018.

Sales, S. (2015). Determinação do efeito do regime hidrológico e da regularização do caudal na ecologia trófica do barbo do Norte (*Luciobarbus bocagei* Steindachner 1864). Dissertation to obtain the master's degree in Management and Conservation of Natural Resources. Universidade de Évora.

Santos, A. and dos Santos, A. (2012). Programa de Monitorização CascaisWatch. IPMA.

SNIRH – Sistema de Informação de Recursos Hídricos (2020). Daily Average Flow, Moinho da Gamitinha. Available at: https://snirh.apambiente.pt/

Sousa, F. and Lourenço, I. (1980). Oceanografia Física do Estuário do Sado. Laboratório de Física da Universidade de Lisboa.

Sousa, M. (2006). Contribuição para a caracterização geoambiental dos sapais do estuário do Sado – aplicação experimental no ensino da geologia. Dissertation to obtain the master's degree in Geology for Teaching. Faculdade de Ciências e Tecnologia, Universidade Nova de Lisboa.

Sutcliffe, A., Brito, A.C., Sá, C., Sousa, F., Boutov, D. and Brotas, V. (2016). Observação da Terra: uso de imagens de temperatura da superfície do mar e cor do oceano para a monitorização de águas costeiras e oceânicas. DGRM, Lisboa, Portugal. E-book available at www.sophia-mar.pt.

Toming, K., Kutser, T., Uiboupin, R., Arikas, A., Vahter, K. and Paavel, B. (2017). Mapping Water Quality Parameters with Sentinel-3 Ocean and Land Colour Instrument Imagery in the Baltic Sea. *In* Remote Sensing 9(10):1070, DOI:10.3390/rs9101070.

Vale, C., Ferreira, A., Micaelo, C., Caetano, M., Pereira, E., Madureira, M. and Ramalhosa, E. (1998). Mobility of contaminants in relation to dredging operations in a mesotidal estuary (Tagus Estuary, Portugal). *In* Water Science and Technology 37(6-7):25-31, PII: S0273-1223(98)00178-4.

Valencia, V., Franco, J., Borja, A., Fontán, A. (2004). Chapter 7 – Hydrography of the southeastern Bay of Biscay. *In* Elsevier Oceanography Series 70:159-194, https://doi.org/10.1016/S0422-9894(04)80045-X.

van Maren, D., van Kessel, T. and Sittoni, C. (2015). The impact of channel deepening and dredging on estuarine sediment concentration. *In* Continental Shelf Research 95:1-14, https://doi.org/10.1016/j.csr.2014.12.010.

Vazquez-Cuervo, J., Gomez-Valdes, J., Bouali, M., Miranda, L., Stocken, T., Tang, W. and Gentemann, C. (2019). Using Saildrones to Validate Satellite-Derived Sea Surface Salinity and Sea Surface Temperature along the California/Baja Coast. *In* Remote Sensing 11(17), https://doi.org/10.3390/rs11171964.

Wolanski, E., Andutta, F., Delhez, E. (2013). Estuarine hydrology. Encyclopedia of Lakes and Reservoirs. Encyclopedia of Earth Sciences Series (238-249). Spring-Verlag. DOI:10.1007/978-1-4020-4410-6_77.

Wollast, R. (1978). Rio Sado Campagne de Mesures de juillet. Technical Report. Secretaria de Estado do Ambiente, Lisboa.

Wollast, R. (1979). Rio Sado Campagne de Mesures d'Avril. Technical Report. Secretaria de Estado do Ambiente, Lisboa.

Zheng, G. and DiGiacomo, P. (2017). Uncertainties and applications of satellite-derived coastal water quality products. *In* Progress in Oceanography 159: 45-72, https://doi.org/10.1016/j.pocean.2017.08.007.

Annexes

Annex I

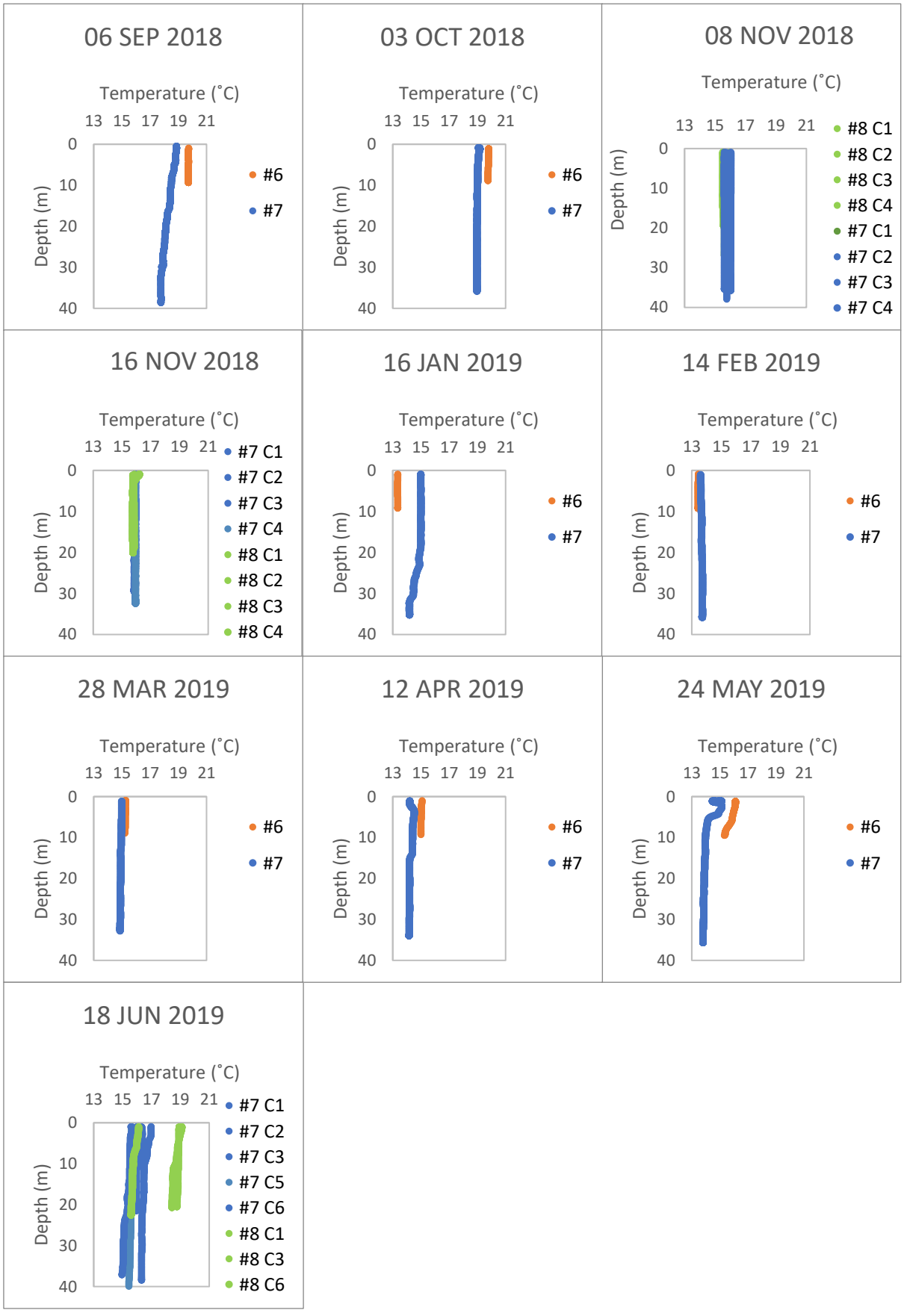

Figure A.1. Temperature profiles obtained in CTD stns. #6 (orange), #7 (blue) and #8 (green), in the period SEP 2018-JUN 2019. C - partial cycle measurement.

Annex II

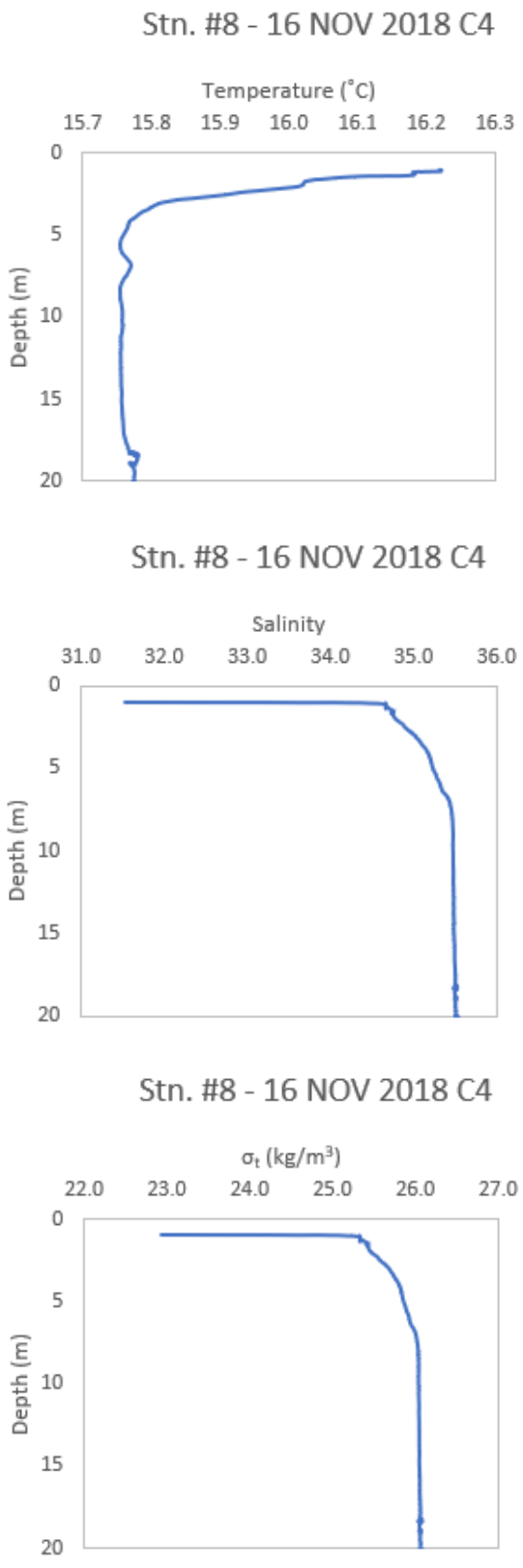

Figure A.2. Temperature, salinity and sigma-t profiles obtained in CTD stn. #8 (C4 - partial cycle measurement no. 4), during the campaign of 16 NOV 2018.

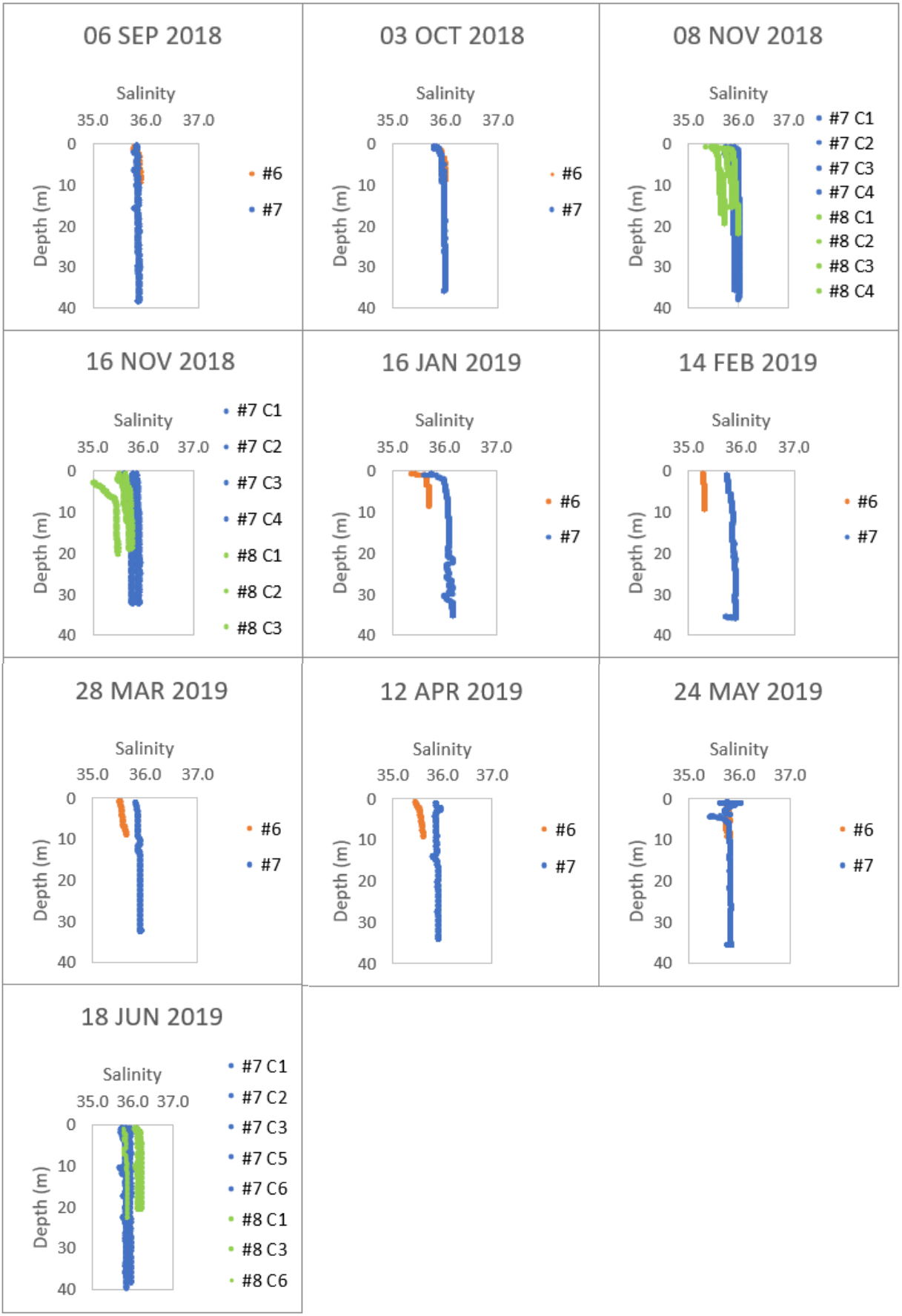

Figure A.3. Salinity profiles obtained in CTD stns. #6 (orange), #7 (blue) and #8 (green), in the period SEP 2018-JUN 2019. C - partial cycle measurement.

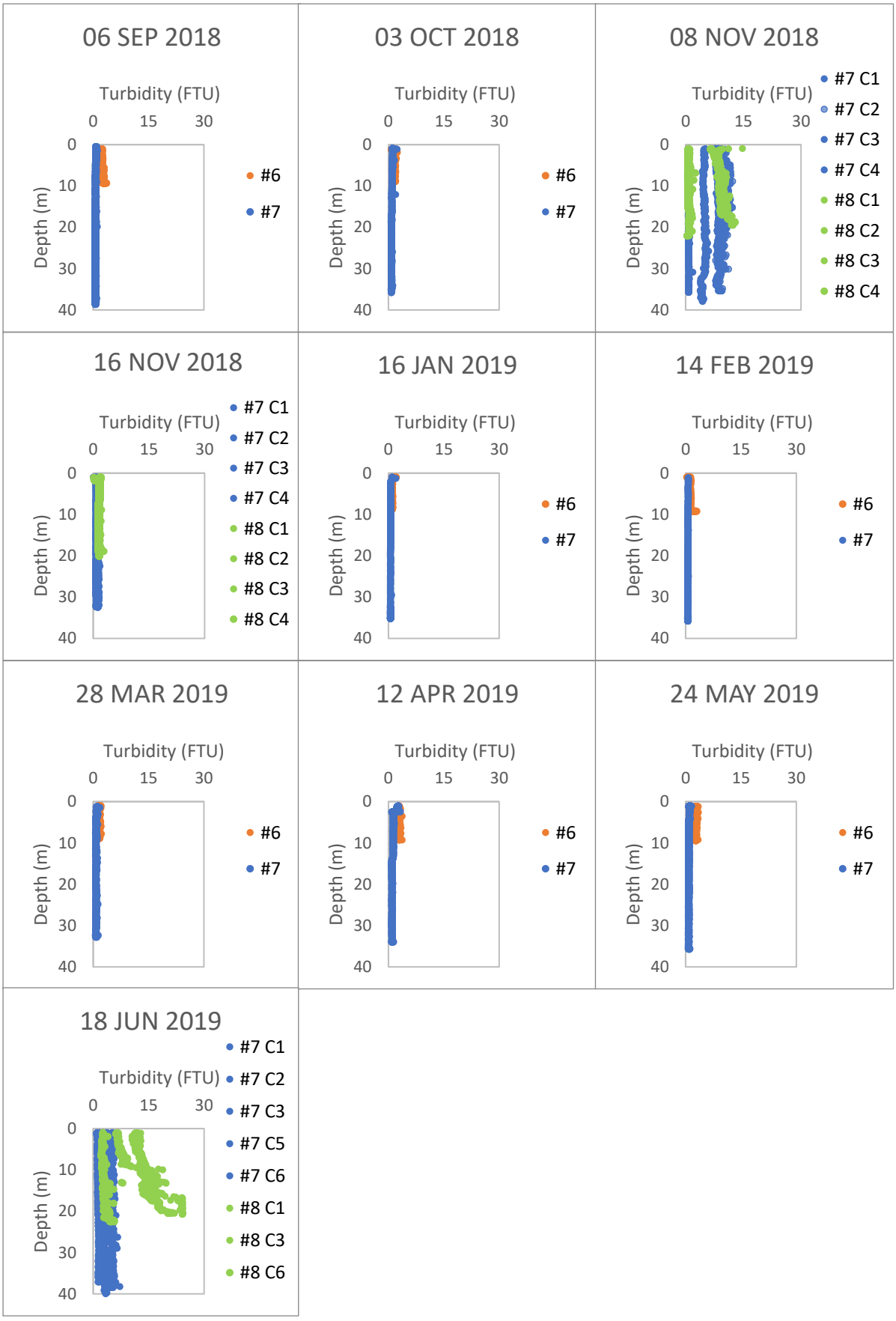

Figure A.4. Turbidity profiles obtained in CTD stns. #6 (orange), #7 (blue) and #8 (green), in the period SEP 2018-JUN 2019. C - partial cycle measurement.

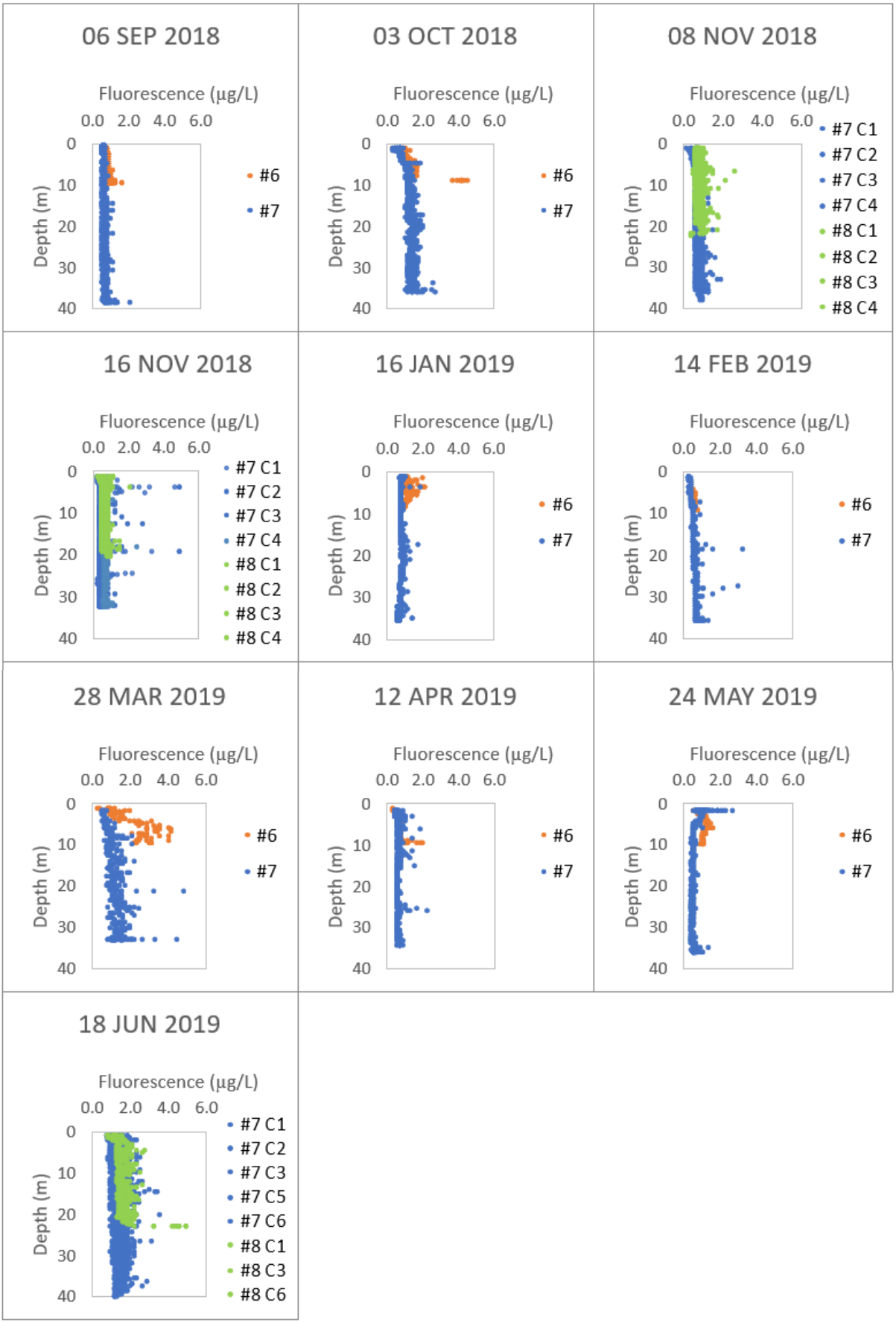

Figure A.5. Fluorescence profiles obtained in CTD stns. #6 (orange), #7 (blue) and #8 (green), in the period SEP 2018-JUN 2019. C - partial cycle measurement.

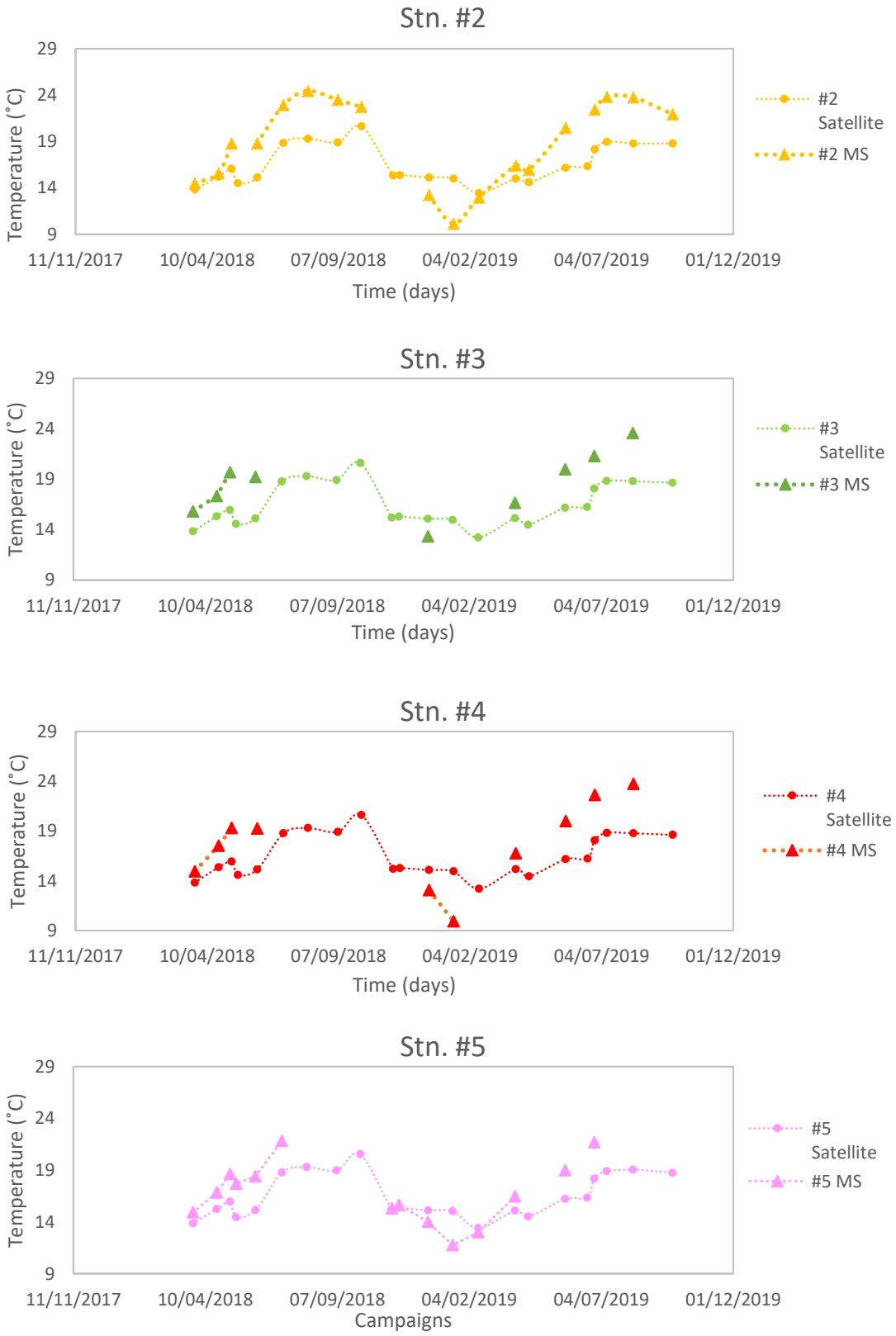

Figure A.6. Temporal variation of the surface temperature data obtained with the CTD, the CS, the MS and the satellite during the sampling campaigns.

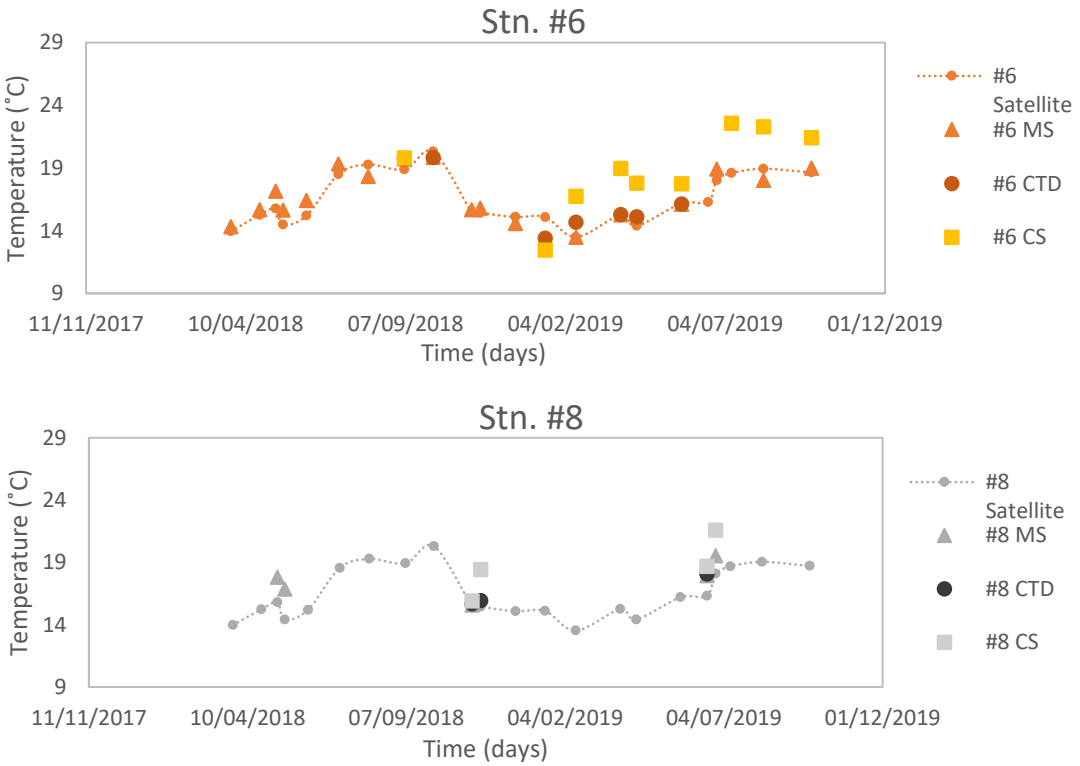

Figure A.6 (continued).

Annex VII

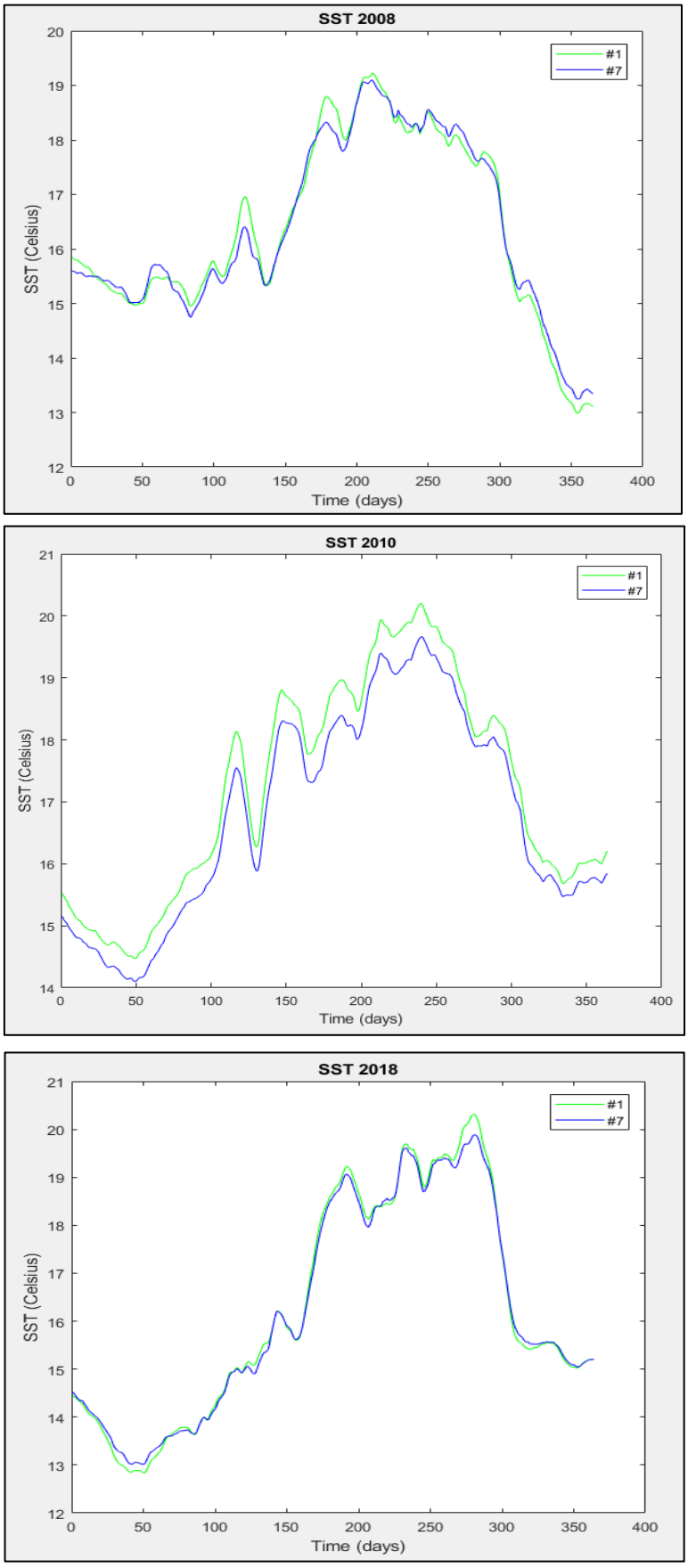

Figure A.7. Example of the SST variation throughout the year of 2008, 2010 and 2018, in one station from the inner area of the estuary (#1) and another from the outermost zone (#7), smoothed with a moving mean filter with a 15-day window.